University of Venda

Design and synthesis of potential malaria cysteinyl protease inhibitors

By

Sedzani A Nethavhani

Student Number: 11573877

Submitted in fulfilment of the requirements for the Degree of

Master of Science (Chemistry)

in the Department of Chemistry

School of Mathematical and Natural Sciences

at the University of Venda

Supervisor: Prof. T. van Ree

Co-supervisor: Prof. I.D.I. Ramaite

Date submitted: August 2015

Declaration

I, Sedzani Alvina Nethavhani, hereby declare that the dissertation for the Master of Science (Chemistry) degree at the University of Venda, hereby submitted by me, has not been submitted previously for a degree at this or any other university, that it is my own work in design and in execution, and that all reference material contained therein has been duly acknowledged.

Signature ..... Date 19.02.2015

Sedzani A. Nethavhani

Main supervisor ..... Date 19.02.2015

Prof. T. van Ree

Co-supervisor ..... Date 19/02/2015

Prof. I. D. I. Ramaite

Plagiarism declaration

I, Sedzani Alvina Nethavhani (Student No: 11573877), hereby declare the following:

- I am aware and acknowledge that plagiarism is wrong. Plagiarism is the use of another person's ideas or published work and to pretend that it is one's own and it is a serious academic offence for which the university may impose severe penalties.
- I declare that this thesis is my own work and that I have correctly acknowledged the work of others. The work has not been previously submitted to the University of Venda or elsewhere for this degree.
- I have not allowed, and will not allow, anyone to copy my work with the intention of passing it off as their own work.

Signature: 

Date: 19.02.2015

Abstract

The overall objective of this project was to design and synthesize cysteinyl protease inhibitors that are envisaged to have antimalarial activity. Several synthesis routes leading to the rigid heterocyclic 2-pyridone scaffold were explored. The syntheses of the 2-pyridones involved constructing and investigating derivatives with hydrophilic and hydrophobic moieties, using a methodology that seems to have a wide scope. Intermediates as well as the target pyridones were docked into the falcipain-2 active site and tested against chloroquine-sensitive and resistant *Plasmodium falciparum* strains; three 3-cyano-2-pyridones showed promising results. Using this collection of synthesis methodologies, a wide variety of di- and tripeptides based on a substituted 2-pyridone scaffold in the P2 position, have become accessible.

Keywords: *Plasmodium; protease; cysteinase; 2-pyridone; antimalarial.*

ACRONYMS AND ABBREVIATIONS

AIDS	Acquired Immune Deficiency Syndrome
CC	Column chromatography
CDC	Centers for Disease Control
FP2	Falcipain-2
GC	Gas chromatography
GIC	Genome International Consortium
HIV	Human Immunodeficiency Virus
IC_{50}	The concentration of an enzyme inhibitor where the response (or binding) is reduced by half.
pLDH	Parasite lactate dehydrogenase
MS	Mass spectrometry
TB	Tuberculosis
TLC	Thin layer chromatography
WHO	World Health Organization
^{13}C-NMR	Carbon-13 nuclear magnetic resonance spectroscopy
^{1}H-NMR	Proton nuclear magnetic resonance spectroscopy

ACKNOWLEDGEMENTS

1. Dr Jenny-Lee Panayides of the Council for Scientific and Industrial Research (Biosciences Molecular and Biomedical Technologies Group) is thanked for performing the antiplasmodial testing.
2. Mr Thomas Makungo is thanked for assistance with the FP2 docking studies.
3. A very big thank you goes to my supervisor, Professor Teuns van Ree as source of inspiration and guidance on this project. His patience and compassionate nature is appreciated.
4. A debt is owed to Dr Paul Mebe for mentoring and nurturing my chemistry knowledge and skills.
5. I thank my husband Mr Lindelani Manyaga for his patience, support and prayers throughout the period of this project.

TABLE OF CONTENTS

Chapter 1

Introduction and Background

Malaria is an infectious disease caused by the mosquito-borne parasite *Plasmodium* and, with HIV and TB, is one of the three major human infectious diseases targeted by the World Health Organization (WHO, 2014). There are four infective species of *Plasmodium* that can be transmitted to humans. The most severe and deadly malaria is caused by *Plasmodium falciparum.* The other species, namely *Plasmodium vivax, Plasmodium ovale* and *Plasmodium malariae* cause a milder form of malaria that is usually not fatal to otherwise healthy humans (White, 2004).

1.1 Malaria as a disease

The disease is a result of multiplication of the malaria parasite within the red blood cells after somebody is bitten by a mosquito, which is called the *vector*. The lifecycle of the *Plasmodium* parasite (Figure 1.1) is complex and involves three stages, which are the exoerythrocytic cycle (A), the erythrocytic cycle (B) and the sporogonic cycle (C). Several sub-stages are numbered 1 to 12 in the following discussion. The sexual phase of the parasite's life-cycle occurs in mosquitoes, which are the vectors for the malaria parasites. The sexual phase, called ***sporogony***, leads to the development of a large number of infecting forms of the parasite within the mosquito that induce disease in the human *host* after their injection by the mosquito bite (1). *Plasmodium* survives in the saliva of female *Anopheles* mosquitoes. When an infected mosquito bites a person, it injects saliva that contains infectious sporozoites into the human bloodstream. After this first stage injection, the sporozoites are carried to the liver by the circulatory system. Once the sporozoites are in the liver cell (2), the cell becomes infected and the sporozoites develop into schizonts (3), which develop into merozoites and the cell ruptures (4). The merozoites migrate to the erythrocytes (5) in the erythrocytic stage and undergo a period of enlargement known as the ring stage trophozoite. The trophozoite is more metabolically active and develops into the merozoite, and the erythrocyte ruptures (6) releasing a large number of merozoites. Apparently, the rupture and reinvasion of erythrocytes at this stage requires proteases; the degradation of haemoglobin by trophozoites also requires proteases. The trophozoites ingest the cytoplasm

and transport it to the large central food vacuole of the parasite. Here, the haemoglobin is metabolized to haem and globin, which is hydrolysed to its constituent amino acids. The food vacuole is acidic in nature with pH 5.0, which is acidic enough to degrade haemoglobin (Krogstad and Schlesinger, 1987).

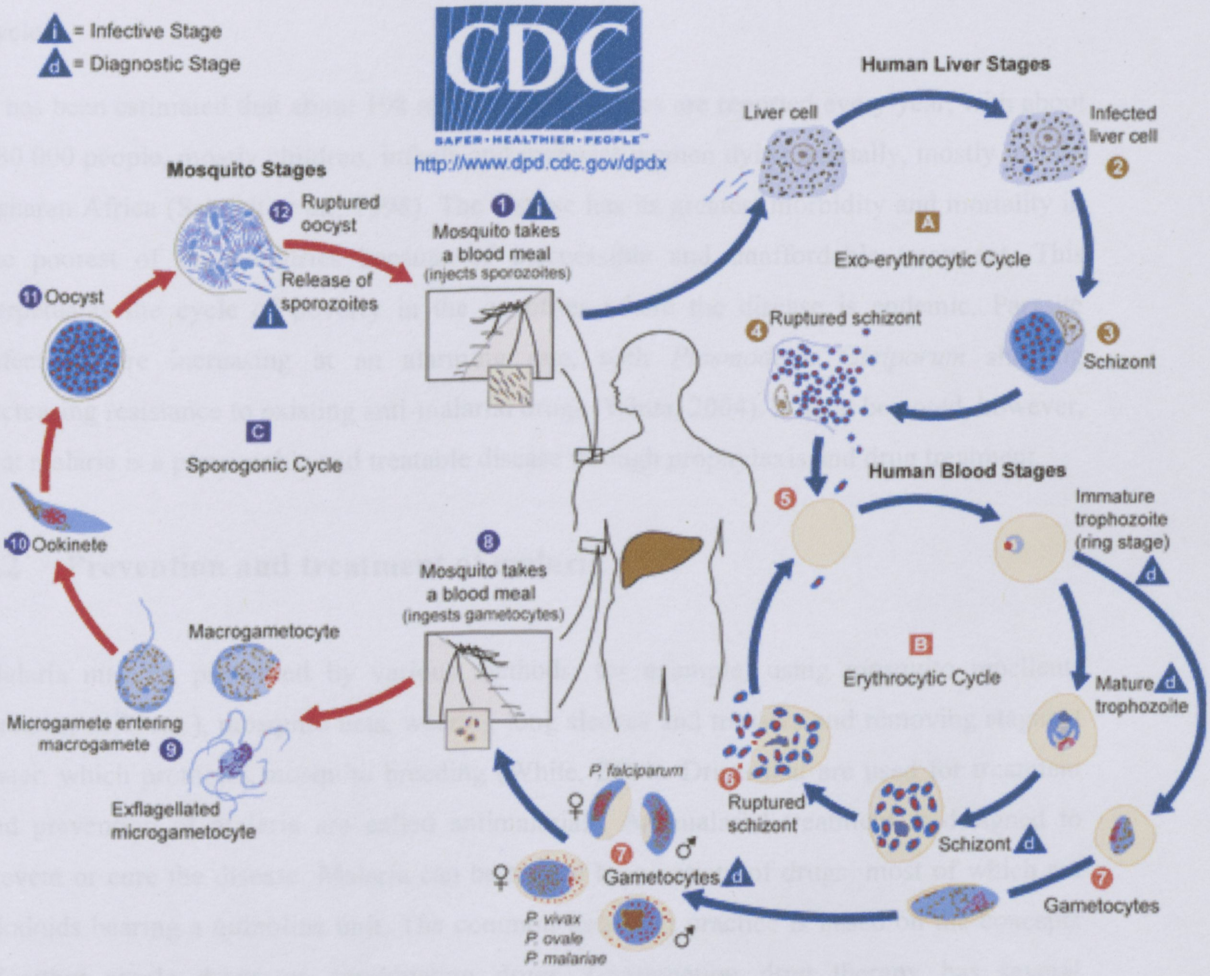

Figure 1.1 The *Plasmodium* lifecycle is complex, consisting of three sub-cycles (CDC, 2013, reproduced under the terms of the Creative Commons attribution license). Sub-cycles: A: Exoerythrocytic cycle; B: Erythrocytic cycle; C: Sporogonic cycle. The sequence of events can be summarized as: 1. Mosquito bite; 2. Host liver cell infection; 3. Schizont formation; 4. Cell rupture and merozoite release; 5. Merozoite entry into human blood stage; 6. Schizont re-infection; 7. Gametocyte development; 8. Gametocyte extraction by mosquito bite; 9. Gamete development; 10. Zygote formation; 11. Oocyst development; 12. Release of sporozoites.

At this stage, the host exhibits malaria symptoms such as fever and chills. The other merozoites in the blood cells develop into female and male gametocytes (7), which are extracted by a biting mosquito (8). Within the mosquito, the gametocytes form female and male gametes (9) in the sporogonic stage. The gametes fuse to form a zygote, which further develops into the oocyst (11). The oocyst undergoes mitotic division to form a large number of sporozoites (12), which then migrate to the mosquito's salivary gland. This completes the cycle.

It has been estimated that about 198 million malaria cases are reported every year, with about 580 000 people, mostly children, infants and pregnant women dying annually, mostly in sub-Saharan Africa (Scheidt *et al.*, 1998). The disease has its greatest morbidity and mortality in the poorest of the countries because of inaccessible and unaffordable treatment. This perpetuates the cycle of poverty in the countries where the disease is endemic. Parasite infections are increasing at an alarming rate, with *Plasmodium falciparum* showing increasing resistance to existing anti-malarial drugs (White, 2004). It must be noted, however, that malaria is a preventable and treatable disease through prophylaxis and drug treatment.

1.2 Prevention and treatment of malaria

Malaria may be prevented by various methods, for example, using mosquito repellents (creams, coils *etc.*), mosquito nets, wearing long sleeves and trousers and removing stagnant water, which promotes mosquito breeding (White, 2004). Drugs that are used for treatment and prevention of malaria are called antimalarials. Antimalarial treatment is designed to prevent or cure the disease. Malaria can be treated by a variety of drugs, most of which are alkaloids bearing a quinoline unit. The common treatment practice is based on the concepts of either single drugs or combination drugs. Combination drug therapy has several advantages: reduced treatment failures, reduced risk of developing resistance, and reduced side-effects. It is important to confirm the infection of suspect malaria cases as soon as possible before starting treatment. Starting treatment simply because malaria is suspected, is not advisable because most malaria symptoms are common for many other diseases.

Malaria has been treated for many years by several single drug therapies. The structures of some of the most common antimalarial drugs are shown in Figure 1.2.

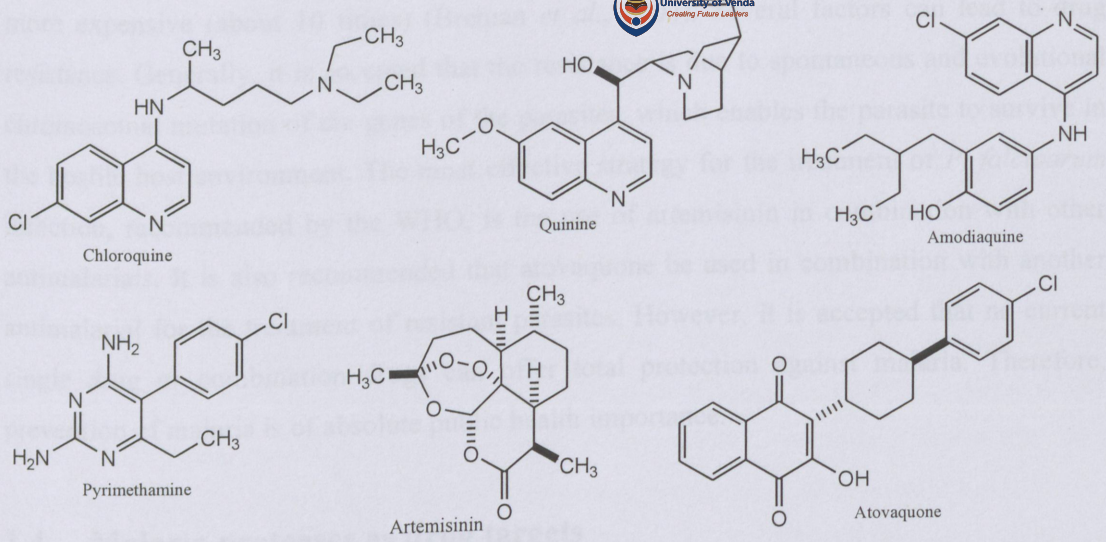

Figure 1.2 Structures of some common antimalarials.

1.3 Treatment and drug resistance

Antimalarial resistance is a major health problem that makes malaria control and treatment less effective. Resistance of *Plasmodium falciparum* to some of the antimalarial drugs, and chloroquine in particular, is spreading fast in many of the countries where malaria is endemic. Antimalarial medication is intended to prevent or cure the disease; there are varieties of antimalarial drugs that are currently used with various properties and specific treatment requirements. The traditional antimalarial drug is quinine, which is less effective and more toxic than chloroquine and is used in areas where a high level of resistance to chloroquine occurs.

Currently the treatment and control of malaria is through chemotherapy with single or combination drug regimens, but it is now common knowledge that resistance to existing antimalarials has rendered the control and treatment often ineffective as a result of the increasing resistance and development of new strains (Breman *et al.*, 2004). Therefore, it is important to continue searching for safe, potent and more effective antimalarial drugs for the control and elimination of malaria.

Malaria is currently mostly treated by combination therapy, because lower doses of individual drugs are used, which result in lower risks of resistance developing, treatment failure and side-effects. It should however be noted that combination drugs are generally

more expensive (about 10 times) (Breman *et al.*, 2004). Several factors can lead to drug resistance. Generally, it is accepted that the resistance is due to spontaneous and evolutional chromosomal mutation of the genes of the parasites, which enables the parasite to survive in the hostile host environment. The most effective strategy for the treatment of *P. falciparum* infection, recommended by the WHO, is the use of artemisinin in combination with other antimalarials. It is also recommended that atovaquone be used in combination with another antimalarial for the treatment of resistant parasites. However, it is accepted that no current single drug or combination drugs can offer total protection against malaria. Therefore, prevention of malaria is of absolute public health importance.

1.4 Malaria proteases as drug targets

The complete genome sequence of the malaria pathogen (Gardner *et al.*, 2002) and that of its host *Homo sapiens* (GIC, 2001) are available. This has enabled the identification of potential enzymes present in the pathogen and absent in the host, so that in principle enzyme inhibitors may be found that target the enzymes of the parasite rather than those of the human host. It is important that the enzyme inhibitors do not interfere with human biological processes. Finding those enzyme targets with the lowest possible similarity to the human enzymes is not easy, because the *Plasmodium* genome consists of 32 million bases and is highly unstable and susceptible to recombination and genome fusion (Maelicke, 1999). Nevertheless, analysis of the genome sequence has provided some important knowledge on metabolic pathways of *Plasmodium* regardless of the life-cycle stages involved (Gardner *et al.*, 2002).

Several of the discovered metabolic pathways are targeted by the existing antimalarial drugs (Gardner *et al.*, 2002). For instance, chloroquine, artemisinin and quinine inhibit the breakdown of haemoglobin to haemozoin in the parasite food vacuole (Dahl and Rosenthal, 2005), fosmidomycin acts in the apicoplast on the DOXP pathway (Ralph *et al.*, 2001), and thiolactomycin and triclosan interfere with fatty acid biosynthesis (Jomaa *et al.*, 1999; Kemp *et al.*, 2002).

1.4.1 Proteases as primary targets

The parasite hydrolyses haemoglobin to provide amino acids for protein synthesis and to maintain osmotic stability (Rosenthal, 2004). Hydrolysis of haemoglobin is therefore a key

catabolic process, and members of the plasmepsin (aspartic proteinases), the falcipain family (cysteine proteinases) and falcilysin (a metallopeptidase) involved in this process, have been identified clearly and occur in all the blood stages. At least four aspartyl proteases and three cysteine proteases have been linked to haemoglobin degradation in the acidic food vacuole (Rosenthal and Meshnick, 1996; Francis *et al.*, 1997a). The falcipains and plasmepsins, therefore, are logical targets for antimalarial drug development.

Among several strategies for the development of antimalarial chemotherapy is the synthesis of protease inhibitors, since parasitic cysteine proteases and aspartic proteases play a major role in the malaria disease (Lv *et al.*, 2010). It is known that cysteine and aspartic protease inhibitors interfere with the life cycle of *Plasmodium falciparum*, the parasite responsible for most of the malaria morbidity and mortality (Verissimo *et al.*, 2008). Proteases are enzymes that, like proteins, are made of a sequence of amino acids linked together by peptide bonds or amide bonds. Each protease is unique with regard to its amino acid sequence.

In the past two decades, di- and tripeptides have become increasingly important in the treatment of malaria by targeting malaria parasite proteases (Caffrey *et al.*, 2000; Rosenthal, 2004). This is because many short peptide sequences have potential pharmacological properties. Both natural and synthetic peptides have for a long time proved to inhibit a broad spectrum of pathogens and microorganisms (Bulet and Stöckling, 2005; Hancock *et al.*, 1995). The peptide sequences (termed *substrates*) are specifically recognized by proteases and hence the interaction between the proteases and the drug (peptide). In malaria drug design, it is important, therefore, to have knowledge of the proteases of the host and the parasite (Ramjee *et al.*, 2006).

Currently, many medicinal chemical and biochemical strategies for developing drugs to attack infectious bacteria and parasites, involve the interference with metabolic pathways of the host parasite and not that of humans. This often means drugs are intended to disrupt or inhibit the natural biosynthesis of the enzyme responsible for a disease, for example, a drug such as the well-known antibiotic, penicillin (Frere *et al.*, 1992). Penicillin inhibits the enzyme that catalyses D-alanine transfer in a very specific way, during the bacterial cell synthesis. In this way, it mimics the natural substrate when it reacts with the enzyme and deactivates it by blocking the OH group at the active site (Scheme 1.1). In its action, penicillin imitates D-alanine and binds with the enzyme, allowing the OH group of serine to

attack the strained β-lactam and open it. Consequently, the synthesis of the bacterial cell walls cannot be completed and the bacteria die.

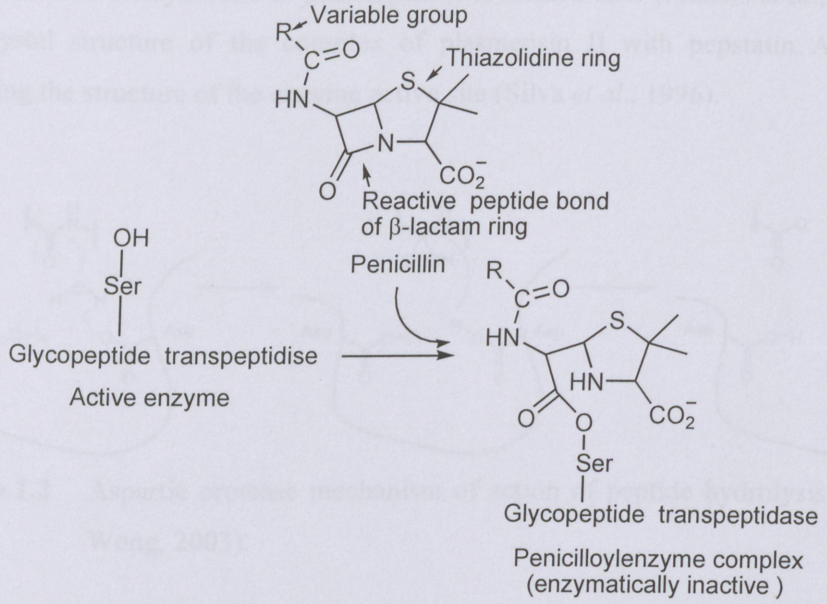

Scheme 1.1 Penicillin inhibits the enzyme that catalyses D-alanine transfer by mimicking the natural substrate (after Frere *et al.*, 1992).

1.4.2 The aspartic proteases

The aspartic proteases are protease enzymes that use an activated water molecule bound to two aspartate residues to catalyze hydrolysis of their peptide substrates (Scheme 1.2). Two classes of aspartic protease have received attention as potential drug targets, *viz.* the pepsin-like family (for example, renin, BACE-1) and the plasmepsins (Blum *et al.*, 2008). About ten plasmepsins have been found in the *Plasmodium falciparum* genome and five of these have been intensively researched, namely plasmepsins I, II, IV, V, and histo-aspartic protease, which is related to the plasmepsins. These are present in the acidic food vacuole of the parasite (Cunico *et al.*, 2009; Ersmark *et al.*, 2006; Rosenthal, 1998; Shenai *et al.*, 2000; Sijwali *et al.*, 2001).

Plasmepsins I and II have received most attention as targets for potential antimalarials. Plasmepsin I is thought to be responsible for initial cleavage of haemoglobin in the hinge region that maintains quaternary structure, after the molecule has been transported to the food vacuole (Gluzman *et al.*, 1994). This strategic cleavage is thought to unravel the

haemoglobin, exposing it to further proteolysis by a cysteinyl protease (falcipain) and plasmepsin II. Plasmepsin I is synthesized shortly after the invasion of the erythrocytes by the parasite, while the synthesis of plasmepsin II is formed later (Francis *et al.*, 1997a). In 1996, the crystal structure of the complex of plasmepsin II with pepstatin A was published, revealing the structure of the enzyme active site (Silva *et al.*, 1996).

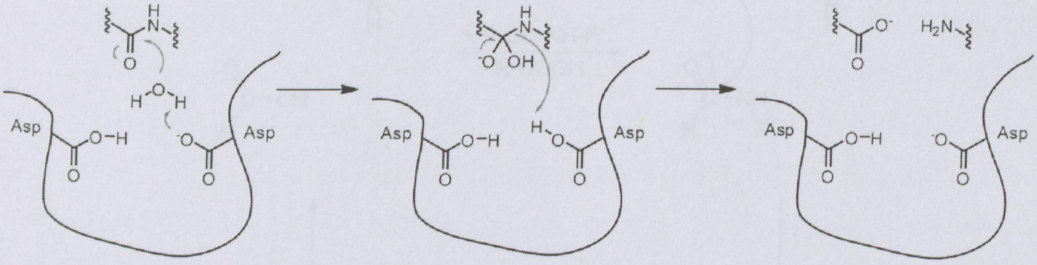

Scheme 1.2 Aspartic protease mechanism of action of peptide hydrolysis (after Brik and Wong, 2003).

1.4.3 The cysteine proteases

The family of cysteine proteases, also known as thiol proteases, are proteolytic enzymes that share a common catalytic mechanism involving a nucleophilic cysteine thiol in a catalytic triad or dyad (Scheme 1.3). The papain-like cysteine proteases, especially FP-1 (Greenbaum *et al.*, 2002), FP-2 (Shenai *et al.*, 2000), FP-2' (Singh *et al.*, 2006), and FP-3 (Sijwali *et al.*, 2001), are found in the *Plasmodium falciparum* food vacuole. The roles of FP-1 had FP-2' are less well understood, but they are certainly involved in haemoglobin degradation, erythrocyte invasion and oocyst production (Kumar *et al.*, 2007; Greenbaum *et al.*, 2002; Goh *et al.*, 2005). FP-2 had FP-3 play key roles in parasite hydrolysis of haemoglobin and are therefore potential chemotherapeutic targets, but falcipains may also be necessary in the initial stages (Gamboa de Domínguez and Rosenthal, 1996).

Falcipain 2 plays a key role in parasite hydrolysis of haemoglobin and is therefore a potential chemotherapeutic target. The binding of haemoglobin to falcipain 2 is regulated by pH, so that the enzyme normally processes haemoglobin within the acidic food vacuole (Ettari *et al.*, 2008).

Falcipain 3 is structurally similar to falcipain 2, but is involved twice in cleaving haemoglobin. Falcipain 3 is essential in asexual growth and this suggests that it also is a

prime target for development of new antimalarials. Falcipain 3 together with falcipain 2, are the major cysteine proteases involved in hydrolysis of haemoglobin. Therefore, targeting this enzyme family is a valid strategy in the development of new malaria chemotherapy (Selzer *et al.*, 1999).

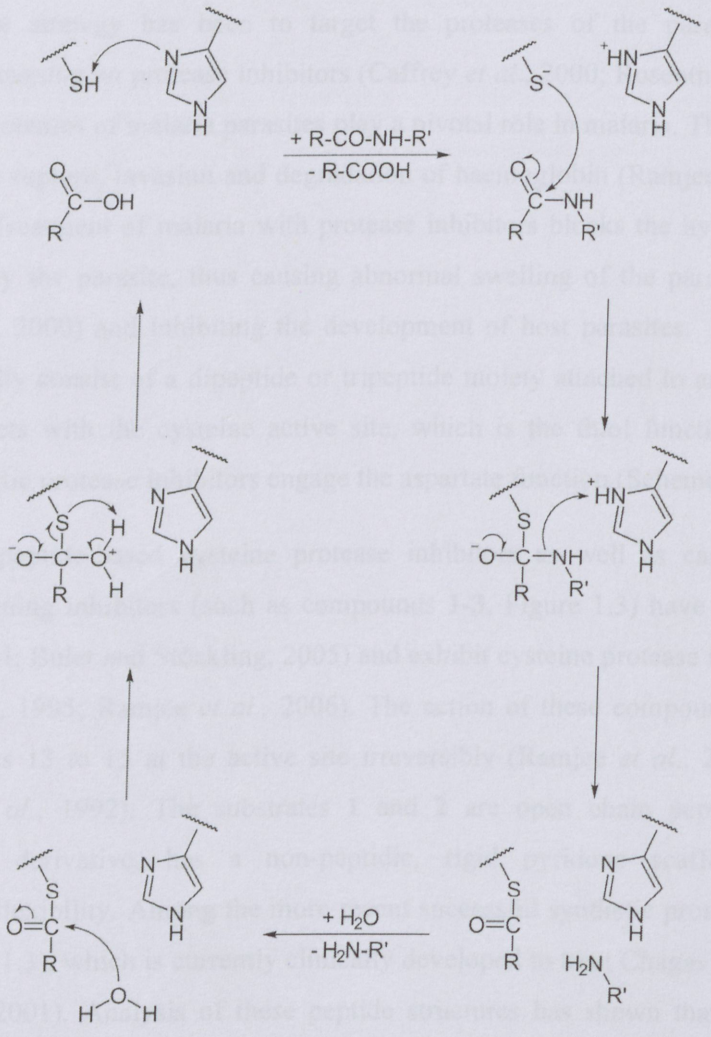

Scheme 1.3 The cysteinyl protease mechanism of action involves the thiol function (after Roberts, 2005).

1.4.4 Inhibition of plasmepsins and falcipains as antimalarial strategy

The falcipains and plasmepsins all generate fragments corresponding to cleavage of the haemoglobin α-33Phe/34Leu bond, and are inhibited synergistically by cysteine and aspartyl

protease inhibitors. These proteases are therefore logical targets for antimalarial drug development.

The synthesis of protease inhibitors is based on mimicking the amino acid sequence of the substrate peptides. In the development of potential antimalarial and HIV/AIDS drugs and antibiotics, the strategy has been to target the proteases of the parasites and viruses, specifically focussing on protease inhibitors (Caffrey *et al.*, 2000; Rosenthal, 2004). Cysteine and aspartic proteases of malaria parasites play a pivotal role in malaria. They are responsible for erythrocyte rupture, invasion and degradation of haemoglobin (Ramjee *et al.*, 2006; Eksi *et al.*, 2004). Treatment of malaria with protease inhibitors blocks the hydrolysis of human haemoglobin by the parasite, thus causing abnormal swelling of the parasite food vacuole (Caffrey *et al.*, 2000) and inhibiting the development of host parasites. Cysteine protease inhibitors usually consist of a dipeptide or tripeptide moiety attached to an electrophile that chemically reacts with the cysteine active site, which is the thiol function (Scheme 1.3). Similarly, aspartic protease inhibitors engage the aspartate function (Scheme 1.2).

A number of peptide-based cysteine protease inhibitors as well as carbonyl and vinyl sulphone containing inhibitors (such as compounds **1-3**, Figure 1.3) have been synthesized (Rosenthal, 2004; Bulet and Stöckling, 2005) and exhibit cysteine protease inhibition activity (Hancock *et al.*, 1995; Ramjee *et al.*, 2006). The action of these compounds is to alkylate cysteine residues 13 to 15 at the active site irreversibly (Ramjee *et al.*, 2006; Eksi *et al.*, 2004; Frere *et al.*, 1992). The substrates **1** and **2** are open chain peptides while **3**, a peptidomimetic derivative, has a non-peptidic, rigid pyridone scaffold, hence less conformational flexibility. Among the more recent successful synthetic protease inhibitors is K777 (**4**, Figure 1.3), which is currently clinically developed to treat Chagas disease (Breman and Holloway, 2001). Analysis of these peptide structures has shown that an aliphatic or heterocyclic ring may serve as a linker binding the inhibitor to the active enzyme site.

A large number of cysteine protease inhibitors have been synthesized to date (*e.g.*, Figure 1.3), and compounds such as tokaramide (**5**, Figure 1.4) (Konno *et al.*, 2011) and pfHDAC-1 (**6**, Figure 1.4) (Patel *et al.*, 2009) have shown promise in mouse models, but most compounds have enjoyed limited practical success (Turk, 2006). The synthetic approach in this study is based on the planned construction of a dipeptide or tripeptide mimic that incorporates the heterocyclic ring of the 2-pyridone scaffold in the P2 position, a phenylalanine analogue at the P1 position and a phthalimido moiety in position P3. The 2-

pyridone scaffold-based derivatives have shown favourable analgesic, anti-inflammatory, antibacterial and anticancer activities in various tests (Lv *et al.*, 2010; Gezegen *et al.*, 2014). The design of inhibitors is usually based on the mimicry of transition states formed during peptide hydrolysis by a cysteinyl protease. Inhibitors mimic the hydrophobic and hydrogen-bonding interactions of the parasite's enzyme, but as potential substrates they also possess disadvantages as potential drugs; for example, they may be susceptible to enzymatic or chemical hydrolysis and further metabolism. These disadvantages may be overcome by systematic chemical modification of the amino acid backbone and/or side chains (Bryant *et al.*, 2009).

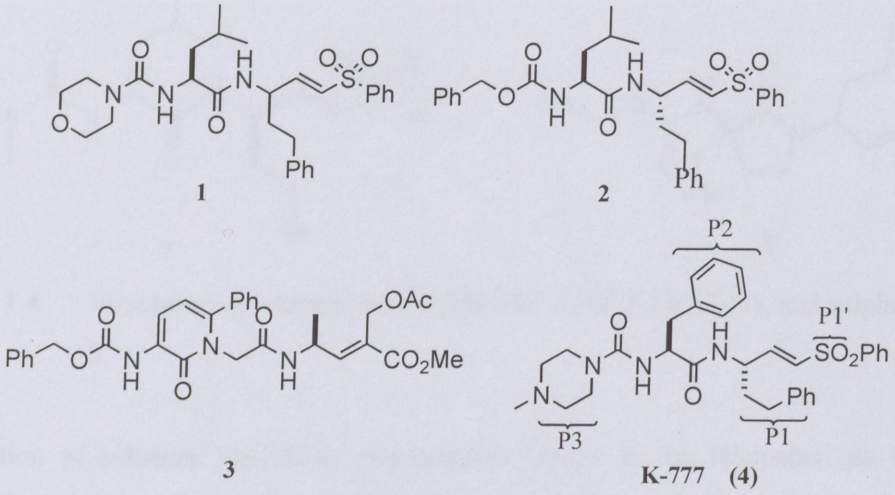

Figure 1.3 Examples of peptidic and peptidomimetic cysteinase inhibitors.

1.5 General inhibitor design principles

So far, most approaches to the synthesis of protease inhibitors have focused on peptidomimetics. Typical cysteine protease inhibitors are di- or tripeptides linked to an electrophilic 'warhead' that reacts reversibly or irreversibly with the cysteine thiol function. Peptidyl vinyl sulfones, such as K11017 (Mu-Leu-Hph-Vsph) (**7**, Figure 1.4) (Kerr *et al.*, 2009b), are potent irreversible inhibitors of falcipains, acting as Michael acceptors of the catalytic cysteine residue.

The malaria cysteine proteases (falcipains) are enzymes that can cleave small peptides by nucleophilic attack by the thiol group on the substrate. They differ structurally sufficiently

from the human cysteine proteases to make them interesting targets for inhibitor design (Sajid and McKerrow, 2002). Of the four falcipains (Dahl and Rosenthal, 2005), falcipain-2 (FP2) and falcipain-3 (FP3) are localized in the food vacuole; they are able to degrade haemoglobin and are the best known.

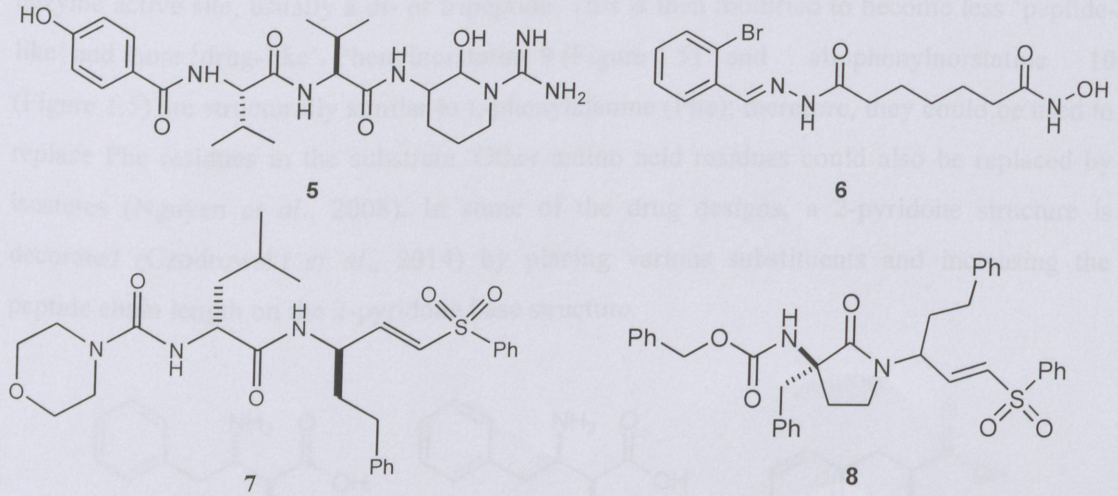

Figure 1.4 Structures of tokaramide (**5**), pfHDAC-1 (**6**), K11017 (**7**), and sulphone **8**.

Elucidation of substrate specificity requirements unique to the falcipains has led to the expectation that specific inhibitors with antimalarial activities may be designed, for example by replacement of certain amino acids near the binding site. Maximal FP2 and FP3 inhibition seems to be consistently obtained by peptidyl analogues with a leucine residue at the P2 position and the unnatural homophenylalanine at position P1 (Lee *et al.*, 2003; Verissimo *et al.*, 2008). Conformationally constrained sulphones, for example compound **8** (Figure 1.4), also demonstrate high FP2 inhibition activity (Scheidt *et al.*, 1998).

Basic structural functions (such as found in quinoline) also seem necessary for transport of the inhibitor to the acidic parasite food vacuole site.

1.6 Specific approaches to peptidomimetic design

1.6.1 Mimicry

Most current frontline approaches to drug design start by mimicking a substrate for an enzyme active site, usually a di- or tripeptide. This is then modified to become less 'peptide-like' and more 'drug-like'. Phenylnorstatine **9** (Figure 1.5) and allophenylnorstatine **10** (Figure 1.5) are structurally similar to L-phenylalanine (Phe); therefore, they could be used to replace Phe residues in the substrate. Other amino acid residues could also be replaced by isosteres (Nguyen *et al.*, 2008). In some of the drug designs, a 2-pyridone structure is decorated (Czodrowski *et al.*, 2014) by placing various substituents and increasing the peptide chain length on the 2-pyridone base structure.

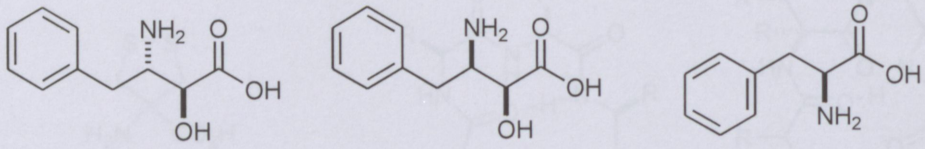

9 **10** L-Phenylalanine

Figure 1.5 L-Phenylalanine and related compounds phenylnorstatine **9** and allophenylnorstatine **10**.

1.6.2 Conformational restriction

Conformational restriction can play an important role in rational design of peptidomimetics, with the aim of reducing conformational flexibility and biodegradability, and improving receptor selectivity. The incorporation of conformational restraints enhances the selectivity, efficiency, stability, and effectiveness of the di- or tripeptide.

The incorporation of chiral and achiral amino acids that have a quaternary α-carbon atom into peptides is a very useful and versatile approach to restrict conformational freedom; as a result, the secondary structure is fixed and the stability towards chemical and enzymatic hydrolysis may be improved, as was demonstrated by peptides containing substructure **11** (Figure 1.6) (Morera *et al.*, 2000).

Many bioactive peptides contain reverse turns, which influence protein folding (Rose *et al.*, 1985), and especially so-called β-turns are well known. They form the basis for recognition

in the interactions of peptides with receptors (Burgess, 2001). The β-turns are often stabilized by intramolecular hydrogen bonds between the first and fourth residues of a tetrapeptide, to form a 10-membered ring **12** (Figure 1.6) (Rose *et al.*, 1985). Particularly interesting is the use of conformationally constrained di- and tripeptide scaffolds (isosteres) into a peptide, causing a specific folding of the peptide chain. A recent example of this approach is the work by Scheffelaar *et al.* (2009) who synthesized 3,4-dihydropyridin-2-ones **13** (Figure 1.6).

Peptide mimics containing *trans*-substituted cyclopropanes stabilize extended conformations of oligopeptides, and it is thought that *cis*-cyclopropanes stabilize a reverse turn (Martin *et al.*, 2000). Replacing the α-carbon, nitrogen, and β-carbon, or the α-carbon, carbonyl, and β-carbon with cyclopropane, two novel modifications (**14** and **15**, Figure 1.6) are possible.

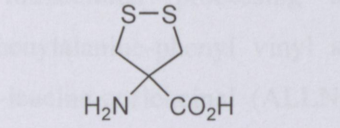

Quaternary cysteine analogue

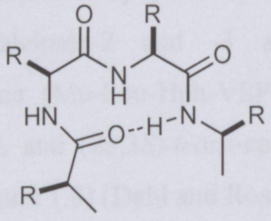

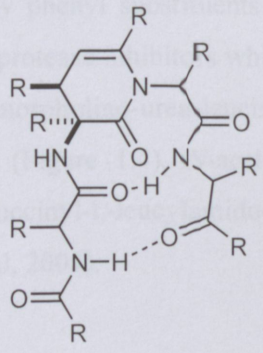

11 12 13

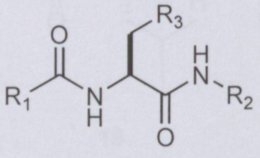

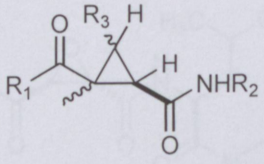

14

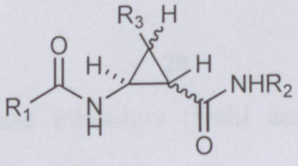

15

Figure 1.6 Examples of structural features causing conformational restriction.

Epoxysuccinyl (**16**) and aziridinyl (**17**) peptides (Figure 1.7) (Hanada *et al.*, 1978) are also irreversible and selective inhibitors of cysteine proteases. In this case, nucleophilic ring opening by the cysteine of the active site results in alkylation and irreversible inhibition of the protease. Bicyclic dipeptide mimetics such as **18** (Figure 1.7) can also provide rigid scaffolds with numerous possibilities of stabilizing β-turns (Qiu *et al.*, 2001).

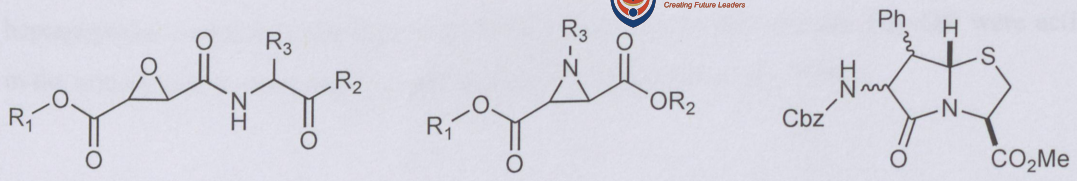

16 17 18

Figure 1.7 Examples of rigid peptidomimetic scaffolds.

1.6.3 Lipophilicity

Introducing hydrophobic, particularly aromatic, moieties in receptor ligands can affect recognition and activation of receptors having lipophilic domains; therefore, many ligand mimics have been designed to contain such an element, especially phenyl substituents or fusions (Giannis and Kolter, 1993). Examples of lipophilic cysteine protease inhibitors which block intracellular processing of falcipain-2 and -3 are morpholino-urea-leucine-homophenylalanine-phenyl vinyl sulfone (Mu-Leu-Hph-VSPh) **7** (Figure 1.4), *N*-acetyl-leucine-leucine-norleucinal (ALLN) **19**, and (2*S*,3*S*)-*trans*-epoxysuccinyl-L-leucylamido-3-methylbutane ethyl ester (E-64d) **20** (Figure 1.8) (Dahl and Rosenthal, 2005).

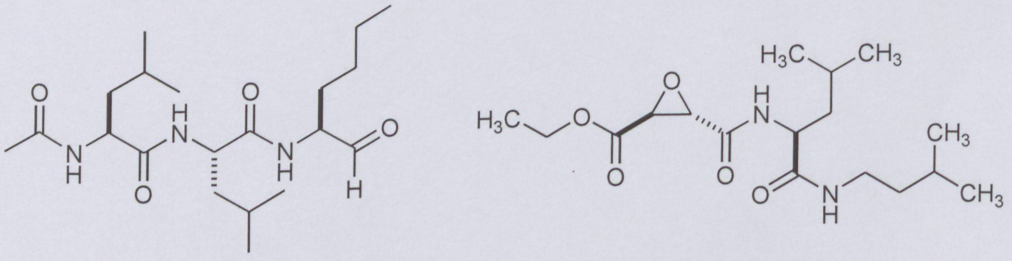

19 20

Figure 1.8 Examples of lipophilic cysteine protease inhibitors (Dahl and Rosenthal, 2005).

1.6.4 Electrophilicity

Electrophilic building blocks such as fumarate and other activated olefins can covalently block the active site Cys residue of FP2 via a Michael-type reaction (Scheme 1.4; Barrett *et al.*, 1982; Machon *et al.*, 2009; Darkins *et al.*, 2007; Santos and Moreira, 2007). For example,

heptapeptides containing the tripeptide RNH-(Phe/Asn/Gly)←Fumarate-Gly-OR were active in the micromolar to nanomolar range against FP2 (Machon *et al.*, 2009).

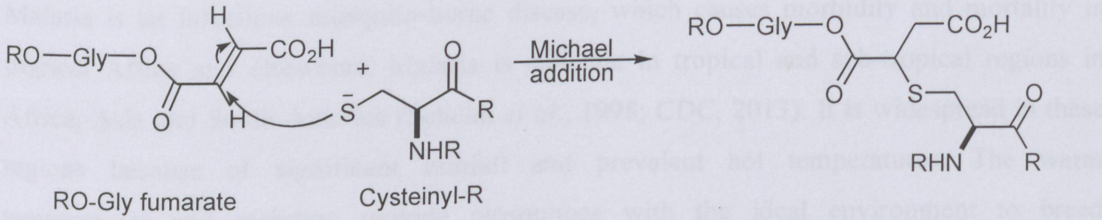

Scheme 1.4 Nucleophilic addition of fumarate to a cysteine residue yields an S-(2-succinyl) substituted cysteinyl residue by Michael addition reaction (Santos and Moreira, 2007). R indicates a peptide chain.

Chapter 2

Motivation, aims and objectives

Malaria is an infectious mosquito-borne disease, which causes morbidity and mortality in tropical Africa and elsewhere. Malaria is endemic in tropical and sub-tropical regions in Africa, Asia and South America (Scheidt *et al.*, 1998; CDC, 2013). It is widespread in these regions because of significant rainfall and prevalent hot temperatures. The warm temperatures and moisture provide mosquitoes with the ideal environment to breed continuously and spread to many places (Scheidt *et al.*, 1998; CDC, 2013). This severe and deadly disease is caused by *Plasmodium falciparum.* The other species, namely, *Plasmodium berghei, Plasmodium vivax, Plasmodium ovale* and *Plasmodium malariae* cause milder forms of malaria that are usually not fatal to humans (Machon *et al.*, 2009).

Malaria is the third of the major infectious diseases after HIV and TB (WHO, 2014), and is one of the deadliest diseases that the world is facing. Malaria causes an estimated 198 million clinical cases and over 580 000 deaths per year, with most of them in Africa, Southeast Asia and South America (Scheidt *et al.*, 1998). According to the World Health Organization, almost 4 billion people, (more than 50% of the world's population) suffer from parasite infections, which can cause chronic infections, leading to severe mortality and morbidity (Desai *et al.*, 2006; WHO, 2014). Parasite infections are increasing at a fast rate, with some of them, like the *Plasmodium falciparum* increasing in resistance to existing antimalarials (White, 2004). Therefore, an urgent provision of more effective antimalarial drugs is required to limit the number of deaths caused by the malaria parasite.

Some common drugs currently used as antimalarials are chloroquine (**21**), quinine (**22**) and artemisinin (**23**) (Figure 2.1). As a result of the growing resistance of the *Plasmodium* parasite to common antimalarial drugs, combination drugs such as artemisinin and atovaquone (**24**) combined with other antimalarials are being used.

Many heterocyclic compounds with a 2-pyridone scaffold have been reported to be effective as inhibitors of *P. falciparum* (Upadhyay *et al.*, 2009) and with antitumor activity, such as the 3,5,6-trisubstituted-2-pyridones **25** (Figure 2.1) (Brik and Wong, 2003). Encouraged by such biological activities much research has been done and continues to attract interest in the synthesis and screening of these types of compounds.

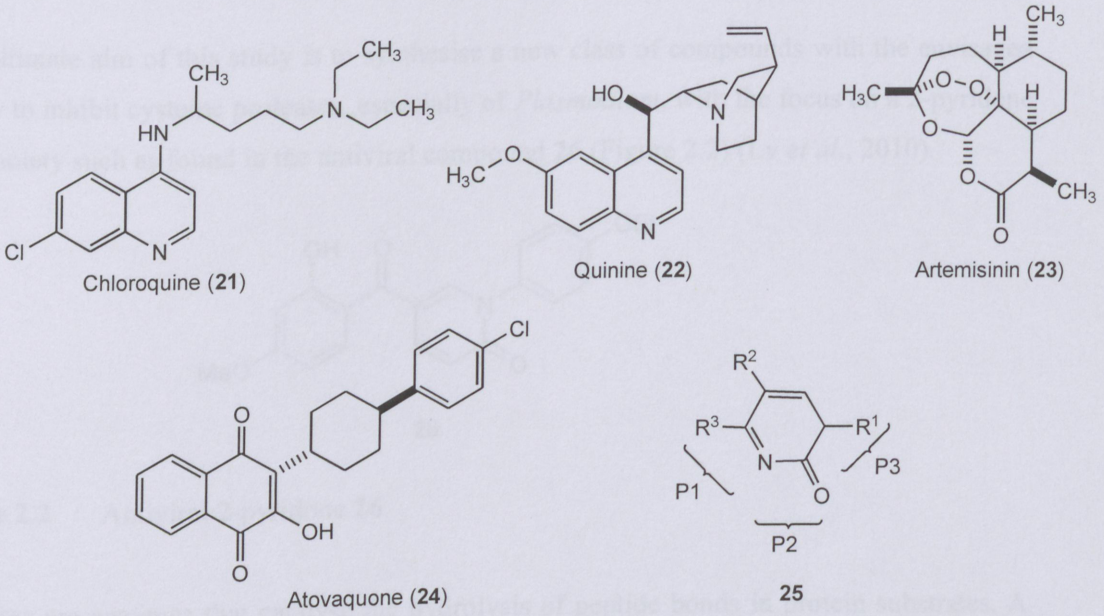

Figure 2.1 Some well-known antimalarial compounds.

As mentioned in Chapter 1, cysteine proteases play a pivotal role in malaria (Sajid and McKerrow, 2002). This study, therefore, focuses specifically on the development of synthesis methodology for cysteine protease inhibitors of *Plasmodium*. Most of the synthetic strategies were designed to produce substances that will mimic the natural substrate and hence will target the enzyme active site. The compounds selected are dipeptidic or tripeptidic, based on a rigid heterocyclic 2-pyridone scaffold. Synthetic strategies based mostly on known literature methods for synthesising 2-pyridone derivatives were chosen. The 2-pyridone scaffold could be an important heterocyclic building block and has been employed over the years by organic chemists for the synthesis of naturally-occurring biologically active alkaloids.

It is hypothesized that antimalarial drug discovery and synthesis have the potential to produce potent and selective lead compounds. It is envisaged that these compounds will exhibit competitive protease inhibition at the enzyme active site.

2.1 Aims

The ultimate aim of this study is to synthesise a new class of compounds with the envisaged ability to inhibit cysteine proteases, especially of *Plasmodium*, with the focus on a 2-pyridone ring moiety such as found in the antiviral compound **26** (Figure 2.2) (Lv *et al.*, 2010).

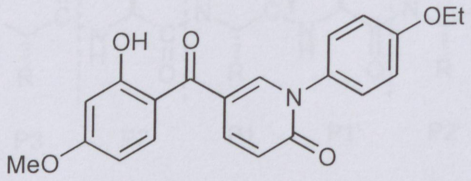

26

Figure 2.2 Antiviral 2-pyridone **26**.

Proteases are enzymes that catalyse the hydrolysis of peptide bonds in protein substrates. A peptide bond cleaved by a protease is called the *scissile bond*. The product of protease-catalysed hydrolysis of a peptide bond is two polypeptides, and new carboxyl and amino termini are formed by lysis of the amide bond (Cronk, 2014; Scheme 2.1). Cysteine or *thiol* proteases catalyse proteolysis by means of nucleophilic attack by the sulfhydryl group of a cysteine residue. Examples of cysteine proteases are papain, cathepsins B and L, caspases, and falcipains.

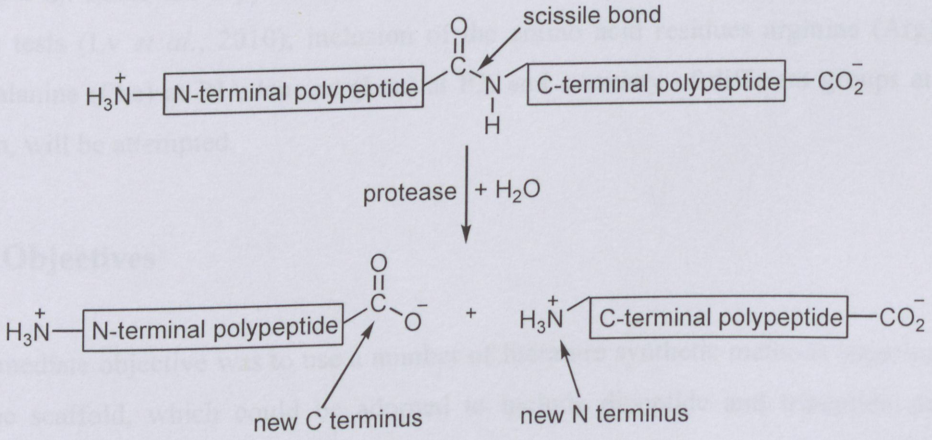

Scheme 2.1 Proteolysis of a scissile bond (after Cronk, 2014).

To assist in the discussion of protease mechanisms and specificities, a brief explanation of the nomenclature used for protease substrates may be helpful (Cronk, 2014). The substrate

residues on the *N*-terminal side of the scissile bond are labelled P1, P2, P3, *etc*., in the *C*-to-*N* direction. The substrate residues on the *C*-terminal side of the scissile bond are indicated by the symbols P1', P2', P3', *etc*., in the *N*-to-*C* direction (Scheme 2.2).

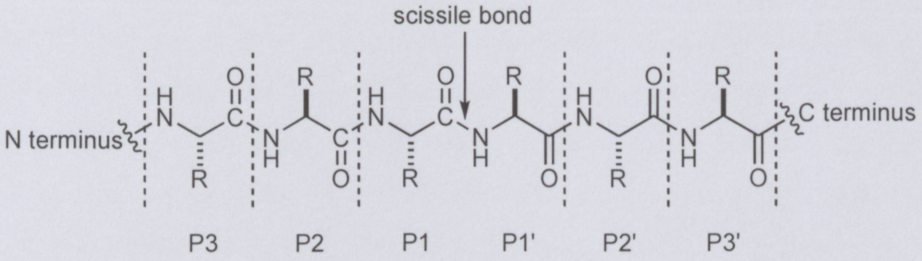

Scheme 2.2 Scissile bond and residues of interest in the proteolysis of a scissile bond (Cronk, 2014).

Protease substrate specificity is provided by the recognition of substrate residues in the P1, P2, P3, ..., and P1', P2', P3', ..., positions. The corresponding enzyme residues are designated using a similar nomenclature: The side chain of the P1 residue is accommodated by the S1 site of the enzyme; other sites of the enzyme are named in corresponding fashion.

In this study, the synthetic approach was initially based on the construction of dipeptide mimics that incorporate the heterocyclic ring of the 2-pyridone scaffold in the P2 position, a phenylalanine analogue at the P1 position and also the phthalimido moiety in position P3 (**54** Scheme **38**). Since the 2-pyridone based derivatives have shown favourable bioactivity in various tests (Lv *et al*., 2010), inclusion of the amino acid residues arginine (Arg) at P1, phenylalanine (Phe) at P1', leucine (Leu) at P2, and a variety of different groups at the P3 position, will be attempted.

2.2 Objectives

The immediate objective was to use a number of literature synthetic methods targeting the 2-pyridone scaffold, which could be adorned to include dipeptide and tripeptide structural features. The study will in future also be extended to non-peptidic compounds with known activity. In this study the aim was to explore syntheses of parasite cysteine protease inhibitors with favourable substrate-inhibitor interactions and that were likely to have drug-like properties (Bryant *et al*., 2009). Non-peptidic fragments such as 5- and 6-membered

heterocyclic rings will also in future be surveyed as potential P2/P3 moieties. The work will be followed by structure-activity studies once one or more potential lead compounds have been discovered.

Chapter 3

Synthesis of 2-pyridone-based drug candidates

The aim of this project was to prepare various 2-pyridone derivatives that may lead to the discovery of new antimalarial drugs. After briefly reviewing the construction methodologies found in the literature, this discussion will focus on the chemistry results. The next chapters will briefly discuss the computer modelling and docking of selected target compounds, which was done in collaboration with a co-student (Makungo, 2015), followed by screening of selected target compounds (done by Dr Panayides of the CSIR).

3.1 Introduction: Literature precedents for the methodologies followed

A broad range of non-natural peptide-mimicking attachments may be used as amide bond replacements to obtain new classes of peptidomimetics. For example, retro-amides, ureas, carbamates, sulphonamides, thiazoles, and triazoles have all been applied as amide bond mimics (Sureshbabu *et al.*, 2008). In this exploratory study, the heterocyclic 2-pyridones **27** (Figure 3.1) are applied as rigid amide bond isosteres. In a later phase, 1,2,4-oxadiazoles **28** (Figure 3.1) may be introduced as ester bond isosteres. The oxadiazoles have been applied to synthesize drug-related molecules, including ligands of benzodiazepine receptors (Watjen *et al.*, 1989), muscarinic receptor agonists (Messer *et al.*, 1997), antiviral compounds, angiotensin II receptor antagonists (Kohara *et al.*, 1995), and HIV-1 reverse transcriptase inhibitors (Medebielle *et al.*, 2005). Their general synthesis involves reaction of an amidoxime (**29**) with an activated carboxyl equivalent, yielding an *O*-acylamidoxime, which is then cyclised to **28** by dehydration (van Ree and Steglich, 1982). The starting material usually is a nitrile **30** (Scheme 3.1) (Sureshbabu *et al.*, 2008).

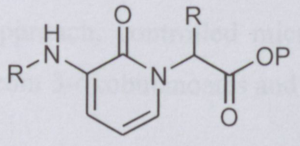

27

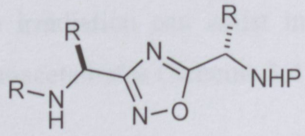

28

Figure 3.1 Examples of amide and ester isosteres.

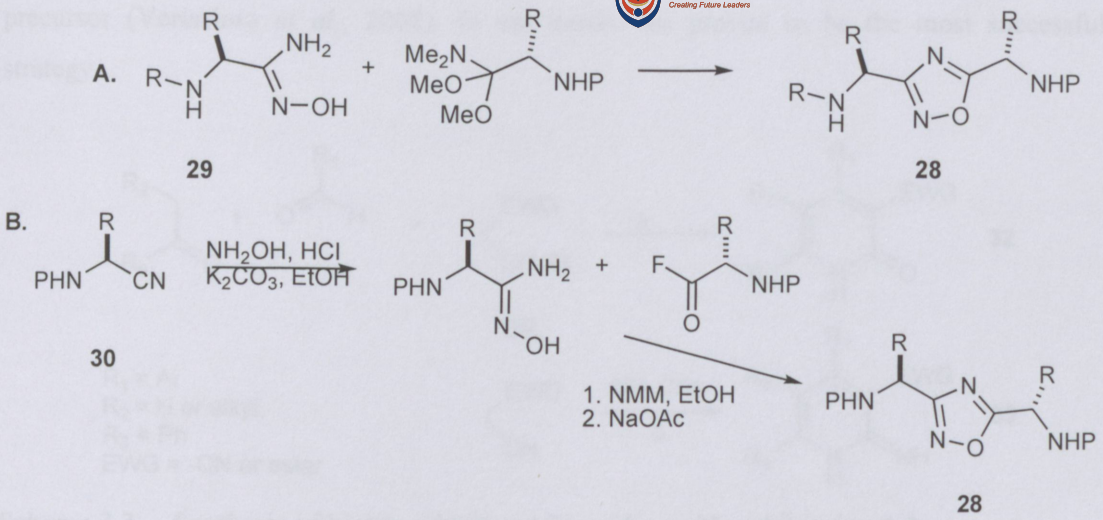

Scheme 3.1 Synthesis of 1,2,4-oxadiazoles: A. From amidoximes; B. From nitriles (Sureshbabu *et al.*, 2008).

N-Unsubstituted dihydro-2-pyridones (**31**, Scheme 3.2) may be synthesised using Horner-Emmons olefination as the key step (Upadhyay *et al.*, 2009). However, this structure is still relatively flexible.

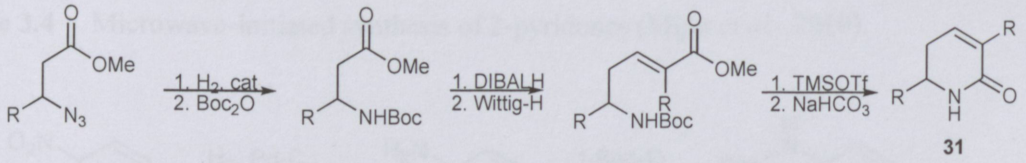

Scheme 3.2 Synthesis of dihydro-2-pyridones **31** (Upadhyay *et al.*, 2009).

Nucleophilic addition of malonic esters to alkynyl imines (Hachiya *et al.*, 2002), or reaction of appropriately substituted acetophenones, aldehydes, and ammonium acetate with ethyl cyanoacetate, or malononitrile (Abadi *et al.*, 2010), may lead to highly substituted 2-pyridones (**32**) or 2-imino-1,2-dihydropyridines (**33**) (Scheme 3.3).

In a similar approach, controlled microwave irradiation can assist in the synthesis of 2-pyridones **34** from 3-oxobutanoates and 2-cyanoacetamides (Scheme 3.4) (Mijin *et al.*, 2010).

Finally, pyridones **39** may be obtained from commercially available 3-nitropyrid-2-one (3-nitro-2-hydroxypyridine) **35**, by selective reduction of the nitro group, followed by protection of the aminopyridinol **36** as a carbamate **37**. The triflate **38** is then condensed with the pyridone fragment **37** to give intermediate **39**, a possible drug candidate with a suitable amide

precursor (Verissimo *et al.*, 2008). In our hands, this proved to be the most successful strategy.

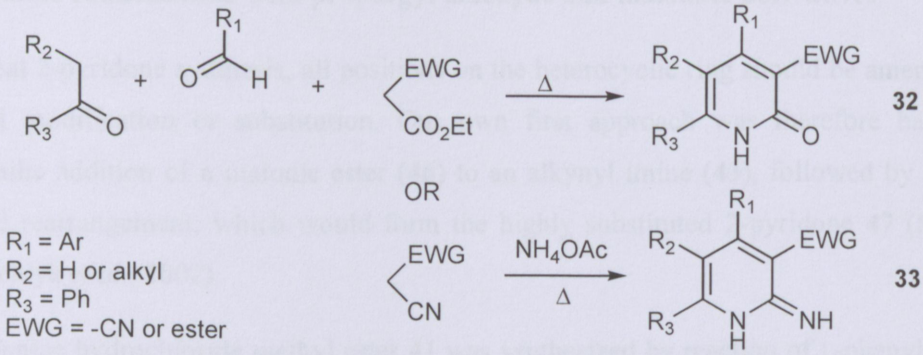

Scheme 3.3 Synthesis of highly substituted 2-pyridones **32** and 2-imino-1,2-dihydropyridines **33** (Hachiya *et al.*, 2002; Abadi *et al.*, 2010).

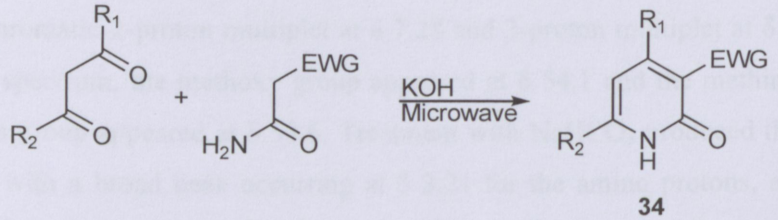

Scheme 3.4 Microwave-initiated synthesis of 2-pyridones (Mijin *et al.*, 2010).

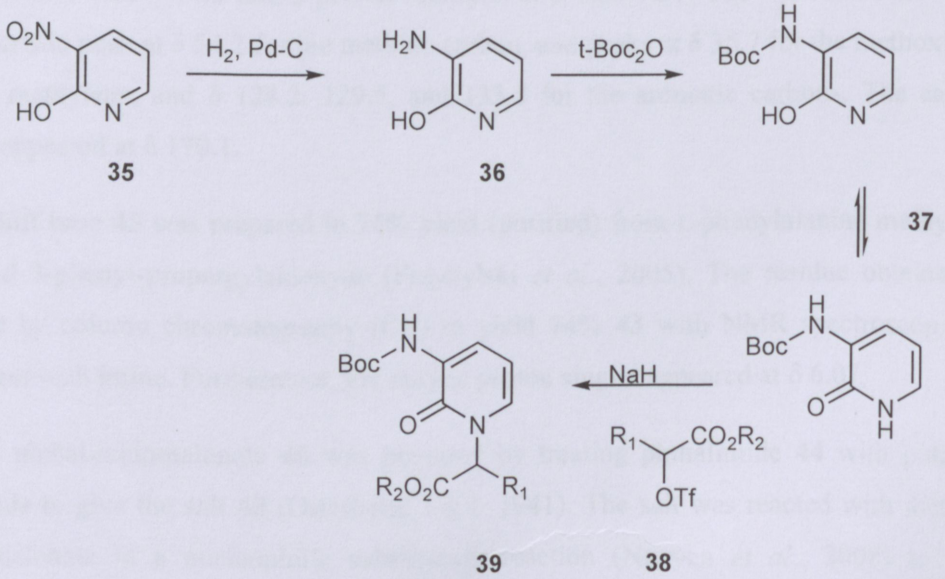

Scheme 3.5 Substituted 2-pyridone synthesis from commercially available 3-nitropyrid-2-one (Verissimo *et al.*, 2008).

3.2 Results and discussion

3.2.1 Imine condensation with propargyl aldehyde and malonate derivatives

In an ideal 2-pyridone synthesis, all positions on the heterocyclic ring should be amenable to chemical modification or substitution. Our own first approach was therefore based on nucleophilic addition of a malonic ester (**46**) to an alkynyl imine (**43**), followed by a base-catalysed rearrangement, which would form the highly substituted 2-pyridone **47** (Scheme 3.6) (Hachiya *et al.*, 2002).

Phenylalanine hydrochloride methyl ester **41** was synthesized by reaction of L-phenylalanine **40** with thionyl chloride in methanol (Tietze and Eicher, 1981). The ^{1}H-NMR of the salt **41** showed a three-proton singlet at δ 3.82 for the methyl ester, two double doublets at δ 3.21 and 3.34 for the methylene group, a double doublet at δ 4.42 for the chiral methine, and the characteristic aromatic 2-proton multiplet at δ 7.28 and 3-proton multiplet at δ 7.37-7.45. In the ^{13}C-NMR spectrum, the methoxy group appeared at δ 54.1 and the methine attached to the ammonium group appeared at δ 53.6. Treatment with $NaHCO_3$ produced the free amino acid ester **42**, with a broad peak occurring at δ 3.21 for the amino protons, a three-proton singlet at δ 3.77 for the methyl ester, a 2-proton multiplet at δ 3.13 to 3.29 for the methylene group, a triplet at δ 4.36 for the chiral methine, and the characteristic aromatic 2-proton multiplet at δ 7.12 – 7.13 and 3-proton multiplet at δ 7.34-7.37. The ^{13}C-NMR showed the characteristic peak at δ 54.2 for the methine carbon, and peaks at δ 35.7 for the methoxy, 53.7 for the methylene, and δ 128.2, 129.5, and 133.8 for the aromatic carbons. The carbonyl carbon appeared at δ 170.1.

The Schiff base **43** was prepared in 74% yield (purified) from L-phenylalanine methyl ester (**42**) and 3-phenyl-propargylaldehyde (Przybylski *et al.*, 2005). The residue obtained was purified by column chromatography (CC) to yield 74% **43** with NMR spectroscopic data consistent with imine. Furthermore, the vinylic proton singlet appeared at δ 6.07.

Diethyl phthalimidomalonate **46** was prepared by treating phthalimide **44** with potassium hydroxide to give the salt **45** (Osterberg, 1927, 1941). The salt was reacted with diethyl 2-bromomalonate in a nucleophilic substitution reaction (Nguyen *et al.*, 2008) to obtain malonate **46** in 46% overall yield. The low yield may be explained by the probable inclusion

of product in the solidified reaction melt. Diethyl 2-(4-methylpiperazino)malonate **48** was prepared similarly (Scheme 3.7).

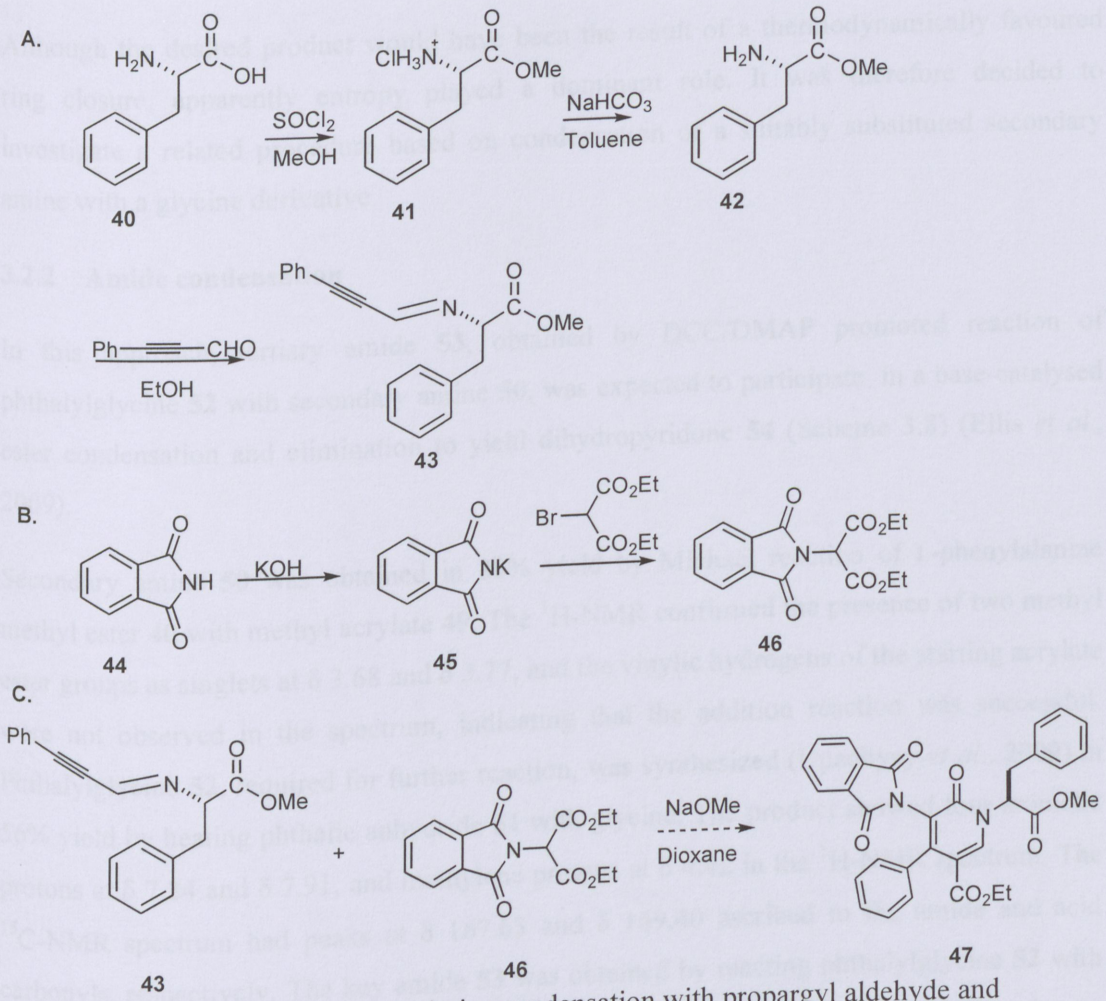

Scheme 3.6 Reaction scheme for imine condensation with propargyl aldehyde and malonate derivatives (Hachiya *et al.*, 2002): A. Synthesis of Schiff base **43**; B. Synthesis of malonate **46**; C. Attempted synthesis of 2-pyridone **47**.

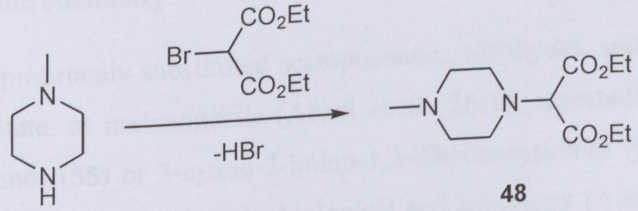

Scheme 3.7 Synthesis of diethyl 2-(4-methylpiperazino)malonate **48**.

In several attempts to prepare one of the 2-pyridone derivatives (**47**, Scheme 3.6), solutions of compounds **43** and **46** or **48** in dioxane were treated with a solution of sodium methoxide

in dioxane and stirred at room temperature. Intractable mixtures were obtained instead of the desired product **47**.

Although the desired product would have been the result of a thermodynamically favoured ring closure, apparently entropy played a dominant role. It was therefore decided to investigate a related procedure based on condensation of a suitably substituted secondary amine with a glycine derivative.

3.2.2 Amide condensation

In this approach, tertiary amide **53**, obtained by DCC/DMAP promoted reaction of phthalylglycine **52** with secondary amine **50**, was expected to participate in a base-catalysed ester condensation and elimination to yield dihydropyridone **54** (Scheme 3.8) (Ellis *et al.*, 2009).

Secondary amine **50** was obtained in 80% yield by Michael reaction of L-phenylalanine methyl ester **40** with methyl acrylate **49**. The ^{1}H-NMR confirmed the presence of two methyl ester groups as singlets at δ 3.68 and δ 3.77, and the vinylic hydrogens of the starting acrylate were not observed in the spectrum, indicating that the addition reaction was successful. Phthalylglycine **52**, required for further reaction, was synthesized (Upadhyay *et al.*, 2009) in 56% yield by heating phthalic anhydride **51** with glycine. The product showed four aromatic protons at δ 7.84 and δ 7.91, and methylene protons at δ 4.42 in the ^{1}H-NMR spectrum. The ^{13}C-NMR spectrum had peaks at δ 167.63 and δ 169.40 ascribed to the amide and acid carbonyls, respectively. The key amide **53** was obtained by reacting phthalylglycine **52** with amine **50** using DCC and DMAP. Unfortunately, all attempts at base-catalysed ring closure failed.

3.2.3 Malonate chemistry

Reaction of appropriately substituted acetophenones, aldehydes, and ammonium acetate with ethyl cyanoacetate, or malononitrile (Abadi *et al.*, 2010), reportedly leads to substituted 3-cyano-2-pyridones (**55**) or 3-cyano-2-imino-1,2-dihydropyridines (**56**) (Scheme 3.9). These compounds are known to have many biological and anticancer (Abadi *et al.*, 2010) activities and are therefore of great interest. Hydrolysis and Hofmann rearrangement of the nitrile would open the way to dipeptide (**57** or **58**) and tripeptide (**59**) mimic syntheses (Scheme 3.10).

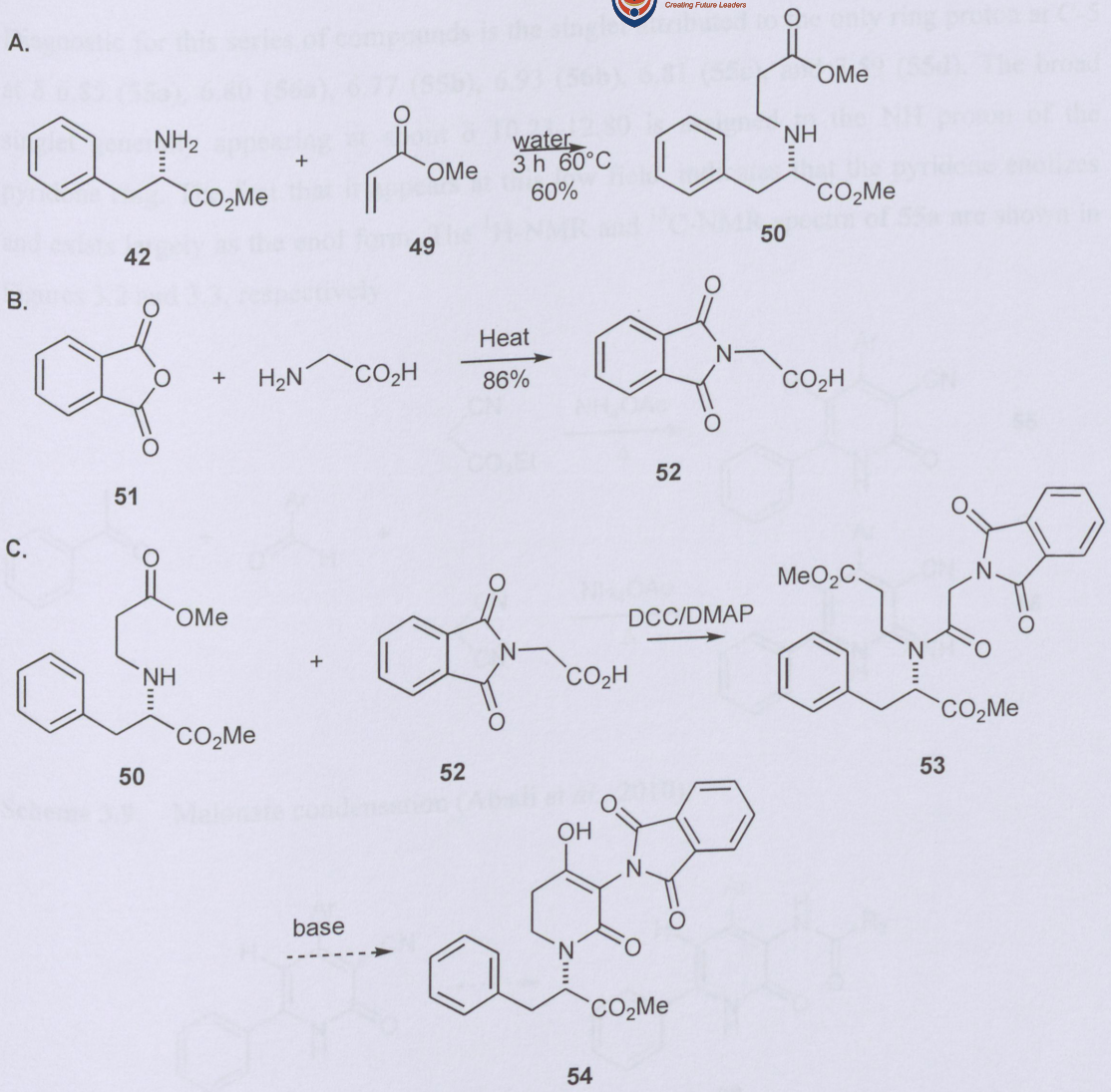

Scheme 3.8 Condensation-cyclization (Ellis *et al.*, 2009): A. Synthesis of amine **50** by Michael reaction; B. Synthesis of phthalimidoglycine **52**; C. Attempted synthesis of 2-pyridone **54**.

In the present case, the general synthesis design consisted of a one-pot reaction as shown in Scheme 3.9, and involved multicomponent aldol and mixed Claisen condensations followed by cyclization involving an ammonium salt. The overall reactions led to the 2-pyridone derivatives (**55**) and the analogous imino derivatives (**56**). Acetophenone, ammonium acetate, the respective aldehyde and ethyl cyanoacetate or malononitrile were heated to reflux in ethanol for up to 12 h to afford solid products. All the compounds obtained (Table 3.1) proved to be diarylcyanopyridine derivatives. The ^{1}H-NMR spectra of all compounds showed the expected characteristic aromatic proton signals with multiple peaks at δ 6.5-8.10.

Diagnostic for this series of compounds is the singlet attributed to the only ring proton at C-5 at δ 6.85 (**55a**), 6.80 (**56a**), 6.77 (**55b**), 6.93 (**56b**), 6.81 (**55c**), and 7.59 (**55d**). The broad singlet generally appearing at about δ 10.23-12.80 is assigned to the NH proton of the pyridone ring. The fact that it appears at this low field, indicates that the pyridone enolizes and exists largely as the enol form. The ^{1}H-NMR and ^{13}C-NMR spectra of **55a** are shown in Figures 3.2 and 3.3, respectively

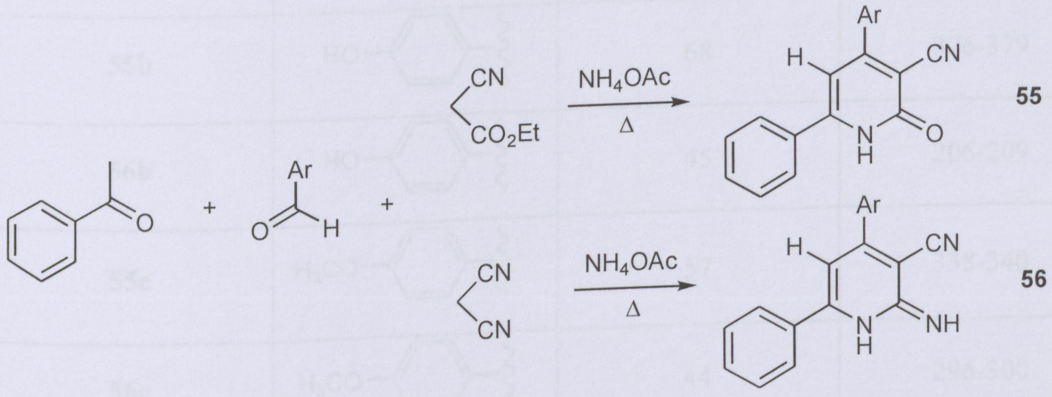

Scheme 3.9 Malonate condensation (Abadi *et al.*, 2010).

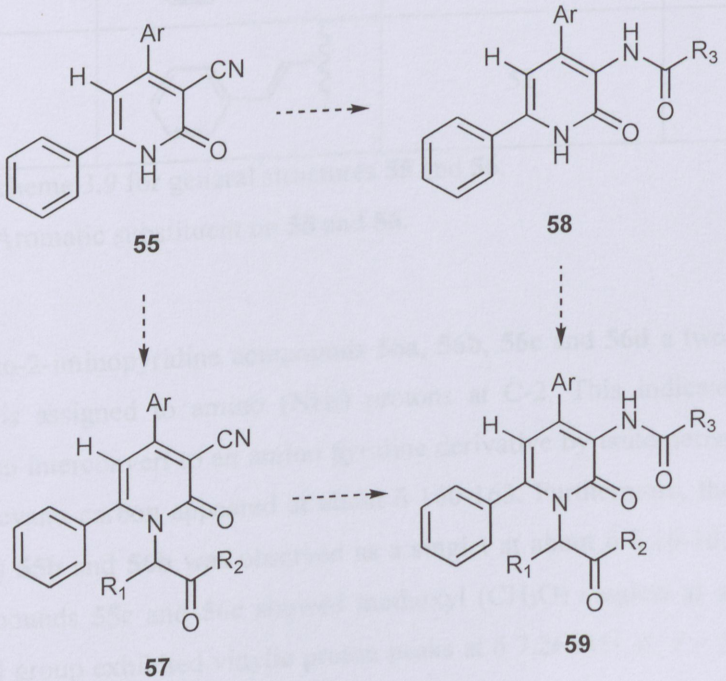

Scheme 3.10 Projected di- and tripeptide mimic syntheses.

Table 3.1 Yields and melting points of synthesized compounds[a].

Compound	Ar[b]	Yield, %	Melting point, °C
55a	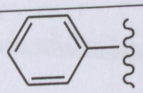	78	332-335
56a	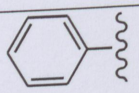	65	185-186
55b	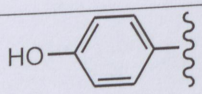	68	376-379
56b	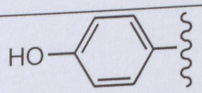	45	206-209
55c	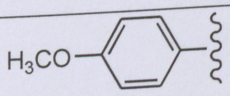	57	338-340
56c	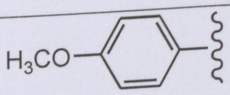	44	296-300
55d	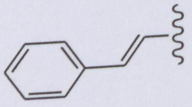	63	301-305
56d	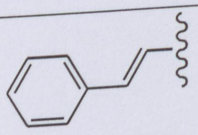	52	244-247

Notes: [a] See Scheme 3.9 for general structures **55** and **56**.

[b] Ar = Aromatic substituent on **55** and **56**.

For the 3-cyano-2-iminopyridine compounds **56a**, **56b**, **56c** and **56d** a two-proton singlet at about δ 5.35 is assigned to amino (NH_2) protons at C-2. This indicates that the imino compounds also interconvert to an amino pyridine derivative by tautomerism. The ^{13}C-NMR signal for the cyano carbon appeared at about δ 160-163. Furthermore, the phenolic proton for compounds **55b** and **56b** was observed as a singlet at about δ 8.10-10.20. The methoxy group of compounds **55c** and **56c** showed methoxyl (CH_3O) singlets at about δ 3.80. The cinnamyl vinyl group exhibited vinylic proton peaks at δ 7.26 (1H, d, J = 16 Hz) and δ 8.01 (1H, d, J = 16 Hz).

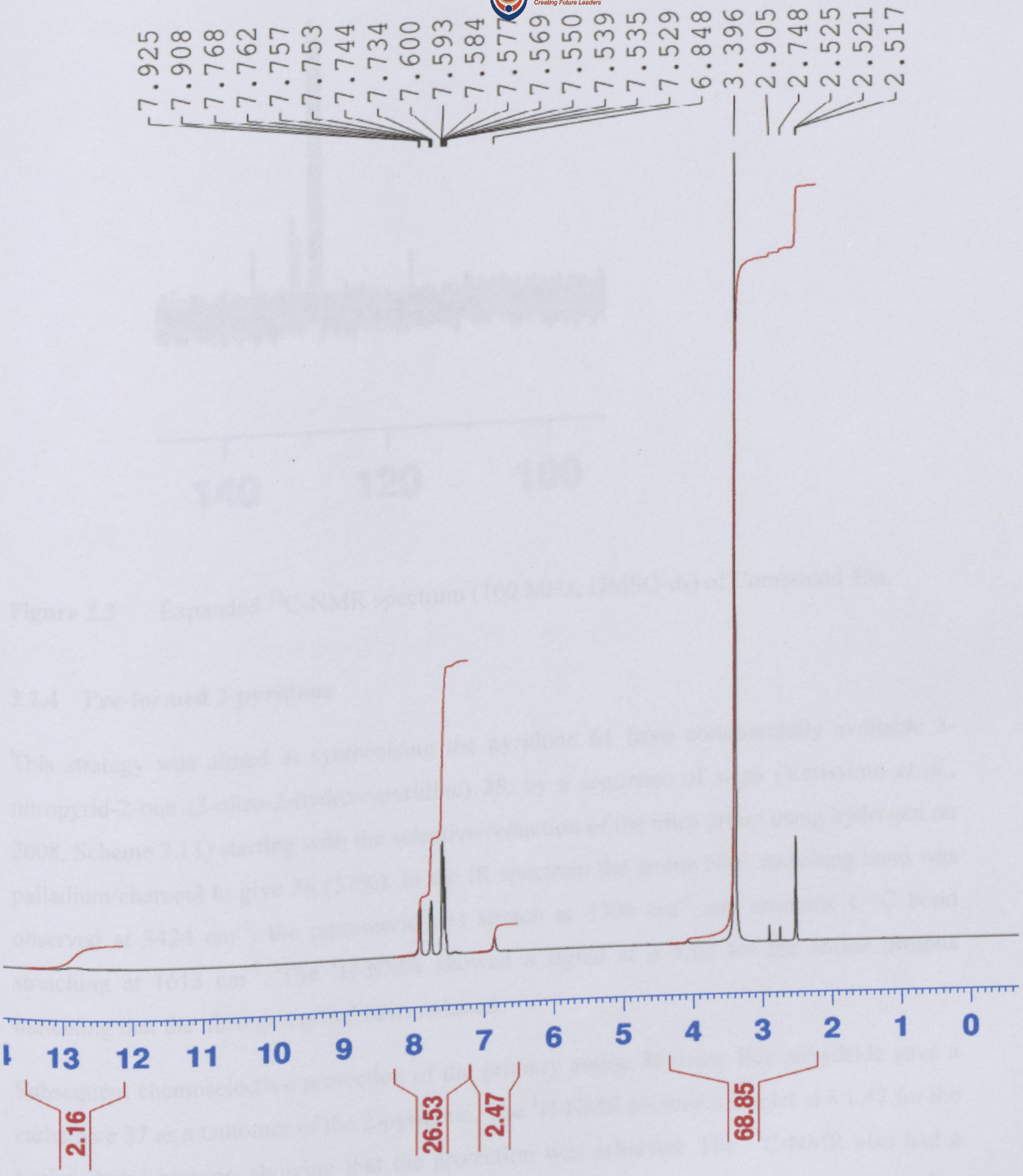

Figure 3.2 ^{1}H-NMR spectrum (400 MHz, DMSO-d_6) of Compound **55a**.

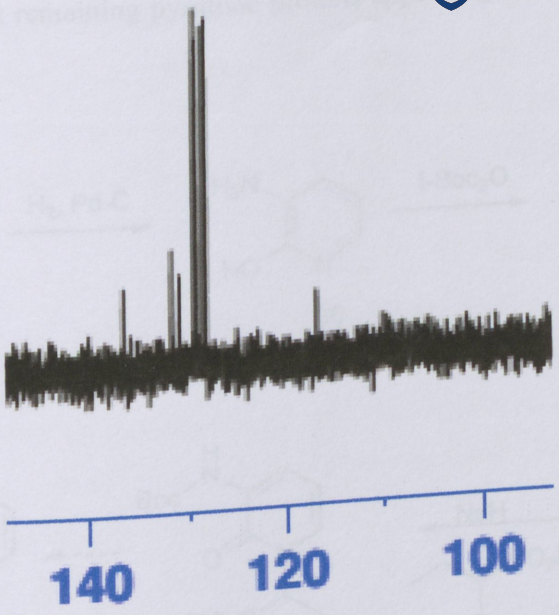

Figure 3.3 Expanded ^{13}C-NMR spectrum (100 MHz, DMSO-d_6) of Compound **55a**.

3.2.4 Pre-formed 2-pyridone

This strategy was aimed at synthesising the pyridone **61** from commercially available 3-nitropyrid-2-one (3-nitro-2-hydroxypyridine) **35**, by a sequence of steps (Verissimo *et al.*, 2008, Scheme 3.11) starting with the selective reduction of the nitro group using hydrogen on palladium/charcoal to give **36** (57%). In the IR spectrum the amine N-H stretching band was observed at 3424 cm^{-1}, the tautomeric OH stretch at 3300 cm^{-1} and aromatic C=C bond stretching at 1613 cm^{-1}. The ^{1}H-NMR showed a signal at δ 5.03 for the amine protons indicating that the nitro group had been reduced.

Subsequent chemoselective protection of the primary amine **36** using Boc anhydride gave a carbamate **37** as a tautomer of the 2-pyridone. The ^{1}H-NMR showed a singlet at δ 1.47 for the tertiary butyl protons, showing that the protection was achieved. The ^{13}C-NMR also had a peak at δ 80.52 assigned to the tertiary carbon bonded to oxygen showing that the amino group was protected. Finally, deprotonation of **37** with NaH, followed by nucleophilic substitution of **60**, yielded Compound **61**. The ^{1}H-NMR of **61** (Fig. 3.4) again displayed the characteristic singlet at δ 1.51 for the tertiary butyl protons, triplets at δ 0.92 and 1.27 for the two methyl groups, respectively, multiplets at δ 1.99 and 2.27 for the acyl CH_2, a quartet at δ 4.22 for the ethyl ester CH_2, a multiplet at δ 5.45 for the acyl methine, a singlet at δ 7.67 for

the NH and the remaining pyridone protons appear as multiplets at δ 6.29, 6.96 and 7.99 ppm.

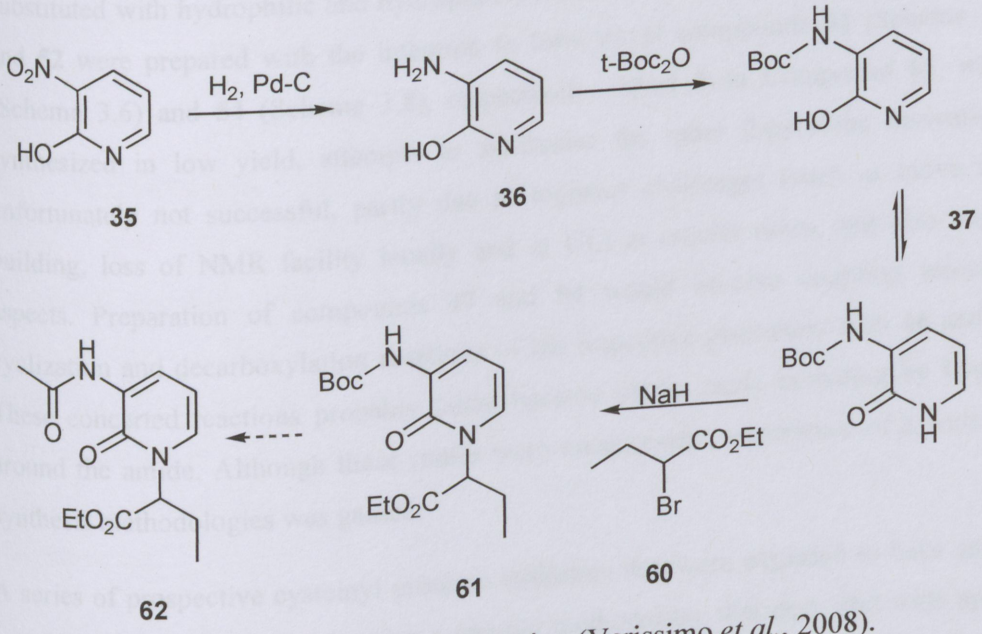

Scheme 3.11 3-Nitro-2-pyridone elaboration (Verissimo *et al.*, 2008).

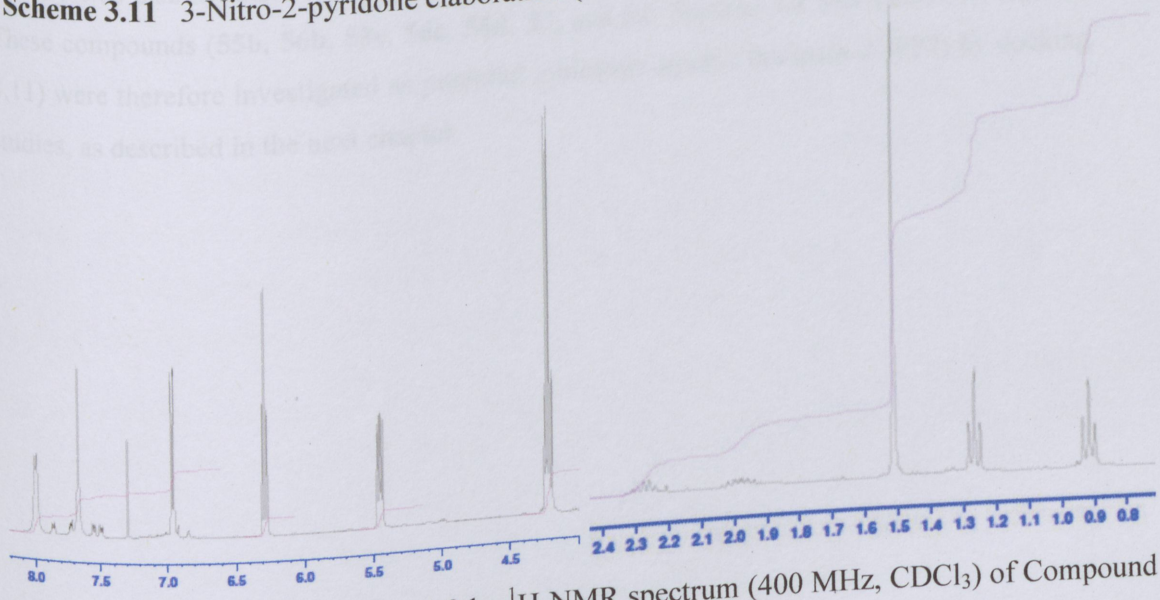

Figure 3.4 Expanded sections of the ^{1}H-NMR spectrum (400 MHz, $CDCl_3$) of Compound **61**.

3.3 Conclusions

The main aim of this project was to synthesise 2-pyridone-derived compounds that may be developed as possible cysteine protease inhibitors as therapeutic agents for malaria. Malaria

is a life-threatening disease and is growing in resistance to current drugs. The synthesis of the 2-pyridone scaffold involved constructing and characterizing 2-pyridone derivatives substituted with hydrophilic and hydrophobic moieties. Key intermediates **37**, **43** and **46**, **50** and **52** were prepared with the intention to form novel compounds **61** (Scheme 3.11), **47** (Scheme 3.6) and **54** (Scheme 3.8), respectively. Apart from Compound **61**, which was synthesized in low yield, attempts to synthesise the other 2-pyridone derivatives were unfortunately not successful, partly due to logistics challenges (such as move to a new building, loss of NMR facility locally and at UL) at crucial times, but also mechanistic aspects. Preparation of compounds **47** and **54** would involve coupling intramolecular cyclization and decarboxylation reactions of the respective precursors with **46** and with **52**. These concerted reactions probably failed because of the steric crowding by large groups around the amide. Although these routes were unsuccessful, experience of a wide range of synthesis methodologies was gained.

A series of prospective cysteinyl protease inhibitors that were expected to have antimalarial activity was also synthesised, using a one-pot methodology that may find wide application. These compounds (**55b**, **56b**, **55c**, **56c**, **55d**, **37**, and **61**; Scheme 3.8 and Table 3.1, Scheme 3.11) were therefore investigated as potential inhibitors against falcipain-2 (FP2) by docking studies, as described in the next chapter.

Chapter 4

Molecular modelling and docking of 2-pyridone-based drug candidates with the FP2-E64 active site

4.1 Introduction

Molecular modelling focuses on computationally simulating the molecular recognition process in biomolecules. It is a process that predicts and optimises the correct orientation of a ligand bound to a protein in a stable complex. Interactions of biological molecules such as proteins, nucleic acids and carbohydrates play a pivotal role physiologically. Furthermore, the relative orientation of the two interacting partners affects the type of response produced by the interaction.

More frequently, docking experiments are useful to find the binding orientation of small drug molecules to their protein partners; this enables prediction of the affinity and activity of the drug. The aim of structure-based drug design is to find and optimise the different interactions between ligands and proteins. To this end, it is necessary to determine the interaction geometries and attractive interactions of these molecules. Usually, direct hydrophilic or hydrophobic contacts between the functional groups of ligands and the protein, are of interest. Interactive forces between host molecules and ligands are mainly due to non-covalent bonding, such as hydrogen bonding and van der Waals forces.

Before a docking experiment can be performed, the 3-dimensional molecular structure of the target protein must be obtained. Protein structures are commonly determined by X-ray crystallography, preferably of the protein/enzyme - substrate crystal. If the target protein is not available in the Protein Databank, its structure can be deduced by homology modelling, which, if done correctly, can reliably predict the structure of the desired protein (Aparoy *et al.*, 2012). The homology modelling method is used to determine the 3D structure of a protein based on proteins with closely homologous structures (Bishop *et al.*, 2008).

FP2 and FP3 are active in the acidic food vacuole, where they cooperate to hydrolyse haemoglobin (Sijwali *et al.*, 2006). The falcipain quaternary structure consists of two main domains, the prodomain and the mature domain. The prodomain further consists of several

different smaller domains (Figure 4.1). The prodomain has unique structural features that enable focussed targeting of the falcipains. The *C*-terminal end of the prodomain is essential for the inhibition of the mature domain (Pandey and Dixit, 2012).

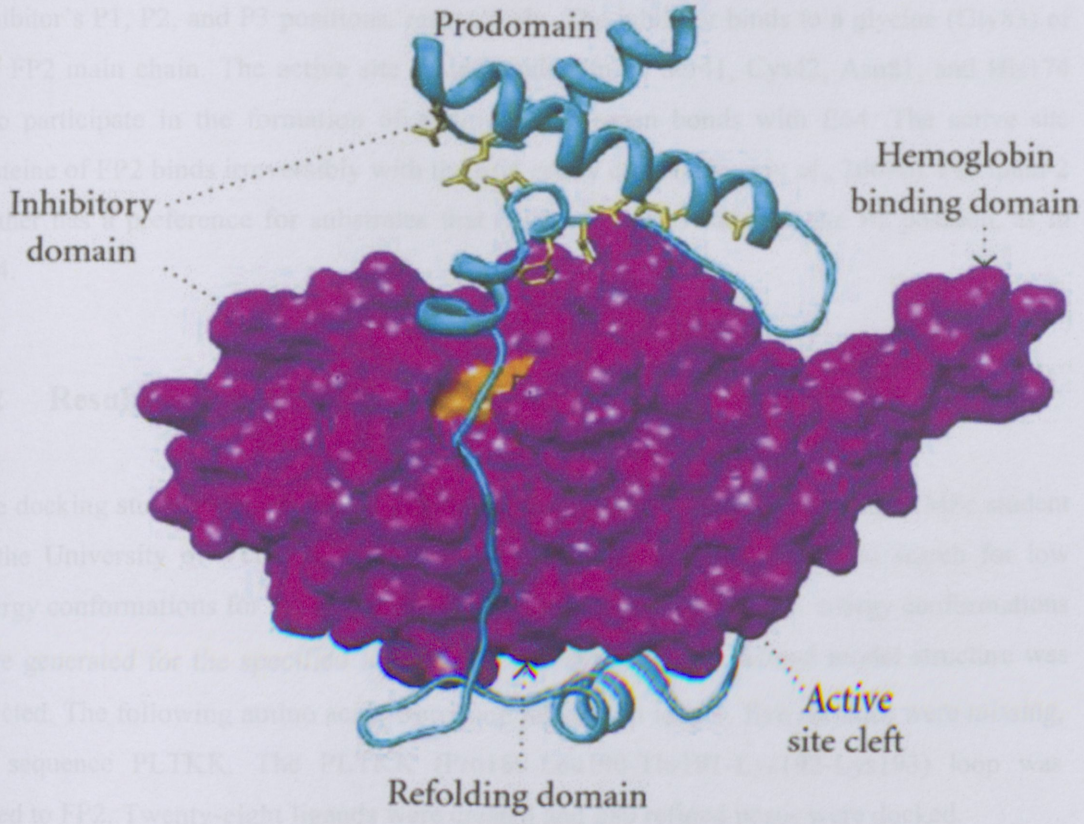

Figure 4.1 Model of pro-FP2, reproduced with permission of the publisher (Pandey and Dixit, 2012).

The 2.9 Å crystal structure of the mature domain of falcipain-2 complexed with the inhibitor E64 has been determined by X-ray crystallography (Kerr *et al*., 2009b), and the profalcipain-2 model shows how certain residues stabilize the inhibitory domain (Figure 4.1). The mature domain is shown in purple, the active site is shown in orange, and the refolding domain and haemoglobin domain are also shown. The prodomain in blue is shown folding over the mature enzyme and forms α helices containing the motifs in yellow. The prodomain of falcipain-2 binds the mature domain in such a way that access of substrate to the active site is blocked, inhibiting the enzyme's catalytic activity (Figure 4.1).

E64 and other vinyl sulfones have been shown to be efficient cysteine protease inhibitors binding the active site of FP2 (Kerr *et al.*, 2009a), which is located in a cleft. The structure of falcipain-2 complexed with these small inhibitors has been determined (Pandey and Dixit, 2012). E64 binds with residues in the S1, S2, and S3 sub-sites of FP2, which interact with the inhibitor's P1, P2, and P3 positions, respectively. The inhibitor binds to a glycine (Gly83) of the FP2 main chain. The active site amino acids Gln36, Ser41, Cys42, Asn81, and His174 also participate in the formation of additional hydrogen bonds with E64. The active site cysteine of FP2 binds irreversibly with the E64 epoxy carbon (Kerr *et al.*, 2009b). Falcipain-2 further has a preference for substrates that have a leucine residue at the P2 position, as in E64.

4.2 Results and discussion

The docking studies were executed in collaboration with Mr Thomas Makungo (MSc student at the University of Venda). The selected model structure was refined to search for low energy conformations for the loops. For each loop selected, several low energy conformations were generated for the specified loop region and the best loop refined model structure was selected. The following amino acids were loop refined: In loop 1, five residues were missing, the sequence PLTKK. The PLTKK (Pro189-Leu190-Thr191-Lys192-Lys193) loop was added to FP2. Twenty-eight ligands were created and 280 refined poses were docked.

The results for the optimized structures are summarized in Table 4.1. Docking poses and protein-ligand interactions are shown in Figures 4.2-4.9.

The docking pose of Compound **55b** into the active centre of FP2 is shown in Fig. 4.2. The docking results reveal that three amino acids, Gln36, Asn81, and His174, located in the binding pocket of the protein, play an important role in the binding, which is stabilized by one electrostatic interaction and three hydrogen bonds. Therefore, it can be anticipated that Compound **55b** could well embed in the active pocket. In addition, the enzyme surface model shown in Fig. 4.2(b) reveals that Compound **55b** occupies an active site of FP2.

In Fig. 4.3, the docking pose of Compound **56b** into the active centre of FP2 is presented. Two amino acids, Gln36 and His174, again play a role in the binding, which is stabilized by one electrostatic interaction and two hydrogen bonds. The docking score is quite low,

however. In addition, the enzyme surface model shown in Fig. 4.3(b) reveals that Compound **56b** occupies an active site of FP2.

Table 4.1 Results of target structure docking with falcipain-2.

Ligand	CDOCKER Energy	Consensus Score	H-Bond Interaction	Electrostatic Interaction
TS14	28.32	4	A:GLN36:HE22 - TS14:O31	A:HIS174:NE2 - TS14:O31 (Attractive charge)
			A:HIS174:HD1 - TS14:O31	
			TS14:H33 - A:ASN81:O	
TS15	19.16	1	A:GLN36:HE22 - TS15:O32	A:HIS174:NE2 - TS15:O32 (Attractive charge)
			A:HIS174:HD1 - TS15:O32	
TS16	6.20	5	A:CYS42:HG - TS16:O36	
TS17	12.11	4	TS17:H37 - A:ASP234:OD2	TS17:N35 - A:ASP234:OD2 (Attractive charge)
TS18	13.37	1	A:CYS42:HG - TS18:O36	
			TS18:H37 - A:CYS42:SG	
TS22	20.74	2	A:CYS42:HG - TS22:O27	
			A:GLY83:HN - TS22:O27	
			TS22:H29 - A:GLY83:O	
TS23	23.41	2	TS23:H44 - A:GLY83:O	
TS25	26.32	2	A:CYS42:HG - TS25:O33	
			A:GLY83:HN - TS25:O31	
			A:HIS174:HD1 - TS25:O32	
			TS25:H35 - A:ASN173:O	

Notes: 1. CDOCKER_ENERGY is reported as the negative value, where a higher value indicates a more favourable binding. This enables the energy to be used like a score. This score includes internal ligand strain energy and receptor-ligand interaction energy, and is used to sort the poses of each input ligand.

2. The codes are:
TS14 = **55b**
TS15 = **56b**
TS16 = **55c**
TS17 = **56c**
TS18 = **55d**
TS22 = **37**
TS23 = **61**
TS25 = **62**

The docking pose of Compound **55c** into the active centre of FP2 is shown in Fig. 4.4. The docking results reveal that only one amino acid, Cys42, plays a role in the binding in the form of a hydrogen bond. The docking score is high, however. In addition, the enzyme surface model shown in Fig. 4.4(b) reveals that Compound **55c** occupies an active site of FP2.

The docking pose of Compound **56c** is shown in Fig. 4.5. Only one amino acid, Asp234, plays a role in the binding, which is stabilized by one electrostatic interaction and one hydrogen bond. The docking score is high, however, probably because of the strong electrostatic forces. The enzyme surface model shown in Fig. 4.5(b) reveals that Compound **56c** occupies an active site of FP2.

The docking pose of Compound **55d** into the active centre of FP2 is shown in Fig. 4.6. The docking results reveal that one amino acid, Cys42, located in the binding pocket of the protein, plays a role in the binding, which is stabilized by two hydrogen-bonding modes. The docking score is low. The enzyme surface model shown in Fig. 4.6(b) reveals that Compound **55d** occupies an active site of FP2.

The docking pose of Compound **37** into the active centre of FP2 is shown in Fig. 4.7. The docking results reveal that two amino acids, Cys42 and Gly83, located in the binding pocket of the protein, play a role in the binding, which is stabilized by and three hydrogen-bonding modes. Therefore, it can be anticipated that Compound **37** could well embed in the active pocket. In addition, the enzyme surface model shown in Fig. 4.7(b) reveals that Compound **37** occupies an active site of FP2.

The docking pose of Compound **61** into the active centre of FP2 is shown in Fig. 4.8. The docking results reveal that only one amino acid, Gly83, located in the binding pocket of the protein, plays a role in the binding, which is stabilized by one hydrogen bond. The enzyme surface model shown in Fig. 4.8(b) reveals that Compound **61** occupies an active site of FP2. In contrast, Compound **62** (Fig. 4.9) presents four hydrogen bonding modes, with amino acids Cys42, Gly83, Asn173, and His174. These residues also appear in interactions with several other compounds.

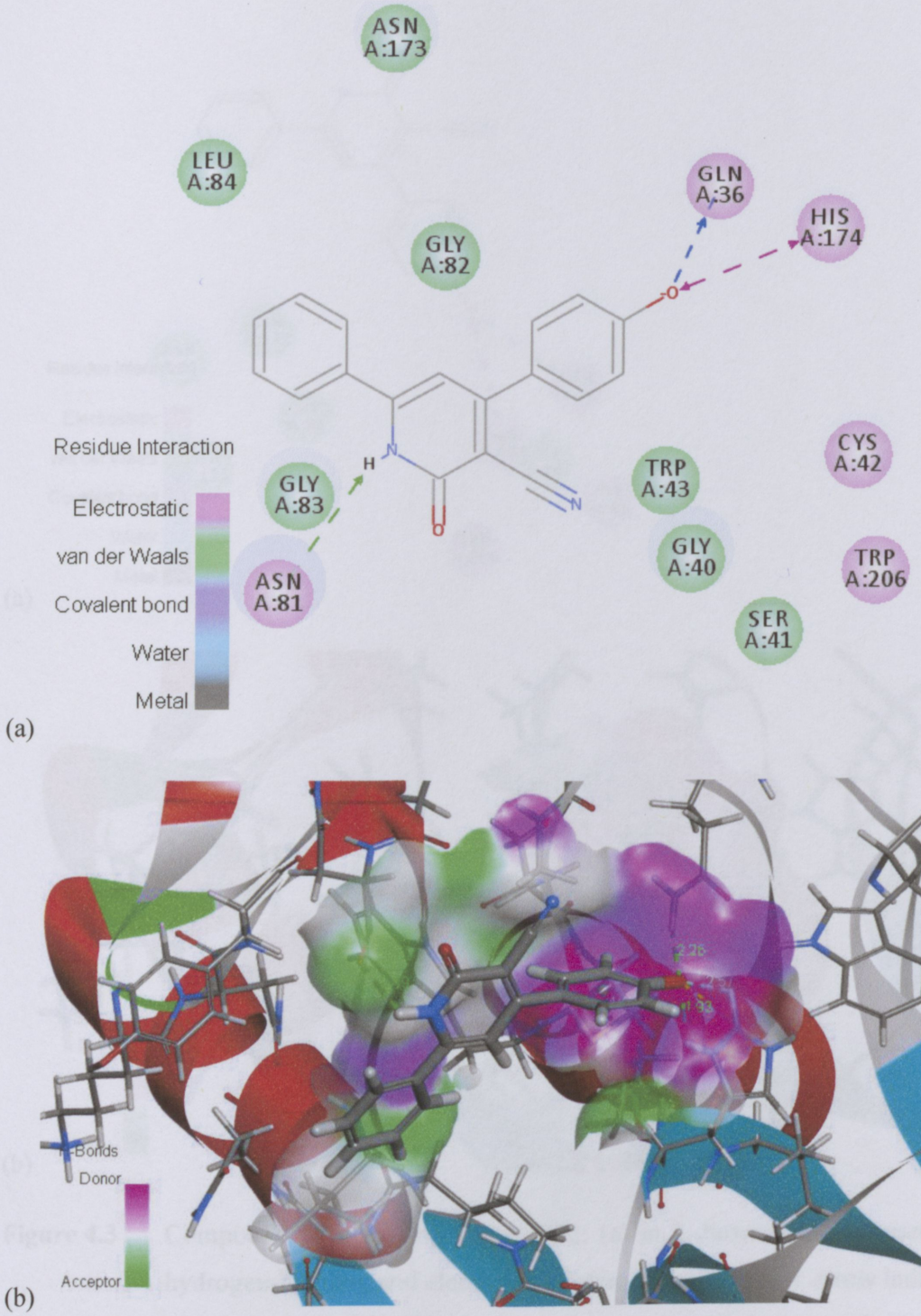

Figure 4.2 Compound **55b** docking versus FP2: (a) in 2-dimensional representation for hydrogen-bonding and electrostatic interactions. The blue and green arrows indicate hydrogen-bonding interactions and the red arrow indicates a pi-sigma or pi-pi interaction; (b) 3D docking model of Compound **55b** docked with FP2.

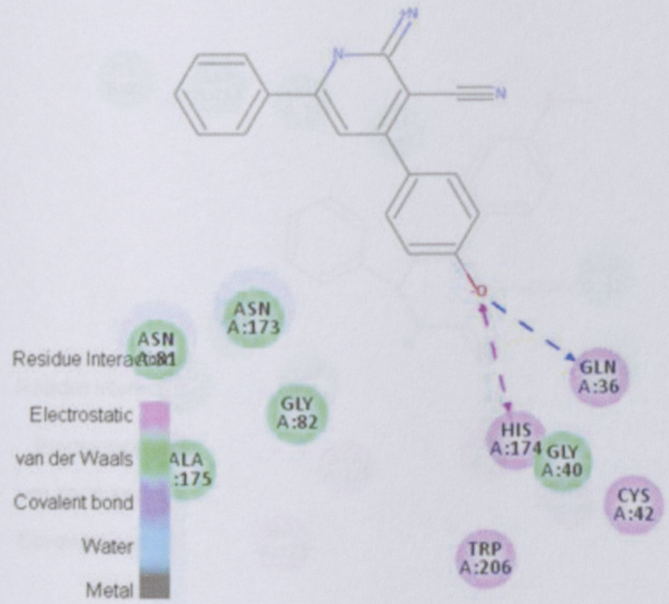

(a)

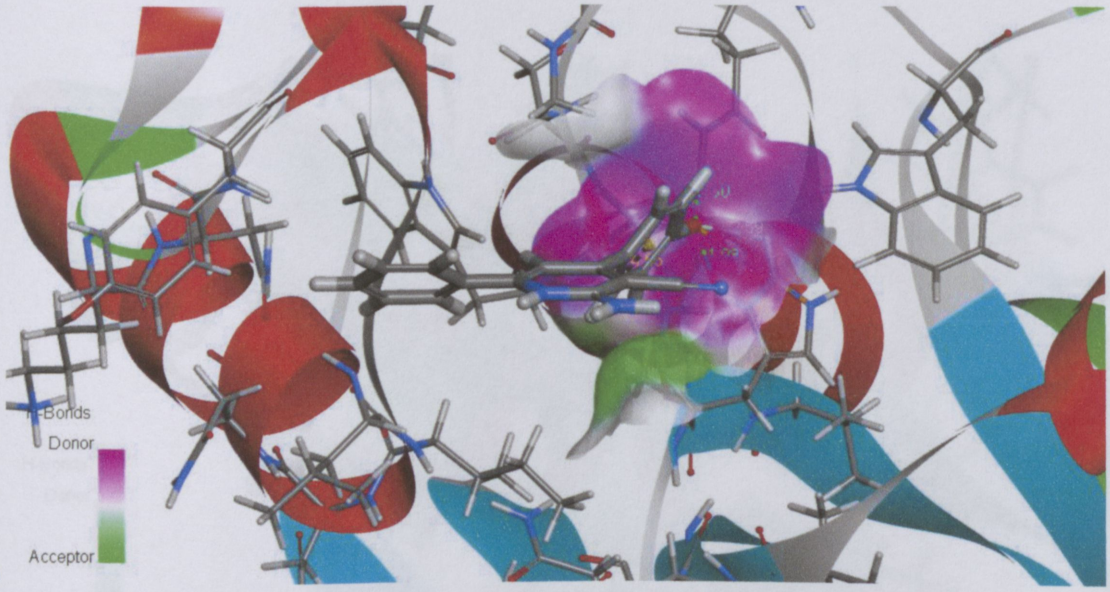

(b)

Figure 4.3 Compound **56b** docking versus FP2: (a) in 2-dimensional representation for hydrogen-bonding and electrostatic interactions. The blue arrow indicates a hydrogen-bonding interaction and the red arrow indicates a pi-sigma or pi-pi interaction; (b) 3D docking model of Compound **56b** docked with FP2.

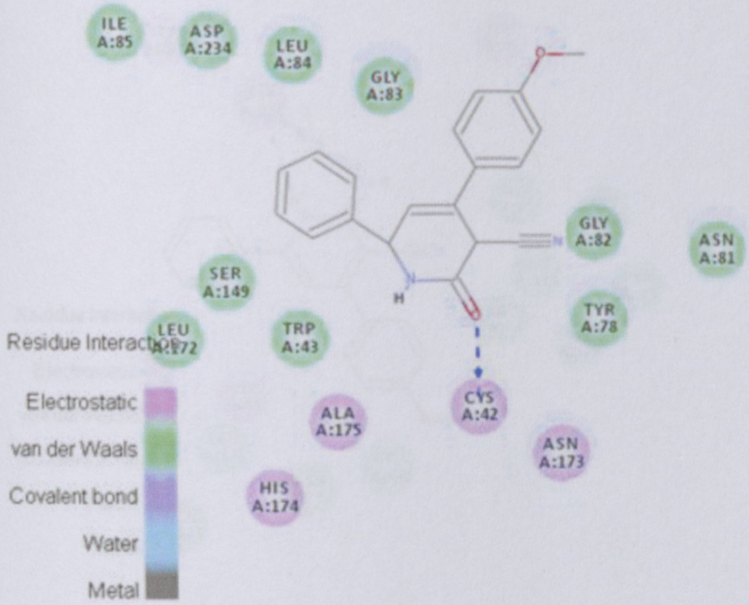

(a)

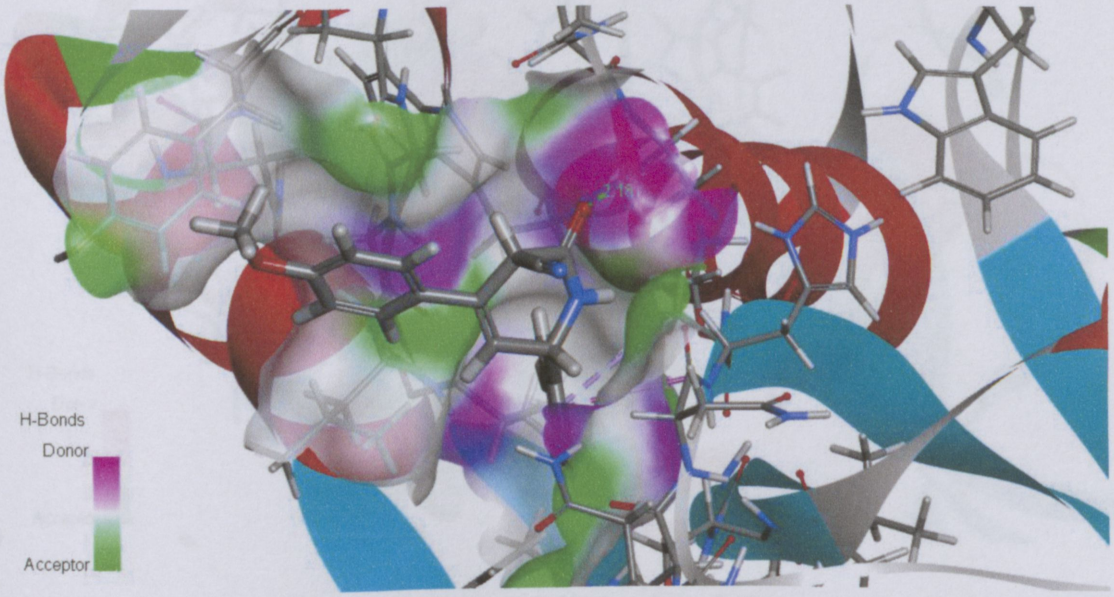

(b)

Figure 4.4 Compound **55c** docking versus FP2: (a) in 2-dimensional representation for hydrogen-bonding and electrostatic interactions. The blue arrow indicates a hydrogen-bonding interaction; (b) 3D docking model of Compound **55c** docked with FP2.

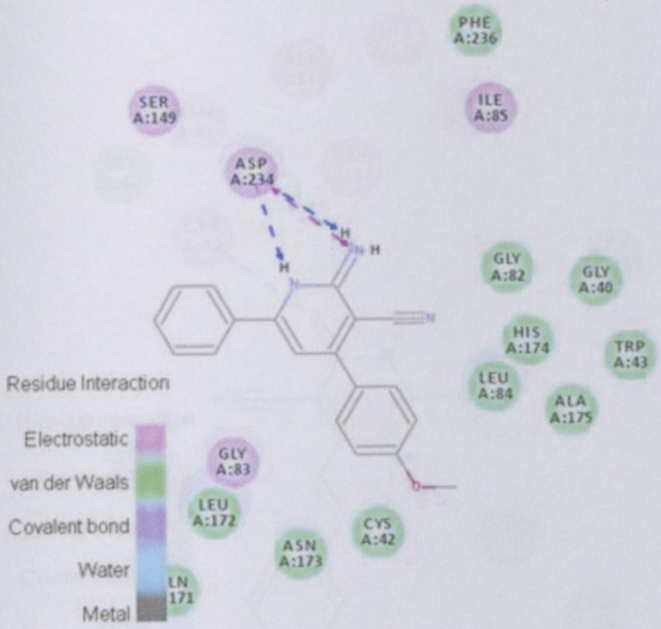

(a)

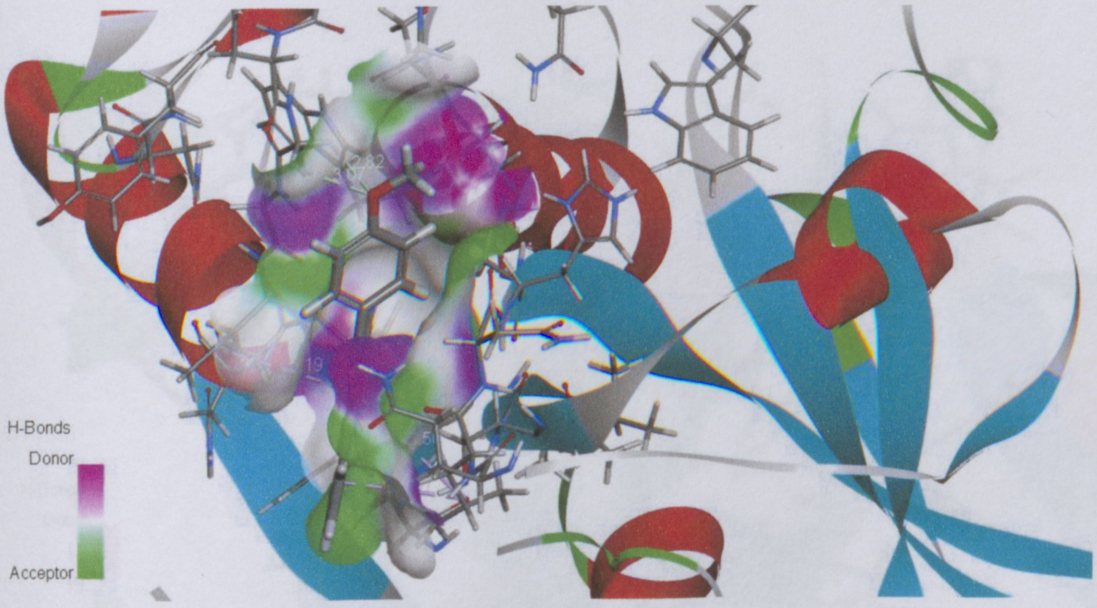

(b)

Figure 4.5 Compound **56c** docking versus FP2: (a) in 2-dimensional representation for hydrogen-bonding and electrostatic interactions. The blue arrow indicates a hydrogen-bonding interaction and the red arrow indicates a pi-sigma or pi-pi interaction; (b) 3D docking model of Compound **56c** docked with FP2.

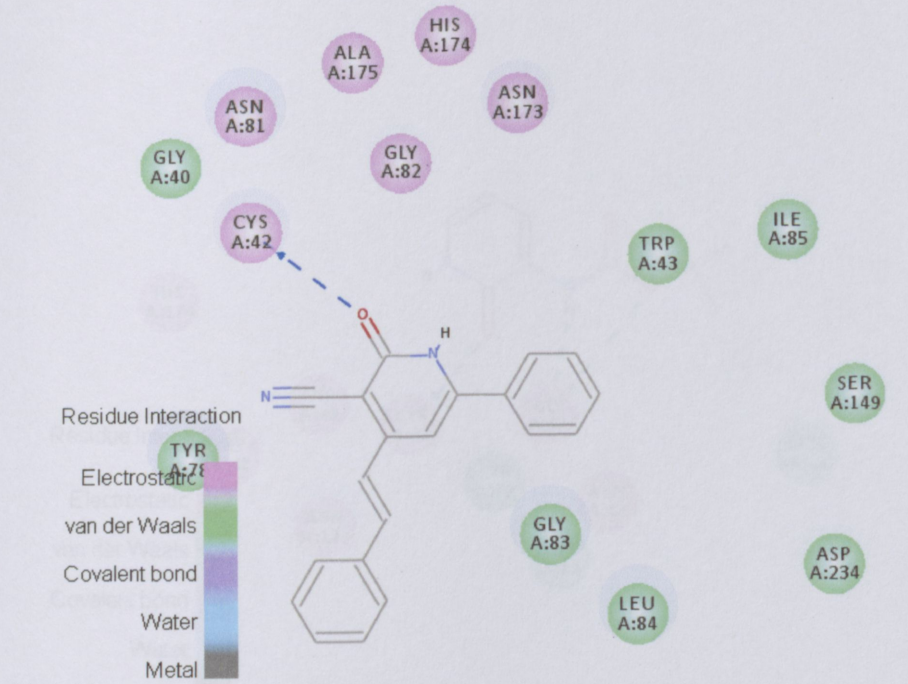

(a)

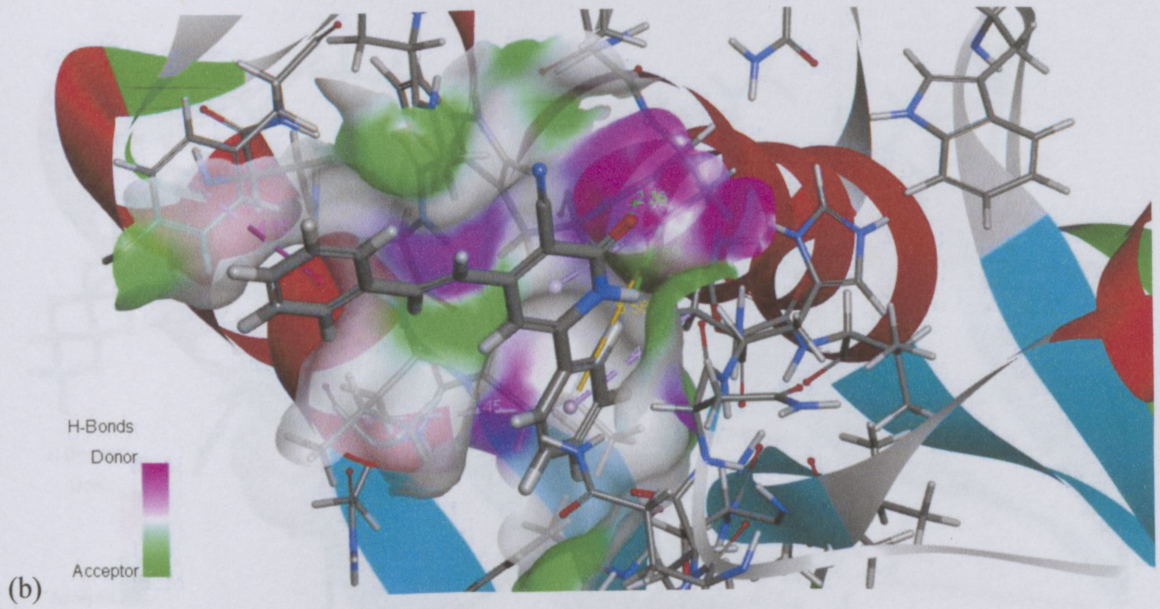

(b)

Figure 4.6 Compound **55d** docking versus FP2: (a) in 2-dimensional representation for hydrogen-bonding and electrostatic interactions. The blue arrow indicates a hydrogen-bonding interaction; (b) 3D docking model of Compound **55d** docked with FP2.

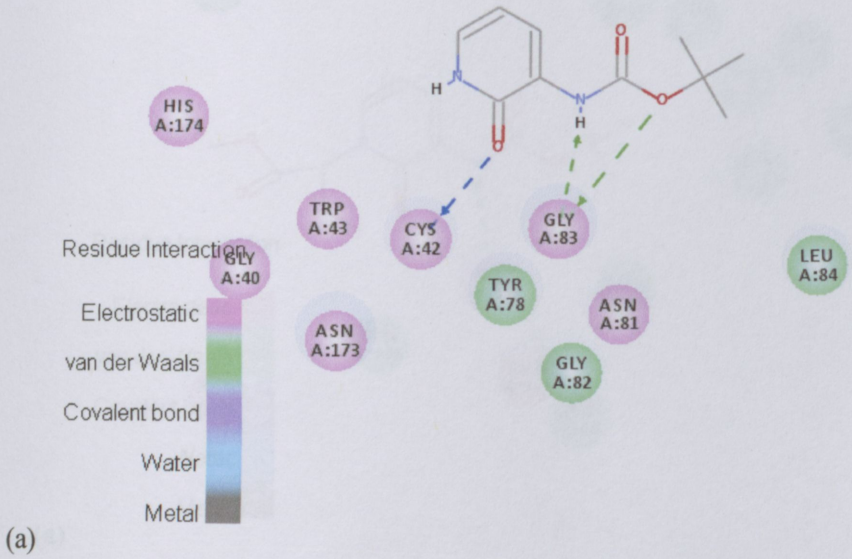

(a)

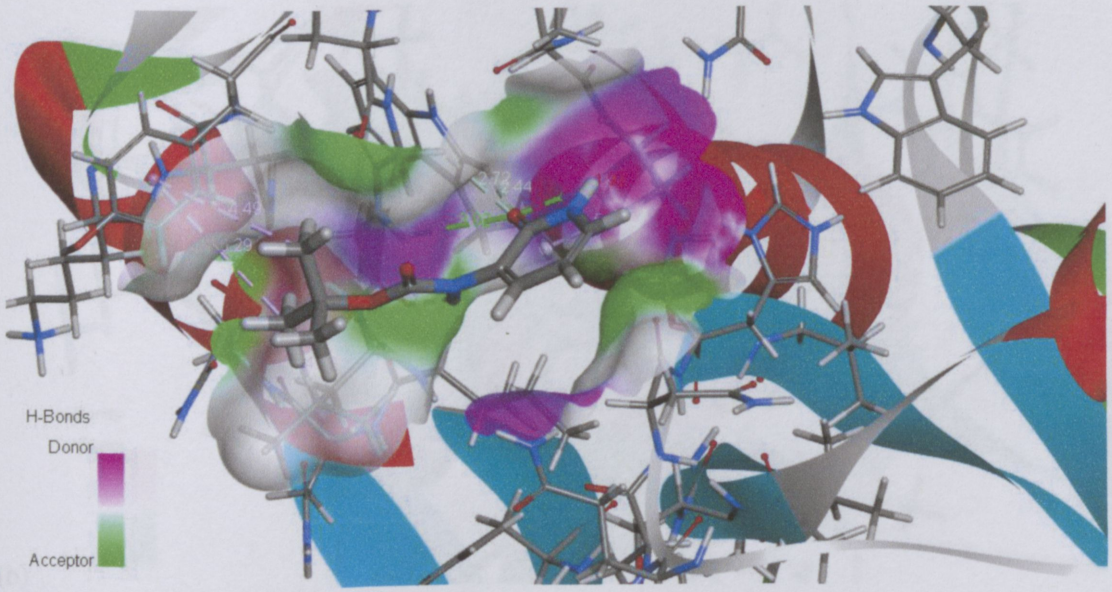

(b)

Figure 4.7 Compound **37** docking versus FP2: (a) in 2-dimensional representation for hydrogen-bonding and electrostatic interactions. The blue and green arrows indicate hydrogen-bonding interactions; (b) 3D docking model of Compound **37** docked with FP2.

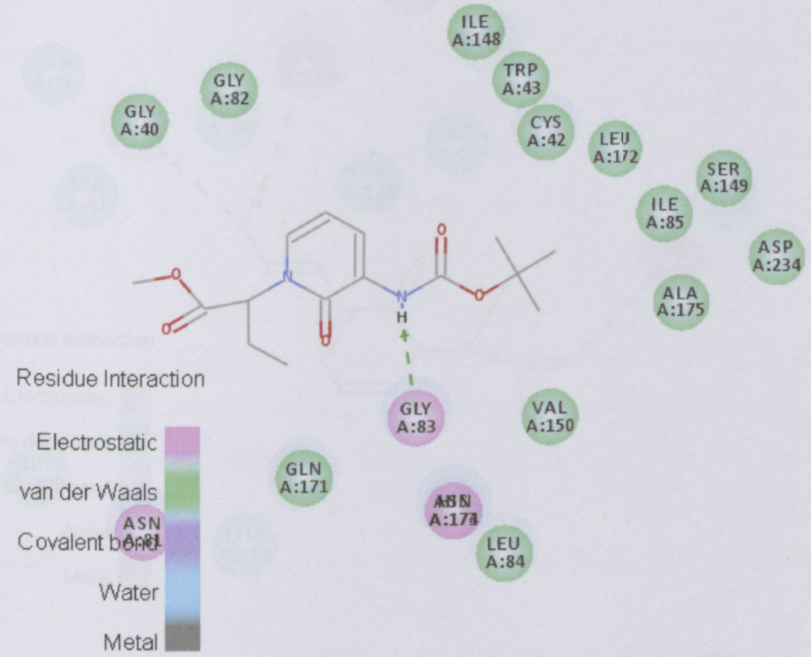

(a)

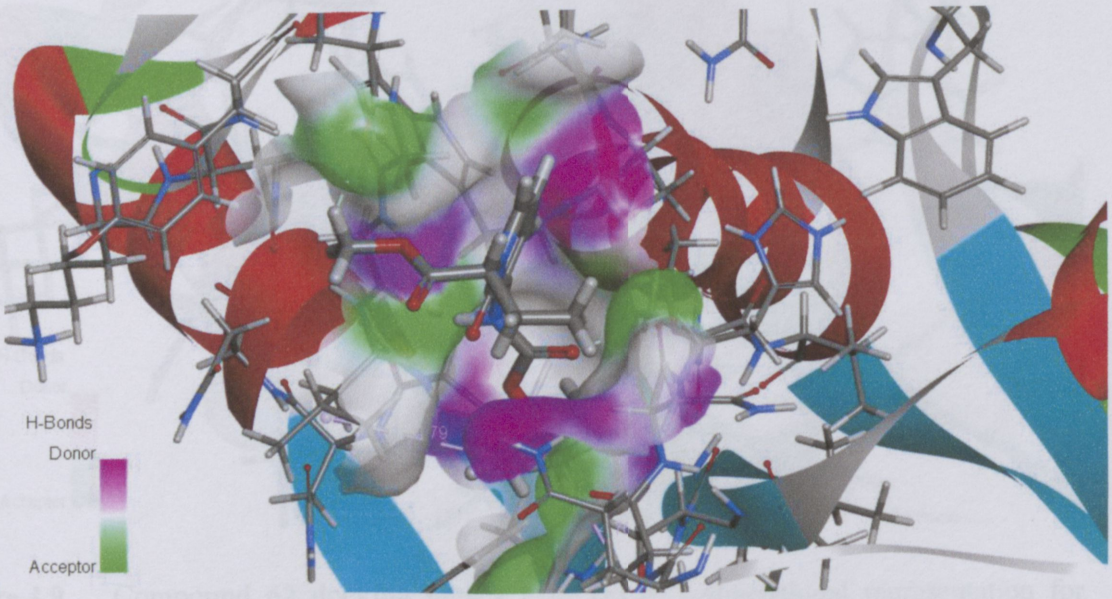

(b)

Figure 4.8 Compound **61** docking versus FP2: (a) in 2-dimensional representation for hydrogen-bonding and electrostatic interactions. The green arrow indicates a hydrogen-bonding interaction; (b) 3D docking model of Compound **61** docked with FP2.

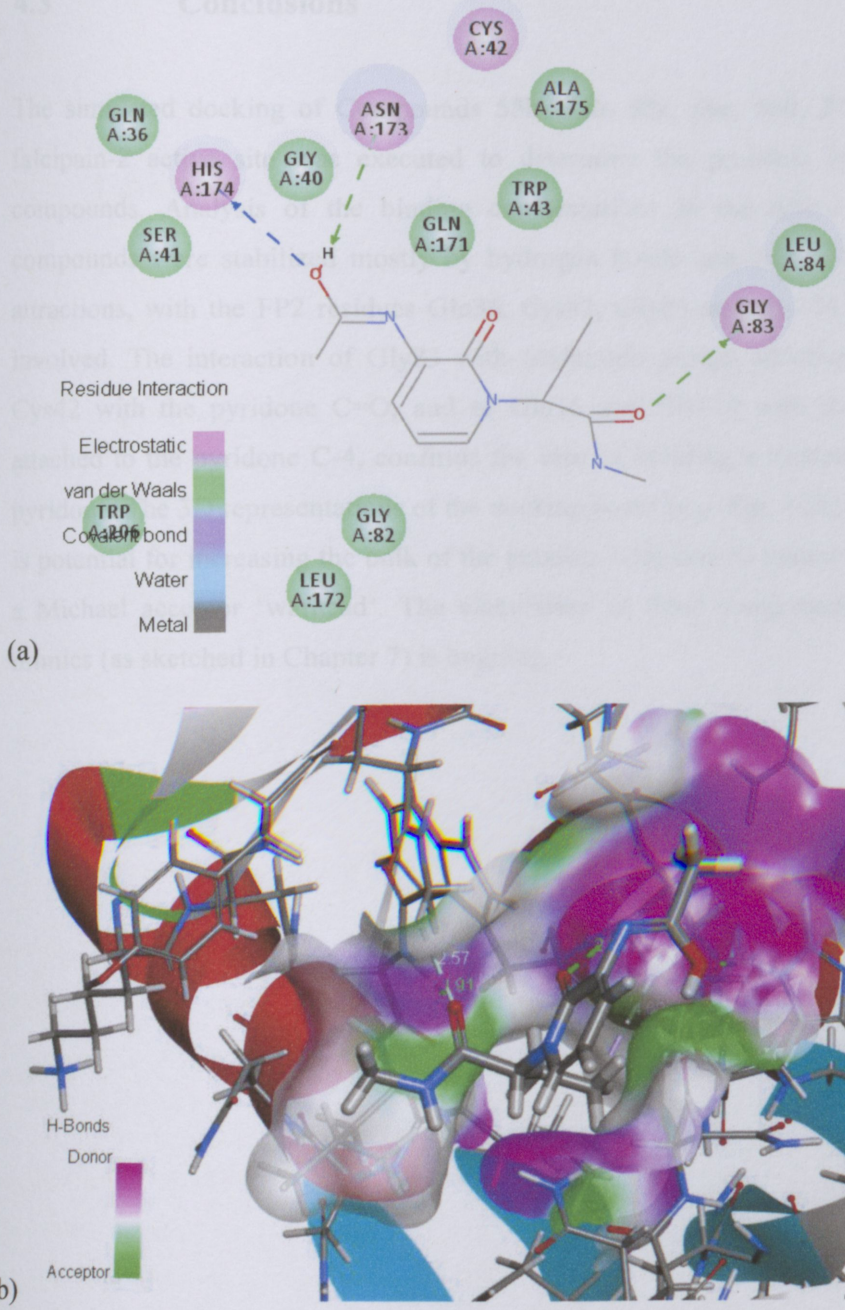

Figure 4.9 Compound **62** docking versus FP2: (a) in 2-dimensional representation for hydrogen-bonding and electrostatic interactions. The blue and green arrows indicate hydrogen-bonding interactions; (b) 3D docking model of Compound **62** docked with FP2.

4.3 Conclusions

The simulated docking of Compounds **55b**, **56b**, **55c**, **56c**, **55d**, **37**, **61**, and **62** with the falcipain-2 active site was executed to determine the probable binding mode of these compounds. Analysis of the binding conformations in the active site showed that the compounds were stabilized mostly by hydrogen bonds and some of them by electrostatic attractions, with the FP2 residues Gln36, Cys42, Gly83 and His174 being most frequently involved. The interaction of Gly83 with acylamido groups attached to the pyridone C-3, Cys42 with the pyridone C=O, and of Gln36 and His174 with the 4-hydroxyoxyphenyl attached to the pyridone C-4, confirms the idea of building a tripeptide mimic based on 2-pyridone. The 3D representations of the docking poses (*e.g.* Fig. 4.2b) clearly show that there is potential for increasing the bulk of the putative inhibitors to induce a better fit, and adding a Michael acceptor 'warhead'. The elaboration of these compounds to di- and tripeptide mimics (as sketched in Chapter 7) is ongoing.

Chapter 5

In vitro antiplasmodial pLDH assays

5.1 Introduction

Five compounds were obtained in sufficient purity and stability to use in antiplasmodial assays. These were executed by Dr Jenny-Lee Panayides of the Council for Scientific and Industrial Research (Biosciences Molecular and Biomedical Technologies Group). The results are presented as received, and the discussion excerpted from the standard narrative provided in the received reports.

The Z' factor reported in these assays measured the *statistical effect size* and is used in high-throughput screening to judge whether the response is large enough to warrant further attention (Zhang *et al.*, 1999). It is defined in terms of four parameters: the means and standard deviations of both the positive and negative controls, and can range between zero and one. A value above 0.5 is interpreted as an excellent assay, with Z' = 1 being the ideal result.

In the single-concentration assays, compounds can be classified as:

Inactive: % parasite viability > 50% at a compound concentration of 10 µM.

Marginally active or Inactive:
% parasite viability > 20% at a compound concentration of 10 µM.

Active: % parasite viability < 20% at a compound concentration of 10 µM.

In the IC_{50} assay, compounds can be classified as:

Inactive: IC_{50} > 10 µM

Moderately active: IC_{50} = 1-10 µM

Active: IC_{50} = 0.1-1 µM

Highly active: IC_{50} < 0.1 µM

Standard antimalarials typically produce the following average IC_{50} values in CSIR assays:

Chloroquine	0.016 µM
Artemisinin	0.021 µM
Mefloquine	0.009 µM

5.2 Results and discussion

5.2.1 Single-concentration antimalarial assays against the 3D7 strain

Compounds **55a**, **56a**, and **55b** were screened against the chloroquine-sensitive 3D7 strain at concentrations 100 µM (Table 5.1), 10 µM (Table 5.2), and 1 µM (Table 5.3) in a single assay, with Z' = 0.89. The assay results indicate that as the concentration decreases from 100 µM to 10 µM, the viability increases showing that these compounds are active (viability 10.748-13.953) only at a concentration of 100 µM and higher. At the concentration of 1 µM the compounds showed no activity.

These results are summarized in Figure 5.1. From the data obtained from the single concentration assay at a concentration of 10 µM, these compounds are classified as *inactive* against the malaria strain 3D7. Normally, only active compounds would be screened in the subsequent IC_{50} assay. However, as all of the compounds submitted were inactive, it was decided to screen them in the subsequent IC_{50} assay against the 3D7 line.

Table 5.1 Single concentration assay against the 3D7 strain at 100 µM.

COMPOUND	% PARASITE VIABILITY	STANDARD DEVIATION
1 – **55a**	13.953	1.78
2 – **56a**	10.748	0.31
3 – **55b**	13.738	0.88
Chloroquine	3.776	0.87
Positive Control	100.000	2.84

Table 5.2 Single concentration assay against the 3D7 strain at 10 µM.

COMPOUND	% PARASITE VIABILITY	STANDARD DEVIATION
1 – **55a**	76.656	4.26
2 – **56a**	83.245	4.69
3 – **55b**	76.404	3.02
Chloroquine	1.994	0.05
Positive Control	100.000	2.84

Table 5.3 Single concentration assay against the 3D7 strain at 1 µM.

COMPOUND	% PARASITE VIABILITY	STANDARD DEVIATION
1 – **55a**	87.610	6.28
2 – **56a**	86.044	5.46
3 – **55b**	82.013	5.47
Chloroquine	1.576	0.30
Positive Control	100.000	2.84

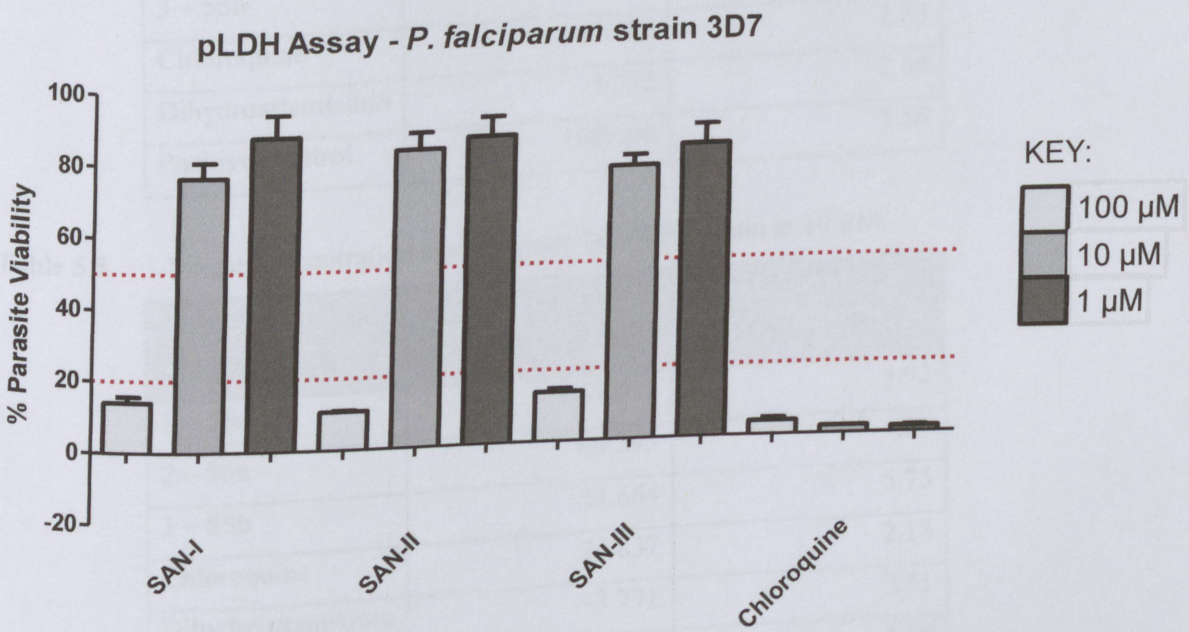

Figure 5.1 Single concentration pLDH assays of compounds against *P. falciparum* strain 3D7. SAN-I = **55a**, SAN-II = **56a**, SAN-III = **55b**.

5.2.2 Single-concentration antimalarial assays against the FCR3 strain

Compounds **55a**, **56a**, and **55b** were screened against the chloroquine-resistant FCR3 strain at concentrations 100 μM (Table 5.4), 10 μM (Table 5.5), and 1 μM (Table 5.6) in a single assay, with Z' = 0.79. At a concentration of 100 μM, the compounds are marginally active, but at concentrations 1 μM and 10 μM, the compounds are inactive.

Two more compounds, **55d** and **55c**, were screened against the resistant FCR3 strain at concentrations 100 μM (Table 5.7), 10 μM (Table 5.8), and 1 μM (Table 5.9) in a single assay, with Z'= 0.74.

These results are summarized in Figures 5.2 and 5.3. From the data obtained from the single concentration assay at a concentration of 10 μM, Compounds **55a**, **56a**, **55b**, and **55d** are classified as *inactive* against the malaria strains 3D7 and FCR3, and Compound **55c** is classified as *marginally active*.

Table 5.4 Single concentration assay against the FCR3 strain at 100 μM.

COMPOUND	% PARASITE VIABILITY	STANDARD DEVIATION
1 – **55a**	32.425	4.40
2 – **56a**	29.211	0.55
3 – **55b**	30.964	3.07
Chloroquine	22.380	2.63
Dihydroartemisinin	-5.232	2.68
Positive Control	100.000	5.56

Table 5.5 Single concentration assay against the FCR3 strain at 10 μM.

COMPOUND	% PARASITE VIABILITY	STANDARD DEVIATION
1 – **55a**	51.071	3.92
2 – **56a**	60.293	4.21
3 – **55b**	53.664	5.75
Chloroquine	26.837	2.18
Dihydroartemisinin	-3.771	2.31
Positive Control	100.000	5.56

Table 5.6 Single concentration assay against the FCR3 strain at 1 µM.

COMPOUND	% PARASITE VIABILITY	STANDARD DEVIATION
1 – **55a**	49.957	5.93
2 – **56a**	55.326	6.86
3 – **55b**	45.026	8.94
Chloroquine	7.204	3.11
Dihydroartemisinin	-0.849	4.09
Positive Control	100.000	5.56

Table 5.7 Single concentration assay against the FCR3 strain at 100 µM.

COMPOUND	% PARASITE VIABILITY	STANDARD DEVIATION
1 – **55d**	25.166	1.53
2 – **55c**	-0.053	1.38
Chloroquine	-18.731	1.29
Positive Control	100.000	4.44

Table 5.8 Single concentration assay against the FCR3 strain at 10 µM.

COMPOUND	% PARASITE VIABILITY	STANDARD DEVIATION
1 – **55d**	56.248	5.38
2 – **55c**	48.418	1.06
Chloroquine	-10.192	2.99
Positive Control	100.000	4.44

Table 5.9 Single concentration assay against the FCR3 strain at 1 µM.

COMPOUND	% PARASITE VIABILITY	STANDARD DEVIATION
1 – **55d**	51.986	13.47
2 – **55c**	57.183	5.46
Chloroquine	-4.584	1.04
Positive Control	100.000	4.44

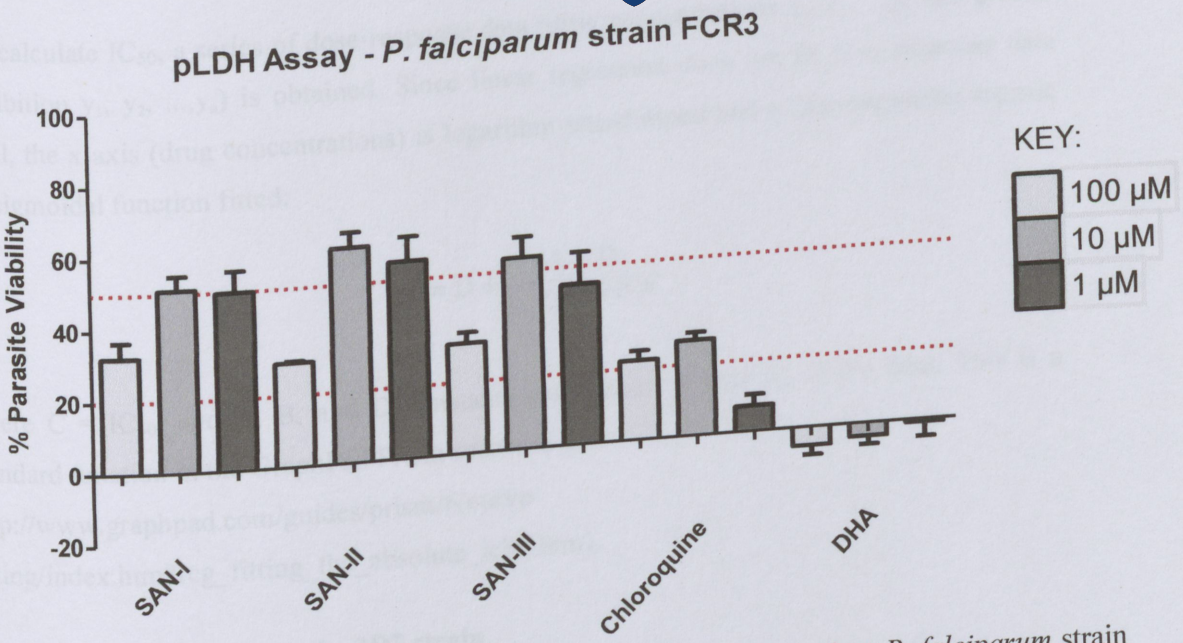

Figure 5.2 Single concentration pLDH assays of compounds against *P. falciparum* strain FCR3. SAN-I = **55a**, SAN-II = **56a**, SAN-III = **55b**.

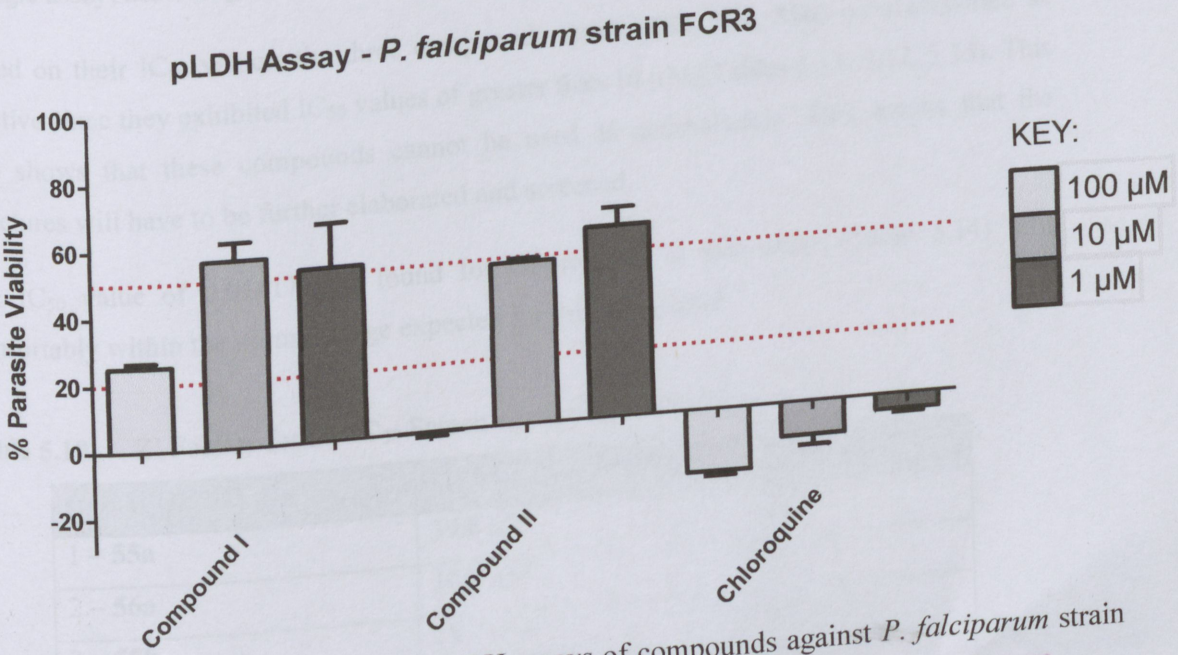

Figure 5.3 Single concentration pLDH assays of compounds against *P. falciparum* strain FCR3. Compound I = **55d**, Compound II = **55c**.

Normally, only active compounds would be screened in the subsequent IC_{50} assay. However, as all of the compounds submitted were inactive, it was decided to screen them in the subsequent IC_{50} assay against the 3D7 and FCR3 lines.

To calculate IC_{50}, a series of dose-response data (drug concentrations x_1, x_2, ...,x_n and growth inhibition y_1, y_2, ...,y_n) is obtained. Since linear regression does not fit dose-response data well, the x-axis (drug concentrations) is logarithm-transformed and a four-parameter logistic or sigmoidal function fitted:

$$y = D + \frac{A - D}{1 + 10^{(x - \log C)B}},$$

where C = IC_{50}, and A, B, and D constants calculated for best fit of the data. This is a standard function in the GraphPad Prism software (*see* http://www.graphpad.com/guides/prism/6/curve-fitting/index.htm?reg_fitting_the_absolute_ic50.htm).

5.2.3 IC_{50} Screen against the 3D7 strain

Compounds **55a**, **56a**, and **55b** were screened against the chloroquine-sensitive 3D7 strain in a single assay, achieving excellent Z' values (Table 5.10).

Based on their IC_{50} values, the three compounds tested (**55a**, **56a**, **55b**) were classified as inactive since they exhibited IC_{50} values of greater than 10 µM (Tables 5.11, 5.12, 5.13). This also shows that these compounds cannot be used as antimalarials. This means that the structures will have to be further elaborated and screened.

The IC_{50} value of 0.01417 µM found for chloroquine in this assay (Table 5.14) falls comfortably within the normal range expected for this compound.

Table 5.10 Z' Factors for the IC_{50} Screen against the 3D7 strain

COMPOUND	CALCULATED IC_{50}	Z' FACTOR
1 – **55a**	39.8 µM	0.84
2 – **56a**	39.8 µM	0.84
3 – **55b**	28.2 µM	0.85
Chloroquine	0.01417 µM	0.87

Table 5.11 Detailed results for Compound **55a** against the 3D7 strain.

Concentration (µM)	Log Conc.	%Parasite Viability	Standard Deviation
100.0	2.000	13.30	0.84
33.3	1.523	57.90	2.71
11.1	1.046	93.58	1.36
3.70	0.568	102.28	0.72
1.23	0.090	101.31	1.07
0.410	-0.357	100.74	1.20
0.137	-0.863	100.37	5.82
0.0457	-1.340	100.66	2.31
0.0152	-1.818	94.82	3.19
0.00508	-2.294	98.65	2.59
0.00169	-2.772	89.41	2.56

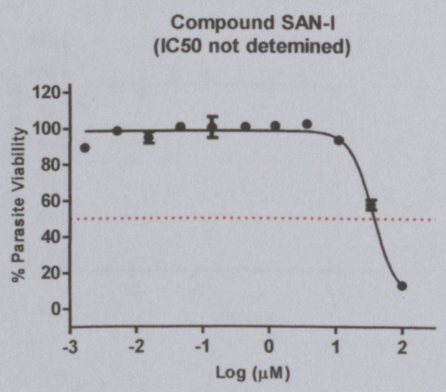

Table 5.12 Detailed results for Compound **56a** against the 3D7 strain.

Concentration (µM)	Log Conc.	%Parasite Viability	Standard Deviation
100.0	2.000	14.60	1.16
33.3	1.523	72.04	5.29
11.1	1.046	97.75	2.70
3.70	0.568	101.32	5.73
1.23	0.090	101.18	8.25
0.410	-0.357	100.05	8.00
0.137	-0.863	102.07	4.89
0.0457	-1.340	97.10	6.68
0.0152	-1.818	98.05	6.60
0.00508	-2.294	95.37	0.85
0.00169	-2.772	91.02	1.29

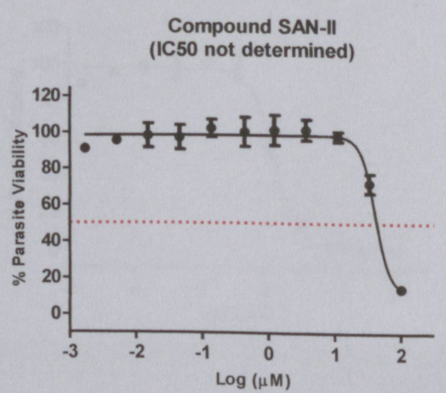

Table 5.13 Detailed results for Compound **55b** against the 3D7 strain.

Concentration (μM)	Log Conc.	%Parasite Viability	Standard Deviation
100	2.000	17.24	1.83
33.3	1.523	32.33	1.40
11.1	1.046	90.71	1.94
3.70	0.568	93.42	1.30
1.23	0.090	96.44	6.06
0.410	-0.357	95.00	1.99
0.137	-0.863	97.97	4.25
0.0457	-1.340	98.56	3.59
0.0152	-1.818	93.04	4.72
0.00508	-2.294	92.42	4.41
0.00169	-2.772	84.32	3.76

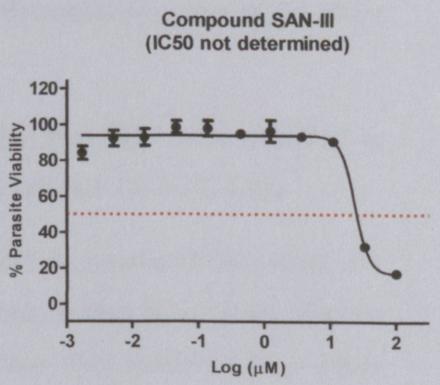

Table 5.14 Detailed results for chloroquine against the 3D7 strain.

Concentration (μM)	Log Conc.	%Parasite Viability	Standard Deviation
1.00	0.000	-1.48	0.12
0.333	-0.478	-0.90	0.63
0.111	-0.955	0.73	0.92
0.0370	-1.432	12.41	3.64
0.0123	-1.910	54.57	4.95
0.00412	-2.385	98.26	7.71
0.00137	-2.863	102.07	5.03
0.000457	-3.340	97.95	5.73
0.000152	-3.818	97.84	2.03
0.0000508	-4.294	94.74	1.73
0.0000169	-4.772	89.17	1.08

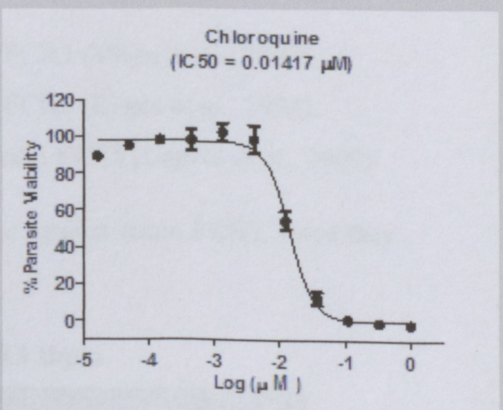

5.2.4 IC_{50} Screen against the FCR3 strain

Compounds **55a**, **56a**, and **55b** were screened against the chloroquine-resistant FCR3 strain in a single assay, achieving excellent Z' values (Table 5.15).

Based on their IC_{50} values, the three compounds tested (**55a**, **56a**, **55b**) were classified as *inactive* since they exhibited IC_{50} values greater than 10 µM (Tables 5.16, 5.17, 5.18).

Two more compounds, **55d** and **55c**, were also screened against the resistant FCR3 strain in a single assay, achieving excellent Z' values (Table 5.19). Based on their IC_{50} values, the two compounds tested (**55d**, **55c**) were classified as *inactive* since they exhibited IC_{50} values greater than 10 µM (Tables 5.20, 5.21).

The IC_{50} values of 0.06530 µM (65 nM) (Table 5.22) and 0.06114 µM (61 nM) (Table 5.23) found in the two separate series for chloroquine, and 0.18 nM (Table 5.24) for dihydroartemisinin, in the above assays fall within the standard range obtained in the CSIR laboratories and is close to those obtained in the literature (Capela *et al.*, 2009). On comparison with the standard IC_{50} obtained for chloroquine (13-16 nM), on average the FCR3 strain offers a 4/5 X protection factor for chloroquine.

Literature Values:

Chloroquine IC_{50} value = ± 160 nM for *P. falciparum* strain FCR3 (Vivas *et al.*, 2007).

Chloroquine IC_{50} value = ± 150 nM for *P. falciparum* strain FCR3 (Evans *et al.*, 1998).

Chloroquine IC_{50} value = 51.1 ± 0.1 nM for *P. falciparum* strain FCR3 (Capela *et al.*, 2009).

These results show that all the compounds tested are *inactive* against strain FCR3, since they exhibit IC_{50} values greater than 10 µM.

Table 5.15 Z' Factors for the IC_{50} Screen against the FCR3 strain.

COMPOUND	CALCULATED IC_{50}	Z' FACTOR
1 – **55a**	79.4 µM	0.70
2 – **56a**	89.1 µM	0.70
3 – **55b**	70.8 µM	0.88
Chloroquine	0.06114 µM	0.88
Dihydroartemisinin	0.0001768 µM	0.86

Table 5.16 Detailed results for Compound **55a** against the FCR3 strain.

Concentration (µM)	Log Conc.	%Parasite Viability	Standard Deviation
100	2.000	35.67	1.96
33.3	1.523	80.66	2.51
11.1	1.046	93.59	2.40
3.70	0.568	108.64	6.25
1.23	0.090	112.92	2.27
0.410	-0.357	115.84	1.80
0.137	-0.863	120.16	2.59
0.0457	-1.340	116.34	2.85
0.0152	-1.818	114.43	1.18
0.00508	-2.294	115.64	3.07
0.00169	-2.772	103.56	2.60

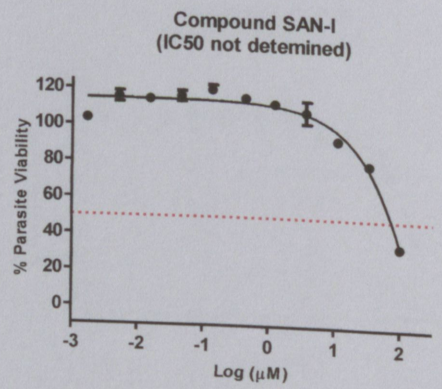

Table 5.17 Detailed results for Compound **56a** against the FCR3 strain.

Concentration (µM)	Log Conc.	%Parasite Viability	Standard Deviation
100	2.000	30.70	4.93
33.3	1.523	99.17	5.31
11.1	1.046	102.84	4.39
3.70	0.568	121.13	1.72
1.23	0.090	119.90	2.47
0.410	-0.357	120.05	6.15
0.137	-0.863	122.38	1.49
0.0457	-1.340	123.79	7.41
0.0152	-1.818	117.11	4.15
0.00508	-2.294	110.96	2.54
0.00169	-2.772	105.91	1.65

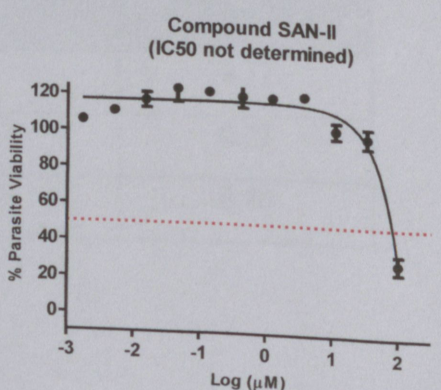

Table 5.18 Detailed results for Compound **55b** against the FCR3 strain.

Concentration (μM)	Log Conc.	%Parasite Viability	Standard Deviation
100	2.000	32.68	1.06
33.3	1.523	74.31	7.27
11.1	1.046	91.80	11.22
3.70	0.568	92.25	5.79
1.23	0.090	100.44	9.31
0.410	-0.357	99.82	8.02
0.137	-0.863	98.59	4.24
0.0457	-1.340	100.87	10.02
0.0152	-1.818	94.63	7.04
0.00508	-2.294	97.87	8.41
0.00169	-2.772	100.44	6.01

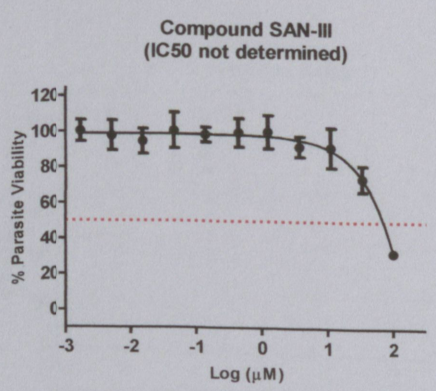

Table 5.19 Z' Factors for the IC_{50} Screen against the FCR3 strain.

COMPOUND	CALCULATED IC_{50}	Z' FACTOR
1 – **55d**	89.1 μM	0.77
2 – **55c**	25.1 μM	0.77
Chloroquine	0.06530 μM	0.80

Table 5.20 Detailed results for Compound **55d** against the FCR3 strain.

Concentration (μM)	Log Conc.	%Parasite Viability	Standard Deviation
100	2.000	48.22	1.82
33.3	1.523	82.81	12.38
11.1	1.046	86.01	4.42
3.70	0.568	93.79	3.66
1.23	0.090	94.95	5.58
0.410	-0.357	99.99	7.44
0.137	-0.863	91.39	11.55
0.0457	-1.340	90.60	11.27
0.0152	-1.818	91.59	6.02
0.00508	-2.294	97.92	7.79
0.00169	-2.772	98.09	9.29

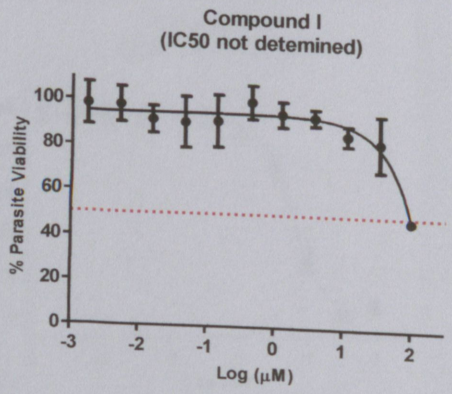

Table 5.21 Detailed results for Compound **55c** against the FCR3 strain.

Concentration (μM)	Log Conc.	%Parasite Viability	Standard Deviation
100	2.000	21.66	3.32
33.3	1.523	43.74	7.59
11.1	1.046	72.93	8.03
3.70	0.568	92.20	5.03
1.23	0.090	99.97	4.49
0.410	-0.357	98.30	6.43
0.137	-0.863	92.68	4.66
0.0457	-1.340	95.13	8.26
0.0152	-1.818	92.89	3.72
0.00508	-2.294	91.34	2.62
0.00169	-2.772	99.48	3.15

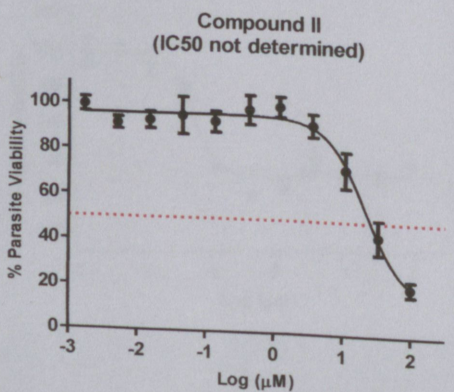

Table 5.22 Detailed results for chloroquine against the FCR3 strain.

Concentration (µM)	Log Conc.	% Parasite Viability	Standard Deviation
1.00	0.000	3.75	2.43
0.333	-0.478	-0.12	2.47
0.111	-0.955	26.69	5.13
0.0370	-1.432	72.78	4.15
0.0123	-1.921	87.86	2.56
0.00412	-2.385	95.83	3.81
0.00137	-2.863	96.32	1.98
0.000457	-3.340	95.45	2.70
0.000152	-3.818	96.96	4.28
0.0000508	-4.294	98.17	5.95
0.0000169	-4.772	99.96	6.31

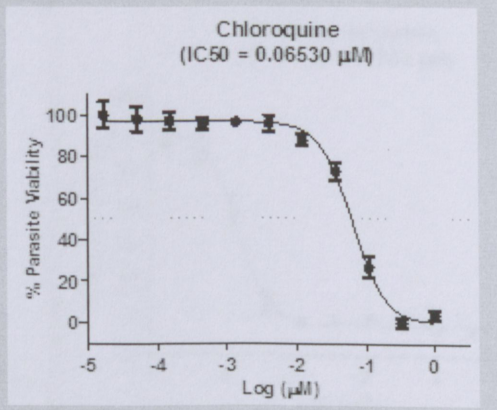

Table 5.23 Detailed results for chloroquine (second series) against the FCR3 strain.

Concentration (µM)	Log Conc.	%Parasite Viability	Standard Deviation
100	2.000	36.68	0.63
33.0	1.523	28.65	3.60
11.1	*1.046**	*46.70**	*1.93**
3.70	0.569	38.39	6.23
1.24	0.092	24.19	3.87
0.412	-0.385	19.44	1.11
0.137	-0.863	35.33	2.21
0.0457	-1.340	77.09	2.61
0.0152	-1.818	91.58	8.21
0.00508	-2.294	99.97	2.06
0.00169	-2.772	97.02	7.73

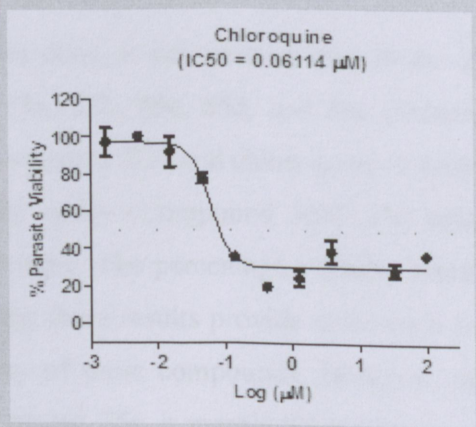

** Indicates data points that were excluded from the final graph as they were considered to be outliers*

Table 5.24 Detailed results for dihydroartemisinin against the FCR3 strain.

Concentration (µM)	Log Conc.	%Parasite Viability	Standard Deviation
1.00	0.000	-10.21	2.72
0.333	-0.478	-5.86	2.05
0.111	-0.955	-5.21	2.82
0.0370	-1.432	-0.67	1.39
0.0123	-1.910	-0.74	2.06
0.00412	-2.385	-1.11	1.85
0.00137	-2.863	-2.80	1.43
0.000457	-3.340	7.66	5.97
0.000152	-3.818	56.57	8.19
0.0000508	-4.294	90.01	7.94
0.0000169	-4.772	100.02	8.30

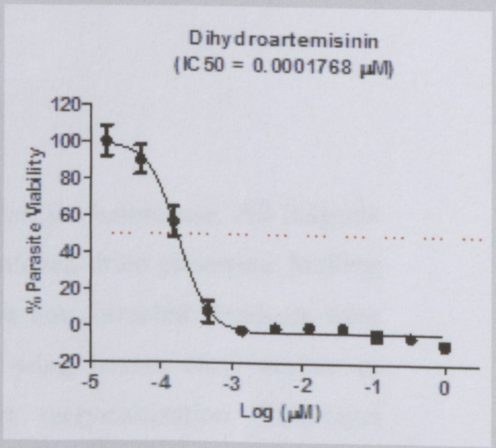

5.3 Conclusions

Based on all the single-concentration assays that were done, it was evident that all the Z' factors warranted further investigation. Compounds **55a**, **55b**, **55c**, **55d**, and **56a** (Scheme 3.9, Table 3.1) were screened against the chloroquine-sensitive 3D7 and chloroquine-resistant FCR3 strains and found to be inactive or marginally active (Compound **55c**). The other compounds were of insufficient stability to warrant testing. The percentage viability results show that the tested compounds have moderate activity; these results provide motivation for further structural modification to improve the efficacy of these compounds. However, the IC_{50} results disappointingly indicate that only one compound, **55c**, is marginally active.

These compounds therefore cannot be used as antimalarials, but need to be further elaborated (as sketched in Chapter 7) and screened.

Chapter 6

Experimental

6.1 General conditions

All reaction and chromatography solvents were dried and distilled before use. All reagents used were commercially sourced. All experiments were run in oven-dried glassware. Melting points were measured with a Büchi SMP apparatus and are not corrected. Products were purified using column chromatography on silica gel 60 using hexane-ethyl acetate or chloroform-methanol mixtures as mobile phase, and by recrystallization. Thin-layer chromatography was performed on precoated TLC plates (silica gel with UV indicator added). NMR spectra were recorded on a Bruker Avance III 400 at the following frequencies: 400 MHz (^{1}H) and 100 MHz (^{13}C). Chemical shifts of ^{1}H and ^{13}C NMR spectra are reported in ppm using residual non-deuterated solvent as an internal standard. Challenges at crucial moments led to several spectra not being recorded. However, circumstantial evidence indicated the identities of all compounds reported below. Infrared spectra were recorded on a Bruker Alpha FTIR spectrometer, when available.

6.2 Imine condensation with propargyl aldehyde and malonate derivatives

L-Phenylalanine methyl ester hydrochloride (41)

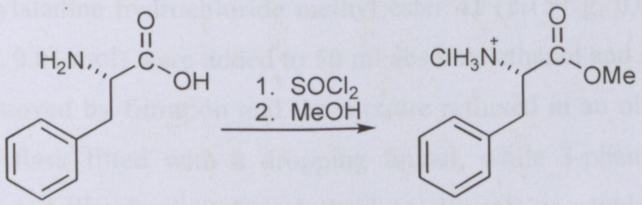

Thionyl chloride (6.0 ml, 82.1 mmol) was added drop-wise to a stirred suspension of L-phenylalanine (9.03 g, 54.7 mmol) in methanol (100 ml) at 0°C. This mixture was stirred for 24 h at room temperature and the solvent was removed by evaporation. The crude product was recrystallized from EtOAc/EtOH (95:5) to give a white solid (8.76 g, 90% yield), m.p. 153 – 155°C (EtOAc/EtOH) (Lit. 159 – 161°C (Tietze and Eicher, 1981)).

^{1}H-NMR (D_2O): δ_H 3.21 (1H, dd, J = 14.6, 7.4, PhC*H*H), 3.34 (1H, dd, J 14.6, 5.2, PhCH*H*), 3.82 (3H, s, CH_3), 4.42 (1H, dd, J = 5.2, 7.4, C*H*), 7.28 (2H, m, Ar-C*H*), 7.37 − 7.45 (3H, m, Ar-C*H*); ^{13}C-NMR (D_2O): δ_C 35.6 (*C*H$_3$), 53.6 (*C*H$_2$), 54.1 (*C*H), 128.2 (Ar-*C*H), 129.3 (2 × Ar-*C*H), 129.4 (2 × Ar-*C*H), 133.7 (Ar-*C*), 170.1 (*C*=O).

L-Phenylalanine methyl ester (42)

Anhydrous $NaHCO_3$ (1.26 g, 0.015 mol) dissolved in about 20 ml water was added to L-phenylalanine hydrochloride methyl ester **41** (2.157 g, 0.01 mol) in 50 ml toluene and the mixture was vigorously stirred for 6 h. The two phases were separated and the aqueous phase was extracted twice with toluene. The toluene phases were combined, dried briefly over anhydrous potassium carbonate, filtered and the solvent evaporated. The amino ester was used immediately or kept in a freezer.

^{1}H-NMR ($CDCl_3$): δ_H 7.34-7.37 (3H, m, Arom), 7.23 (d, 1H, Arom), 7.21 (d, 1H, Arom), 4.36 (t, 1H, >C*H*-), 3.77 (s, 3H, -OC*H*$_3$), 3.29-3.13 (m, 2H, -C*H*$_2$-); ^{13}C-NMR ($CDCl_3$): δ_C 35.7 (-*C*H$_3$), 53.7 (-*C*H$_2$-), 54.2 (>*C*H-), 128.2 (Arom), 129.5 (Arom), 133.8 (Arom), 170.1 (>*C*=O).

Synthesis of imine (Schiff base) 43

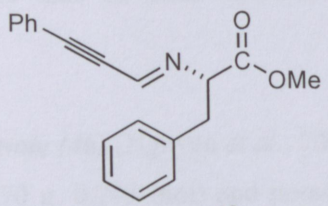

43

L-Phenylalanine hydrochloride methyl ester **41** (2.157 g, 0.01 mol) and anhydrous Na_2CO_3 (1.06 g, 0.01 mol) were added to 50 ml absolute ethanol and stirred for 3 h. The NaCl formed was removed by filtration and the mixture refluxed in an oil bath at 85˚C in a 250 ml two-necked flask fitted with a dropping funnel, while 3-phenylpropargyl aldehyde (1.423 g, 0.0105 mol dissolved in 50 ml absolute ethanol) was added drop-wise. After 3 h heating under reflux, the solution was concentrated under reduced pressure to 10 ml. After cooling to room temperature, the mixture was left overnight in the fridge. The solvent was evaporated to give a brownish residue (2.16 g, 74%). The residue was purified by CC (hexane-ethyl acetate 4:1) and gave **43** as a light brown syrupy product.

^{1}H-NMR ($CDCl_3$): δ_H 2.6 (1H, d, benzylic *H*), 3.10 (1H, d, benzylic H), 3.50 (1H, t, α-*H*), 3.78 (3H, s,-OCH_3), 6.07 (1H, s, vinylic *H*), 7.31-7.64 (10H, m, aryl).

Synthesis of diethyl 2-phthalimidomalonate (46)

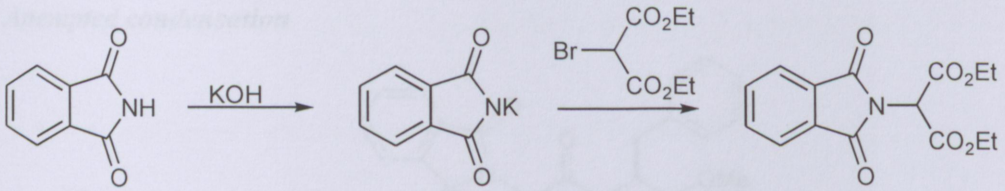

44 **45** **46**

Potassium phthalimide (45)

Phthalimide **44** (50 g, 0.338 mol) and 1 L absolute ethanol were heated gently under reflux for about fifteen minutes or until no more of the phthalimide dissolved. The hot solution was decanted from any solid into a specially prepared solution of KOH (19.1 g, 0.34 mol, prepared as follows: 19.07 g KOH was dissolved in 19 ml water. To this solution was then added 56.3 ml absolute ethanol). A precipitate of potassium phthalimide **45** separated at once. The mixture was stirred and cooled quickly to room temperature, and the precipitate was filtered with suction. The crystals were washed with 100 ml acetone to remove any unchanged phthalimide, and then air-dried to yield 47 g (68%) potassium phthalimide (Osterberg, 1927, 1941).

Diethyl 2-phthalimidomalonate (46) (Nguyen *et al.*, 2008)

Diethyl 2-bromomalonate (70 g, 0.293 mol) and potassium phthalimide **45** (55 g, 0.2 mol) were intimately stirred together. The mixture was stirred every ten minutes. As the temperature started to drop, the mixture was heated in an oil bath at 110°C for one hour to ensure completion of the reaction. The mixture was then poured into a mortar where it solidified to a solid mass. The cooled mixture was ground with water to leach as much of the produced KBr as possible, and filtered. The precipitate was again ground with water and filtered, and finally washed thoroughly with water. The wet precipitate was then heated with 134 ml benzene to boiling. After cooling, the insoluble KBr and phthalimide were removed by filtration. The benzene solution was dried over calcium chloride, and after filtration the benzene was removed by evaporation under vacuum. The hot residue was poured into a mortar and left to solidify on cooling. The resulting crystalline mass was then ground with small amounts of diethyl ether (4x 20 ml), filtered, and washed with small amounts of ether

until white. The yield of diethyl phthalimidomalonate (**46**) was 20.39 g (46%), melting at 73-74°C (Lit. 73-74°C (Nguyen *et al.*, 2008)). Spectral data corresponded to those of Nguyen *et al.* (2008).

Attempted condensation

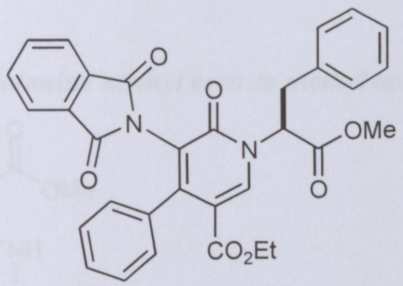

47

A solution of sodium methoxide (0.4 mmol) in 2 ml dioxane was added to a solution of malonate **46** (0.153 g, 0.5 mmol) in 2 ml dioxane. Crude alkynyl imine **43** (59 mg, 0.2 mmol) in 2 ml dioxane was then added while stirring at room temperature. The reaction mixture was heated under reflux for several hours and then cooled to room temperature. Brine (10 ml) was added to quench the reaction, and the mixture was extracted with 3x15 ml dichloromethane. The combined extracts were dried with anhydrous sodium sulphate and filtered. The solvent was evaporated to give 0.74 g of brownish syrup and the residue was purified by TLC and CC using hexane-ethyl acetate 4:1 as mobile phase. No satisfactory spectra could be recorded.

Diethyl 2-(4-methylpiperazino)malonate (48)

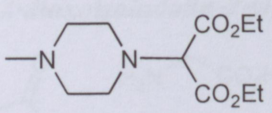

48

To a stirred solution of 58.7 g (0.2 mol) 1-methylpiperazine in 100 ml dried benzene, 70.12 g (0.294 mol) of diethyl 2-bromomalonate was added drop-wise, and the mixture was stirred for 2 d. The mixture was filtered and evaporated to yield a liquid, which was purified by column chromatography over silica gel, eluting with CH_2Cl_2 (58 g, 76.5%).

^{1}H-NMR ($CDCl_3$): δ_H 1.27 (6H, t, ester -C*H*$_3$), 2.25 (3H, s, >NC*H*$_3$), 2.47 (4H, s, 2x piperazine -CH_2-), 2.60 (4H, s, 2x piperazine -CH_2-), 4.00 (1H, s, C*H*). ^{13}C-NMR ($CDCl_3$):

δ_C 14.1 (>N-*C*H_3), 45.97 (ester *C*H_3), 50.08 (piperazine –*C*H_2-), 55.18 (piperazine –*C*H_2-), 61.25 (ester –*C*H_2-), 70.77 (*C*H), 166.88 (*C*=O).

6.3 Amino ester condensations with amino acid derivatives

Michael addition of L-phenylalanine methyl ester to methyl acrylate

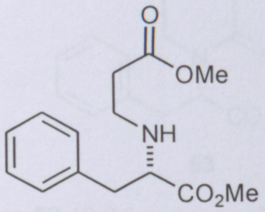

50

L-Phenylalanine methyl ester **42** (2.32 g, 0.01 mol) and methyl acrylate **49** (0.08 g, 0.01 mol) were added to 10 ml methanol and stirred for 24 h. The solution was evaporated to yield **50**, a new compound, as a yellowish syrup (2.12 g, 0.008 mol, 80%), which showed a single spot on TLC.

^{1}H-NMR (CD_3OD): δ_H 3.13-3.29 (4H, m, -C*H*$_2$-); 3.68 (3H, s, -OC*H*$_3$), 3.72 (2H, t, -C*H*$_2$-), 3.77 (3H, s, -OC*H*$_3$), 4.36 (1H, t, >C*H*-), 7.21 (1H, d, Arom), 7.23 (1H, d, Arom), 7.37-7.34 (3H, m, Arom); ^{13}C-NMR (CD_3OD): δ_C 35.7 (-*C*H_3), 53.7 (-*C*H_2-), 54.2 (>*C*H-), 128.2 (Arom), 129.5 (Arom), 133.8 (Arom), 170.1 (>*C*=O).

Phthalylglycine (2-(1,3-dioxoisoindolin-2-yl)acetic acid) (52) (Upadhyay *et al.*, 2009)

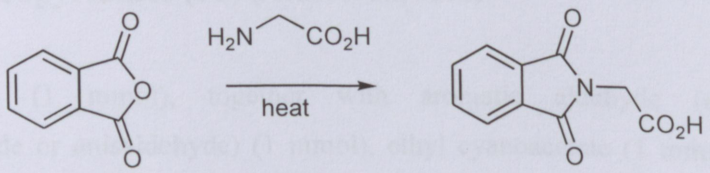

Phthalic anhydride **51** (2.96 g, 19.98 mmol, 1 eq) and glycine (1.53 g, 20.37 mmol, 1.02 eq) were melted and stirred in an oil bath at 135-150°C for 30 min. The mixture was cooled to room temperature, dissolved in 30 ml hot methanol, and then 30 ml cold water was added. The precipitate was filtered, washed with 100 ml water and dried *in vacuo*. Recrystallization from a mixture of acetic acid/H_2O = 1/1 gave the desired products as off-white powder to give 2.3 g (56 %) 2-(1,3-dioxoisoindolin-2-yl)acetic acid **52**. The product was used without further purification. M.p. 185°C (Lit. 193–196°C (Upadhyay *et al.*, 2009)).

^{1}H-NMR (CD_3OD): δ_H 4.42 (2H, s, CH_2), 7.84 (2H, dd, arom), 7.91(2H, dd, arom); ^{13}C-NMR (CD_3OD): δ_C 38.17 (CH_2), 122.97 (*C*H, arom), 131.93 (=*C*<), 134.21 (*C*H, arom), 167.63 (*C*=O imide), 169.40 (*C*=O acid).

Tertiary amide 53

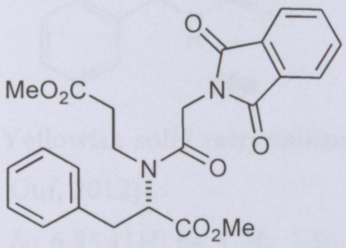

53

The Michael adduct **50** (0.26 g, 1 mmol) was dissolved in 20 ml anhydrous dichloromethane and cooled to 0°C. A mixture of dicyclohexylcarbodiimide (DCC) (0.21 g, 1.01 mmol), *N,N*-dimethylaminopyridine (DMAP) (0.01 g, 0.1 mmol) and 2-(1,3-dioxoisoindolin-2-yl)acetic acid **52** (0.205 g, 1 mmol) was added to this solution while stirring at 0°C until the reaction was complete (monitored by TLC). The precipitated dicyclohexylurea, indirect evidence of amide formation, was removed by filtration. The filtrate was evaporated and the residue purified by CC with CH_2Cl_2 as eluent to give 0.2 g of a liquid product. However, the NMR spectra were inconclusive and not consistent with those expected for **53**.

6.4 Synthesis of 3-cyano-2-pyridones (55) and 3-cyano-2-imino-1,2-dihydropyridines (56) (Abadi *et al.*, 2010)

Acetophenone (1 mmol), together with aromatic aldehyde (*e.g.* benzaldehyde, cinnamaldehyde or anisaldehyde) (1 mmol), ethyl cyanoacetate (1 mmol), and ammonium acetate (8 mmol) were dissolved in ethanol (30 ml) and heated overnight under reflux (15-16 h; TLC monitor). The precipitate obtained was filtered, washed with ethanol and dried (anh. K_2CO_3). The precipitate was purified either by recrystallization (as indicated), or by column chromatography on silica gel, eluting with dichloromethane.

2-Oxo-4,6-diphenyl-1,2-dihydropyridine-3-carbonitrile (55a)

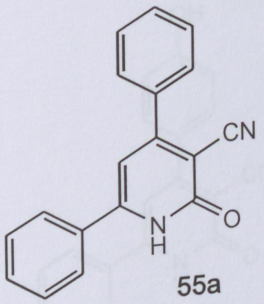

55a

Yield: 0.19 g (78%). Yellowish solid recrystallized from acetic acid, m.p. 332-335°C (Lit. >300°C (El-Sayed and Ouf, 2012)).

^{1}H-NMR (DMSO-d_6): δ_H 6.85 (1H, bs, C*H*), 7.56 (6H, m, arom), 7.75 (2H, m, arom), 7.91 (2H, m, arom), 12.8 (bs, 1H, N*H*); ^{13}C-NMR (DMSO-d_6): δ_C 116.9, 128.2, 128.7, 129.3, 129.4, 130.9, 131.7, 136.5.

2-Imino-4,6-diphenyl-1,2-dihydropyridine-3-carbonitrile (56a)

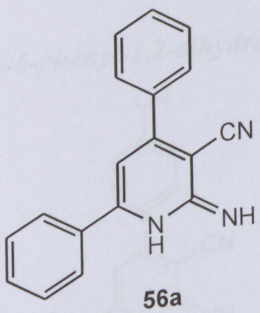

56a

Yield: 0.17 g (65%). Yellowish solid recrystallized from ethanol, m.p. 185°C (Lit. 186-187°C (El-Sayed and Ouf, 2012)).

^{1}H-NMR (DMSO-d_6): δ_H 5.35 (2H, s, NH_2), 6.80 (1H, s, C*H*), 7.55 (6H, m, arom), 7.65 (2H, m, arom), 8.05 (2H, d, J = 4.0 Hz, Ph); ^{13}C-NMR (DMSO-d_6): δ_C 116.4, 119.1, 129.0, 129.2, 129.9, 137.9, 150.3, 162.8.

4-(4-Hydroxyphenyl)-2-oxo-6-phenyl-1,2-dihydropyridine-3-carbonitrile (55b)

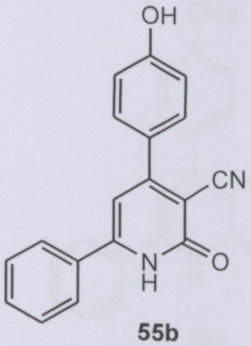

55b

A new compound, yield: 0.19 g (68%). Yellowish solid recrystallized from a mixture of DMF-ethanol (1:10), m.p. 376-379°C.

^{1}H-NMR (DMSO-d_6): δ_H 6.77 (1H, s, C*H*), 6.93 (2H, dd, J = 8.8, 2.8 Hz, arom), 7.54 (3H, m, arom), 7.64 (2H, dd, J = 8.8, 2.8 Hz, arom), 7.87 (2H, m, arom), 7.96 (1H, s, O*H*), 10.23 (1H, bs, N*H*); ^{13}C-NMR (DMSO-d_6): δ_C 116.1, 117.5, 126.9, 128.1, 129.4, 130.6, 131.5, 160.3, 162.8.

4-(4-Hydroxyphenyl)-2-imino-6-phenyl-1,2-dihydropyridine-3-carbonitrile (56b)

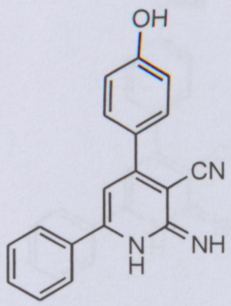

56b

A new compound, yield: 0.13 g (45%). Yellowish solid recrystallized from a mixture of DMF-ethanol (1:10), m.p. 206-209°C.

^{1}H-NMR (DMSO-d_6): δ_H 5.31 (2H, s, NH_2), 6.93 (1H, s, C*H*), 6.99 (2H, dd, J = 8.8, 2.8 Hz, arom), 7.58 (3H, m), 7.66 (2H, dd, J = 8.8, 2.8 Hz, arom), 7.93 (2H, m, arom), 7.43 (1H, s, O*H*); ^{13}C-NMR (DMSO-d_6): δ_C = 116.1, 117.5, 126.9, 128.1, 129.4, 132.6, 135.5, 161.3, 163.5.

4-(4-Methoxyphenyl)-2-oxo-6-phenyl-1,2-dihydropyridine-3-carbonitrile (55c)

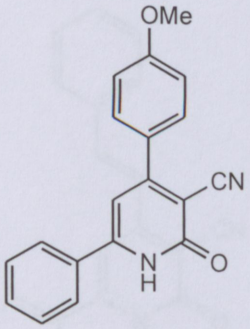

55c

A new compound, yield: 0.16 g (57%), m.p. 333-338°C.

IR (cm^{-1}): 3455, 2220, 1650; ^{1}H-NMR (DMSO-d_6): δ_H 3.87 (3H, s, -OCH_3), 6.81 (1H, bs, C*H*), 7.14 (2H, d, J = 8.8 Hz, arom), 7.76 (2H, dd, J = 8.8 Hz, arom), 7.57 (3H, m, arom), 7.90 (2H, m, arom), 12.74 (1H, s, NH); ^{13}C-NMR (DMSO-d_6): δ_C 55.9, 128.2, 128.5, 129.4, 130.5, 131.6, 161.6.

2-Imino-4-(4-methoxyphenyl)-6-phenyl-1,2-dihydropyridine-3-carbonitrile (56c)

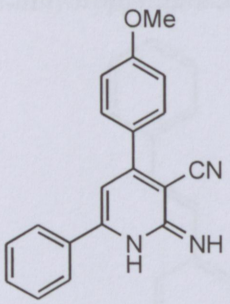

56c

Yield: 0.13 g, m.p. 296-300°C (d).

IR (cm^{-1}): 3136 (arom C-H), 2220 (CN), 1643 (arom C=C).

NMR: The compound decomposed rapidly in solution, so that no satisfactory spectra could be obtained.

E-2-oxo-6-phenyl-4-styryl-1,2-dihydropyridine-3-carbonitrile (55d)

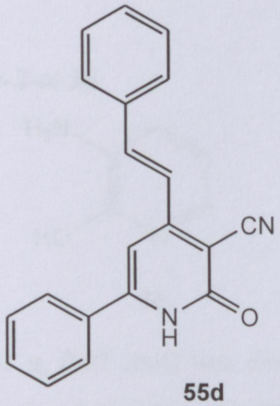

55d

A new compound, yield: 0.19 g (63%), m.p. 301-350°C.

IR (cm^{-1}): 3024 (arom CH), 2928 (NH), 2214 (CN), 1642 (C=O); ^{1}H-NMR (DMSO-d_6): δ_H 7.26 (1H, d, J = 16 Hz, vinylic),7.49 (2H, m, aromatic), 7.58 (1H, d, aromatic), 7.59 (1H, s, pyridyl), 7.73 (1H, d, arom), 7.90 (1H, d, arom), 8.01 (1H, d, J = 18 Hz, vinylic); ^{13}C-NMR (DMSO-d_6): δ_C 116.4, 122.5, 128.2, 129.1, 129.3, 129.4, 129.6, 131.5, 140.4.

E-2-imino-6-phenyl-4-styryl-1,2-dihydropyridine-3-carbonitrile (56d)

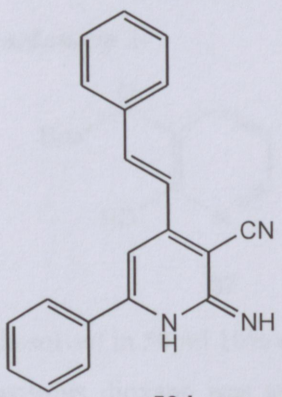

56d

Yield: 0.15 g, m.p. 244-247°C (d).

IR (cm^{-1}): 3187 (C=NH), 2927 (NH), 2196 (CN), 1672 (arom C=C).

NMR: The compound decomposed rapidly in solution, so that no satisfactory spectra could be obtained.

6.5 Substituted 2-pyridones from 3-nitropyrid-2-one (Verissimo *et al.*, 2008)

Synthesis of 3-aminopyridin-2-ol 36

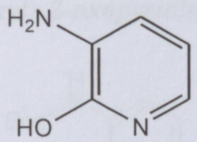

36

3-Nitro-2-pyridone **35** (1.401 g, 0.01 mol) was dissolved in 70 ml ethanol, 0.1g Pd-C was added and the mixture was stirred at room temperature under a H_2 atmosphere for 2d. The catalyst was removed by filtration, washed with ethanol and the combined solution was evaporated. The product was purified by crystallization from ethanol-water to yield **36** as yellow crystals (0.8 g, 57%), m.p. 121-124°C (Lit. 124°C (Nam *et al.*, 2011)).

IR (cm^{-1}): 3424 (NH), 3300 (OH), 1613 (arom C=C); ^{1}H-NMR (DMSO-d_6): δ_H 5.03 (2H, s, -N*H*$_2$), 6.02 (1H, s, arom C*H*), 6.45 (1H, d, arom C*H*), 6.63 (1H, d, arom C*H*), 11.39 (1H, bs, OH); ^{13}C-NMR (DMSO-d_6): δ_C 106.72, 111.49, 120.59, 139.29, 158.19.

tert-Butyl 2-hydroxypyridin-3-yl carbamate 37

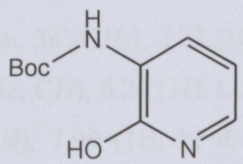

37

Amine **36** (1.10 g, 0.01 mol) was dissolved in 50 ml 10% aq. acetic acid. A solution of Boc_2O (2.23 g, 0.01 mol) in 50 ml anhydrous dioxane was added drop-wise to the well-stirred solution. The mixture was stirred overnight and 400 ml water was then added. The mixture was washed with 3 x 100 ml diethyl ether. The aqueous phase was basified with 2 N NaOH to pH 14 and extracted with 3x 200 ml diethyl ether. The combined extract was washed with 2x 150 ml water, dried over anhydrous Na_2SO_4, filtered, and concentrated under reduced pressure to yield a new compound **37** as white crystals (1.3 g, 64%), m.p. 162-164°C.

IR (cm^{-1}): 3425 (NH), 3394 (OH), 3129 (arom. CH), 2978 (aliphatic CH), 1722 (C=O), 1644, 1620 (C=C), 1113 (C-O); ^{1}H-NMR (DMSO-d_6): δ_H 1.47 (9H, s, C*H*$_3$), 6.21 (1H, s, arom C*H*), 7.70 (1H, d, arom C*H*), 7.72 (1H, s, N*H*), 7.80(1H,d, aromatic), 11.96 (1H, s, OH); ^{13}C-NMR (DMSO-d_6): δ_C 28.3 (*C*H$_3$), 80.52 (quat. *C*), 105.87 (aromatic *C*H), 121.19 (aromatic *C*H),

127.08 (aromatic quat. *C*), 129.50 (aromatic *C*-N), 152.61 (pyridone *C*=O), 157.51 (Boc *C*=O).

Ethyl 2-(3-(tert-butoxycarbonyl)-2-oxopyridin-1(2H)-yl)butanoate 61

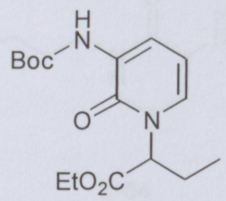

61

Compound **37** (0.210 g, 0.010 mol) was dissolved in 10 ml anhydrous THF and NaH (0.44 g, 0.011 mol, 60% in petrol) carefully added, under an inert atmosphere (Ar). After stirring 30 to 60 min, bromoester **60** (2.146 g, 0.011 mol) was added and stirring continued 2h, while carefully increasing the temperature to 50°C under an inert atmosphere (Ar, TLC monitor). After cooling, the reaction was quenched by addition of 10 ml water, followed by repeated extraction with ethyl acetate, to yield a new compound, **61**, as an oil that was purified by CC with dichloromethane as solvent. Yield: 0.324 g (10 %).

^{1}H-NMR ($CDCl_3$): δ_H 0.92 (3H, t, J = 7.4 Hz, 4'-CH_3), 1.27 (3H, t, J = 7.2 Hz, CH_3-CH_2-O), 1.51 (9H, s, *t*-butyl CH_3), 1.99 (1H, m, 3a'-CH_2), 2.27 (1H, m, 3b'-CH_2), 4.22 (2H, q, J = 7.2 Hz, -CH_2-O), 5.45 (1H, dd, J = 5.2 Hz, C*H*), 6.29 (1H, t, J = 7.2, arom C*H*), 6.96 (1H, dd, J = 5.2 Hz, arom C*H*), 7.67 (1H, s, N*H*), 7.99 (1H, br d, J = 6.8 Hz, arom C*H*); ^{13}C-NMR ($CDCl_3$): δ_C 10.37 (acyl-CH_3), 14.09 (ester-CH_3), 24.06 (acyl-CH_2), 28.24 (*t*-butyl CH_3), 61.74 (ester-CH_2), 80.67 (quat. *C*), 106.67 (aromatic *C*H), 119.30 (aromatic *C*H), 126.16 (aromatic quat. *C*), 129.63 (aromatic *C*-N), 152.79 (pyridone *C*=O), 157.37 (Boc *C*=O), 168.94 (ester-*C*=O).

6.6 Molecular modelling and docking studies

The 3D X-ray structure of the FP2 crystal structure (PDB ID: 3BPF) complexed with **E-64** was chosen as the template to compare the docking modes with falcipain-2 of the synthesised compounds. The crystal structure was obtained from the RCSB Protein Data Bank (http://www.rcsb.org/pdb/home/home.do). Molecular docking was performed using the CDOCKER protocol within Discovery Studio 4.0. For ligand preparation, the 3D structures

of the compounds were generated and minimized using Discovery Studio 4.0. For enzyme preparation, hydrogen atoms were added, and water and impurities were removed. The molecular docking was performed by inserting each compound into the binding pocket of Chain A of FP2, based on the binding mode.

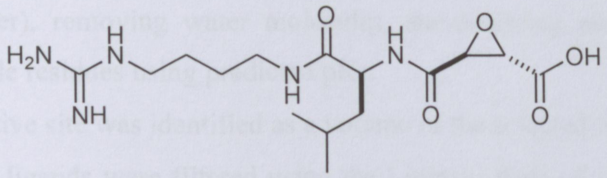

E-64

The protein report for Chain A showed the following:

1. Gap between residues Asn188 and Gly194
2. Incomplete residues: Asn188
3. Ligand: $C_{15}H_{30}N_5O_5$ (E64-242)
4. Crystallographic Resolution: 2.90 Ångstrom
5. Number of Amino Acids: 236
6. Two PDB active sites: AC1 (Gln36, Gly40, Ser41, Cys42, Trp43) and AC5 (Gln209)
7. Chain A amino acid sequence:

QMNYEEVIKK YRGEENFDHA AYDWRLHSGV TPVKDQKNCG SCWAFSSIGS
VESQYAIRKN KLITLSEQEL VDCSFKNYGC NGGLINNAFE DMIELGGICP
DGDYPYVSDA PNLCNIDRCT EKYGIKNYLS VPDNKLKEAL RFLGPISISV
AVSDDFAFYK EGIFDGECGD QLNHAVMLVG FGMKEIVNGE KHYYYIIKNS
WGQQWGERGF INIETDESGL MRKCGLGTDA FIPLIE

The site sphere was selected based on the ligand binding location of E64-242, the E64-242 molecule was removed and each compound was then placed using the molecular docking procedure. The interaction modes of the enzyme and docked ligand were analysed after molecular docking. Ten docking poses were saved for each ligand and the final docked conformation was scored.

Methodology

- The Clean Protein protocol was executed to correct connectivity, add missing atoms, and correct names.

- The Prepare Protein protocol from Discovery Studio was used to prepare FP2 for docking.
- The protocol prepares the protein by running tasks like inserting missing atoms in incomplete residues, modelling missing loop regions, deleting alternate conformations (disorder), removing water molecules, standardizing atom names and protonating titratable residues using predicted pKs.
- The active site was identified as a volume of the selected ligand.
- Eleven ligands were filtered using the Lipinski Rule of 5 (Lipinski *et al.*, 1997) and they were further prepared for docking using the Prepare Ligands protocol where 28 ligands were created.
- The 28 prepared ligands were screened against the prepared FP2 using CDOCKER in Discovery studio 4.0.
- CDOCKER is a grid-based molecular docking method that employs CHARMm to generate random ligand conformations through high temperature molecular dynamics.
- Docked conformations were scored using various scoring functions (LigScore1, LigScore2, PLP1, PLP2, Jain, PMF and PMF04), followed by consensus scoring which uses the combination of various scoring functions to identify ligands that score high in more than one scoring function.
- CDOCKER_ENERGY was also considered in selecting ligands that scored high. It is reported as the negative value, where a higher value indicates a more favourable binding. This enables the energy to be used like a score. This score includes internal ligand strain energy and receptor-ligand interaction energy, and is used to sort the poses of each input ligand.

6.7 *In vitro* antiplasmodial pLDH assay

The in vitro antiplasmodial assays were performed by Dr Jenny-Lee Panayides of the CSIR, Pretoria.

6.7.1 Assay background

The *in vitro* antimalarial activities of test samples against a CQ-sensitive and a CQ-resistant strain of the malaria parasite were measured by assessing parasite survival after drug exposure using a colorometric parasite lactate dehydrogenase (pLDH) enzyme assay. The

lactate dehydrogenase enzyme occurs in all the cells of the parasite; its function is to catalyse the formation of pyruvate from lactate by reducing the co-enzyme NAD^+ (nicotinamide adenine dinucleotide) to NADH.

In the pLDH assay, the NAD^+ analogue APAD (3-acetylpyridine adenine nucleotide) is reduced to APADH and in turn, a yellow Nitro Blue tetrazolium/phenazine ethosulphate reagent is converted to purple formazan crystals. The absorbance was read at 620 nm using a multiwell spectrophotometer (Tecan Infinite F500, iControl 1.5). Formazan formation is directly proportional to pLDH activity, which in turn is indicative of the number of parasites in the cultures following drug exposure. Assay specificity is ensured by the inability of human LDH, found in the host red blood cells, to use APAD as a co-factor.

The inhibitory activity of each compound was determined by preparing test samples in parasite culture medium in transparent 96-well flat bottom plates (Greiner Bio-one) – 100 µM, 10 µM, 1 µM concentrations (n = 3 for each data point). Parasitized red blood cells were added to give a final concentration of 1% haematocrit at 2% parasitaemia, and the plates were incubated for 48 hours before proceeding with the pLDH assay. The percentage parasite survival in each well was calculated relative to the control wells receiving no drug. The 50% inhibitory concentration (IC_{50}) values were obtained from the dose–response curve, using non-linear dose–response curve fitting analyses with GraphPad Prism v.5 software.

6.7.2 Assay conditions

Five compounds were screened against the 3D7 and FCR3 strains.

- Test compound concentrations: 100 µM, 10 µM and 1 µM
- Reference standards: 100 µM, 10 µM and 1 µM (chloroquine and dihydroartemisinin)
- Incubation Time: 48 hours
- Read-out: Abs_{620}
- First, single-concentration assays were done against both *P. falciparum* strains. Normally, if no significant activity were found in this assay, no further analyses would be done. However, in this case full IC_{50} studies were also executed for all samples.

Chapter 7

Conclusions

The area of heterocyclic-based drug discovery has developed significantly over the past decade. A number of commercial and academic groups have been and are actively engaged in synthetic design and synthesis of heterocyclic-based lead compounds and drugs, because some of these are known to be inhibitors of proteins related to diseases such as malaria, cancer, HIV and Chagas disease. The effective synthesis of lead compounds is assisted by molecular modelling experiments and chemical structural modification of potentially active compounds derived from natural products and synthetic intermediates. The discovery of new antimalarial drugs, that would supersede the current clinical antimalarial drugs that are compromised by the resistance to *P. falciparum,* has been elusive to date. Consequently, there is an urgent need to design and develop new potent antiplasmodial agents.

This project set out to synthesise potential cysteine protease inhibitors as therapeutic agents for malaria. This is a life-threatening disease, and unfortunately is growing in resistance to current drugs. The syntheses of these compounds were based on construction of heterocyclic compounds based on a 2-pyridone scaffold. This involved constructing and investigating 2-pyridone derivatives with hydrophilic and hydrophobic moieties. The compounds were expected to be inhibitors of cysteine protease, one of the enzymes essential for the haemoglobin breakdown cascade of the virulent parasite *Plasmodium falciparum*.

The synthesis of potential lead compounds was also assisted by molecular modelling experiments. As the understanding of the parasite's enzyme-ligand interactions grows, it should be possible to design molecules as lead compounds that would mimic the structural activity of natural ligands.

The synthetic strategies used were based on the synthesis of a 2-pyridone scaffold. Some key intermediates (Scheme 7.1, compounds **37**, **43** and **46**, **50** and **52**) were prepared towards the synthesis of 2-pyridone derivatives. These intermediates were synthesized with the intention to form lead compounds **61**, **47** and **54**, respectively.

Attempts to synthesise the 2-pyridone derivatives **47** and **54** (Scheme 7.1) were unfortunately not successful, partly due to logistics challenges (such as move to a new building, loss of NMR facility locally and at UL) at crucial times. Preparation of compounds **47** and **54**

involved coupling intramolecular cyclization and decarboxylation reactions of the respective intermediates **43** with **46**, and **50** with **52**. The reaction mechanisms are concerted and conceivably failed because of steric factors apparent in the large substituents crowding around the amide. These reactions need to be further explored.

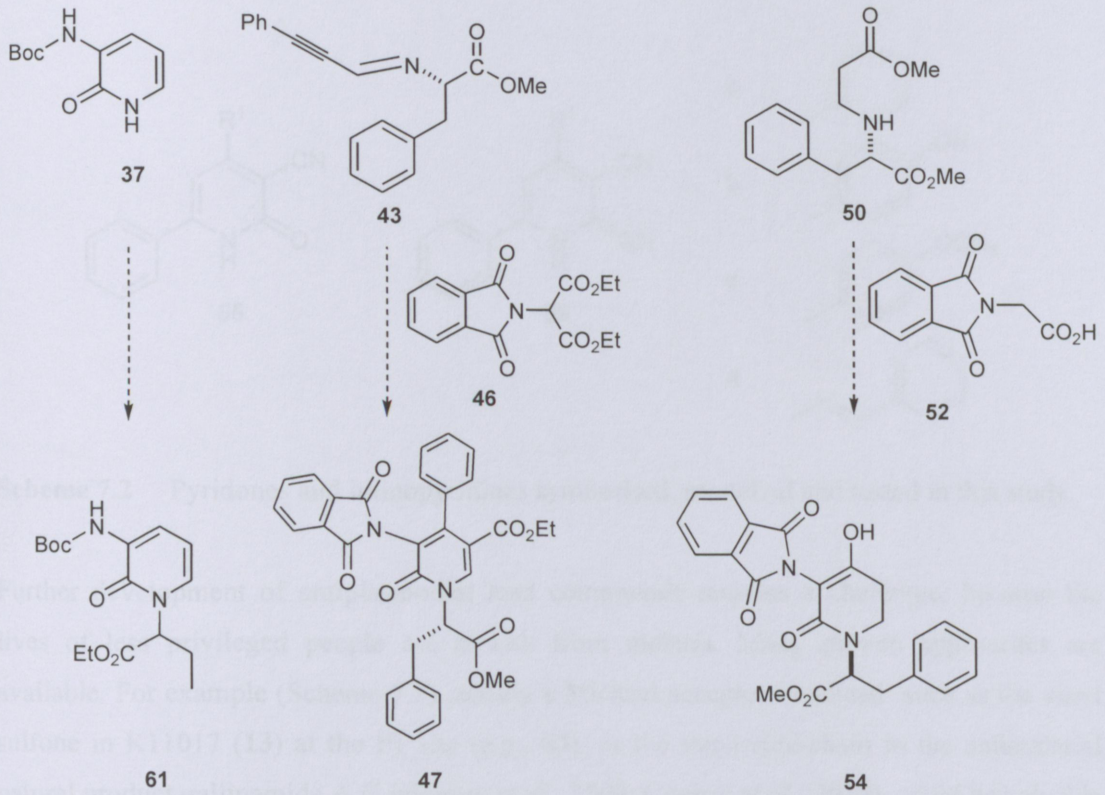

Scheme 7.1 Originally intended syntheses of pyridones.

A series of prospective cysteinyl protease inhibitors that are envisaged to have antimalarial activity (Scheme 7.2) was also synthesised, using a methodology that seems to have a wide scope. Eight related compounds (Compounds **55b**, **56b**, **55c**, **56c**, **55d**, **37**, **61**, and **62**) were tested as inhibitors against falcipain-2 (FP2) by docking studies, with three compounds, **55b**, **55c**, and **56c**, showing promising results. The scope of this methodology needs to be expanded in further studies.

These compounds were docked into the falcipain-2 active site to determine their probable binding modes. Analysis of the binding conformations in the active site showed that the

compounds were stabilized mostly by hydrogen bonds and some of them by electrostatic attractions, with the FP2 residues Gln36, Cys42, and His174 being most frequently involved.

Antimalarial testing of five compounds (Compounds **55a**, **56a**, **55b**, **55d**, and **55c**) showed that Compounds **55b** and **55c** have the potential to lead to discovery of significant antimalarial activity.

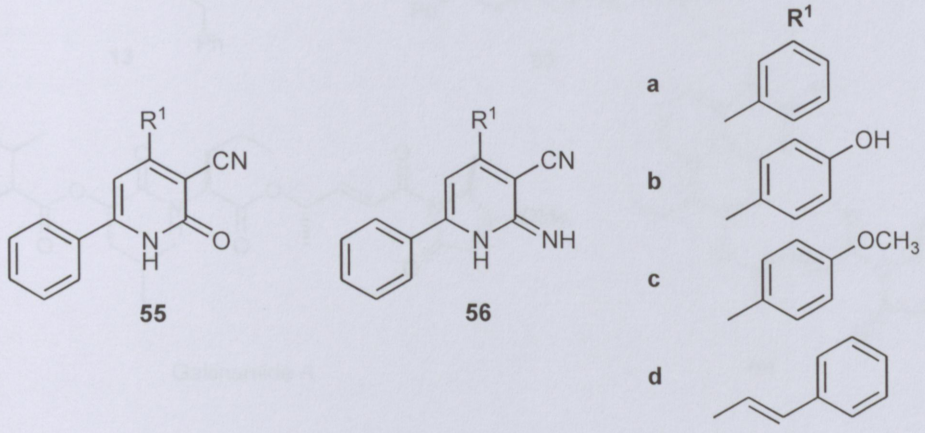

Scheme 7.2 Pyridones and iminopyridines synthesised, modelled and tested in this study.

Further development of antiplasmodial lead compounds remains a challenge, because the lives of less privileged people are at risk from malaria. Many proven approaches are available. For example (Scheme 7.3), adding a Michael acceptor 'warhead' such as the vinyl sulfone in K11017 (**13**) at the P1 site (*e.g.*, **63**), or the vinyl side-chain in the antimalarial natural product gallinamide A (Linington *et al.*, 2009; Conroy *et al.*, 2014), could be valuable avenues to explore in future (*e.g.*, **64**).

The search for potentially active antimalarial agents is multifaceted. It ideally involves collaborative programmes directed towards development of antiplasmodial therapies, involving medicinal chemists, biochemists, microbiologists and pharmacologists. It is hoped that the information gained by this study may contribute to the design and synthesis of new antimalarial lead compounds that have distinct structural features.

The synthesized derivatives of compounds **55** and **56** (Scheme 7.2) and similar compounds (Scheme 7.3) afford more scope for further chemical transformation and biological screening. Other envisaged structural modifications would involve preparation of *N*-alkyl substituted 2-pyridone derivatives. Particularly motivating for future studies are the results of the *in vitro*

assays of some derivatives of compounds **55** and **56**, which exhibited low to medium activity in antimalarial assays.

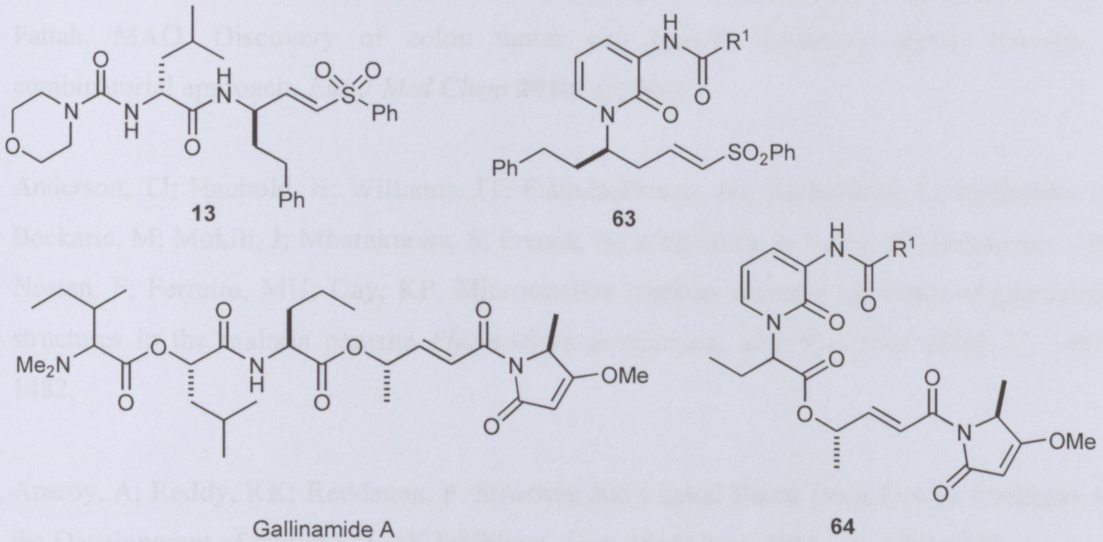

Scheme 7.3 Possible future targets for development.

References

Abadi, AH; Abouel-Ella, DA; Lehmann, J; Tinsley, HN; Gary, BD; Piazza, GA; Abdel-Fattah, MAO. Discovery of colon tumor cell growth inhibitory agents through a combinatorial approach, *Eur J Med Chem* **2010**, *45*, 90-97.

Anderson, TJ; Haubold, B; Williams, JT; Estrada-Franco, JG; Richardson, L; Mollinedo, R; Bockarie, M; Mokili, J; Mharakurwa, S; French, N; Whitworth, J; Velez, ID; Brockman, AH; Nosten, F; Ferreira, MU; Day, KP. Microsatellite markers reveal a spectrum of population structures in the malaria parasite *Plasmodium falciparum*, *Mol Biol Evol* **2000**, *17*, 1467-1482.

Aparoy, A; Reddy, KK; Reddanna, P. Structure and Ligand Based Drug Design Strategies in the Development of Novel 5- LOX Inhibitors, *Curr Med Chem* **2012**, *19*, 3763-3778.

Barrett, AJ; Kembhavi, AA; Brown, MA; Kirschke, H; Knight, CG; Tamai, M; Hanada, K. l-*Trans*-epoxysuccinylleucylamido(4-guanido)butane (E-64) and its analogues as inhibitors of cysteine proteases including cathepsins B, H and L, *Biochem J* **1982**, *201*, 189-198.

Bishop, AOT; de Beer, TAP; Joubert, F. Protein homology modelling and its use in South Africa, *SA J Science* **2008**, *104*, 2-6.

Blum, A; Böttcher, J; Sammet, B; Luksch, T; Heine, A; Klebe, G; Diederich, WE. Achiral oligoamines as versatile tool for the development of aspartic protease inhibitors, *Bioorg Med Chem* **2008**, *16*(18), 8574-8586.

Breman, JG; Alilio, MS; Mills, A. Conquering the Intolerable Burden of Malaria: What's New, What's Needed: A Summary, *Am J Trop Med Hyg* **2004**, *71*, 1–15.

Breman, JG; Holloway, CN. Malaria surveillance, *Am J Trop Med Hyg* **2001**, *64*, 1.

Brik, A; Wong, CH. HIV-1 protease: mechanism and drug discovery, *Org Biomol Chem* **2003**, *1*, 5-14.

Bryant, C; Kerr, ID; Debnath, M; Ang, KKH; Ratnam, J; Ferreira, RS; Jaishankar, P; Zhao, DM; Arkin, MR; McKerrow, JH; Brinen, LS; Renslo, AR. Novel non-peptidicvinylsulfones targeting the S2 and S3 subsites of parasite cysteine proteases, *Bioorg Med Chem Lett* **2009**, *19*, 6218-6221.

Bulet, P; Stöckling, R. Insect Antimicrobial Peptides: Structures, Properties and Gene Manipulation, *Protein Peptide Lett* **2005**, *12*, 3 – 11.

Burgess, K. Solid-Phase Syntheses of β-Turn Analogues To Mimic or Disrupt Protein-Protein Interactions, *Acc Chem Res* **2001**, *34*, 826-835.

Caffrey, CR; Scory, S; Steverding, D. Cysteine proteases of trypanosome parasites, Novel targets for chemotherapy, *Curr Drug Targets* **2000**, *1*, 155-162.

Capela, R; Oliveira, R., Gonçalves, L.M., Domingos, A., Gut, J., Rosenthal, P.J., Lopes, F., Moreira, R. Artemisinin-dipeptidyl vinyl sulfone hybrid molecules: Design, synthesis and preliminary SAR for antiplasmodial activity and falcipain-2 inhibition, *Bioorg Med Chem Lett* **2009,** *19*, 3229-3232.

CDC. *DPDx - Laboratory Identification of Parasitic Diseases of Public Health Concern.* Centers for Disease Control and Prevention, Atlanta, GA, USA. **2013**. http://www.cdc.gov/dpdx/malaria/index.html, last visited on 24.08.2015.

Conroy, T; Guo, JT; Elias, N; Cergol, KM; Gut, J; Legac, J; Khatoon, L; Liu, Y; McGowan, S; Rosenthal, PJ; Hunt, NH; Payne, RJ. Synthesis of Gallinamide A Analogues as potent Falcipain Inhibitors and Antimalarials, *J Med Chem* **2014**, *57*, 10557-10563.

Cronk, JD. **2014**. BIOCHEMISTRY Dictionary, http://guweb2.gonzaga.edu/faculty/cronk/biochem/P-index.cfm?definition=protease. Last visited on 02.02.15.

Cunico, W; Gomes, CR; Facchinetti, V; Moreth, M; Penido, C; Henriques, MG; Varotti, FP; Krettli, LG; Krettli, AU; da Silva, FS; Caffarena, ER; de Magalhães, CS. Synthesis,

antimalarial evaluation and molecular modeling studies of hydroxyethylpiperazines, potential aspartyl protease inhibitors, part 2, *Eur J Med Chem* **2009**, *44*(9), 3816-3820.

Czodrowski, P; Hölzemann, G; Barnickel, G; Greiner, H; Musil, D. Selection of Fragments for Kinase Inhibitor Design: Decoration is Key, *J Med Chem* **2014**, *58*, 457-465.

Dahl, EL; Rosenthal, PJ. Biosynthesis, localization, and processing of falcipain cysteine proteases of *Plasmodium falciparum*, *Mol Biochem Parasitol* **2005**, *139*, 205.

Darkins, P; Gilmore, BF; Hawthorne, SJ; Healy, A; Moncrieff, H; McCarthy, N; McKervey, MA; Brömme, D; Pagano, M; Walker, D. Synthesis of peptidylenediones: selective inactivation of the cysteine proteases, *Chem Biol Drug Res* **2007**, *69*, 170-179.

Desai, PV; Patny, A; Gut, J; Rosenthal, PJ; Tekwani, B; Srivastava, A; Avery, M. Identification of Novel Parasitic Cysteine Protease Inhibitors by Use of Virtual Screening. 2. The Available Chemical Directory, *J Med Chem* **2006**, *49*(5), 1576-1584.

Ekici, ÖD; Götz, MG; James, KE; Li, ZZ; Rukamp, BJ; Asgian, JL; Caffrey, CR; Hansell, E; Dvorák, J; McKerrow, JH; Potempa, J; Travis, J; Mikolajczyk, J; Salvesen, GS; Powers, JC. Aza-peptide Michael acceptors: a new class of inhibitors specific for caspases and other clan CD cysteine proteases, *J Med Chem* **2004**, *47*, 1889-1892.

Eksi, S; Czesny, B; Greenbaum, DC; Bogyo, M.; Williamson, KC. Targeted disruption of *Plasmodium falciparum* cysteine protease, falcipain1, reduces oocyst production, not erythrocytic stage growth, *Mol Microbiol* **2004**, *53*, 243-250.

Ellis, DA; Blazel, JK; Tran, CV; Ruebsam, F; Murphy, DE; Li, L-S; Zhao, J; Zhou, Y; McGuire, HM; Xiang, AX; Webber, SE; Zhao, Q; Han, Q; Kissinger, CR; Lardy, M; Gobbi, A; Showalter, RE; Shah, AM; Tsan, M; Patel, RA; LeBrun, LA; Kamran, R; Bartkowski, DM; Nolan, TG; Norris, DA; Sergeeva, MV; Kirkovsky, L. 5,5'- and 6,6'-Dialkyl-5,6-dihydro-1*H*-pyridin-2-ones as potent inhibitors of HCV NS5B polymerase, *Bioorg Med Chem Lett* **2009**, *19*, 6047-6052.

El-Sayed, HA; Ouf, NH. An efficient and facile multicomponent synthesis of 4,6-diarylpyridine derivatives under Solvent-Free Conditions, *Nat Sci* **2012**, *10*(9), 59-63.

Erdmann, D. *Histamine H2 and H3 Receptor Antagonists: Synthesis and Characterization of Radiolabelled and Fluorescent Pharmacological Tools*. Doctoral thesis, University of Regensburg, **2010**.

Ersmark, K; Samuelsson, B; Hallberg, A. Plasmepsins as potential targets for new antimalarial therapy, *Med Res Rev* **2006**, *26*(5), 626–666.

Ettari, R; Nizi, E; Di Francesco, ME; Dude, MA; Pradel, G; Vičík, R; Schirmeister, T; Micale, N; Grasso, S; Zappalà, M. Development of Peptidomimetics with a Vinyl Sulfone Warhead as Irreversible Falcipain-2 Inhibitors, *J Med Chem* **2008**, *51*(4), 988–996.

Evans, SG; Butkow, N; Stilwell, C; Berk, M; Kirchmann, N; Havlik, I. Citalopram Enhances the Activity of Chloroquine in Resistant *Plasmodium in Vitro* and *in Vivo, J Pharmacol Experim Therapeut* **1998,** 286, 172-174.

Francis, SE; Sullivan, DJ; Goldberg, DE. Hemoglobin metabolism in the malaria parasite *Plasmodium falciparum*, *Annu Rev Microbiol* **1997**, *51*, 97–123.

Frere, JM; Nguyen-Disteche, M; Coyette, J; Joris, B. *Mode of action: interaction with the penicillin-binding proteins*, **1992**. Chapman and Hall, Glasgow, Scotland, pp. 148-195.

Gamboa de Domínguez, ND; Rosenthal, PJ. Cysteine proteinase inhibitors block early steps in hemoglobin degradation by cultured malaria parasites, *Blood* **1996**, *87*, 4448-4454.

Gardner, MJ; Hall, N; Fung, E; White, O; Berriman, M; Hyman; RW; Carlton, JM; Pain, A; Nelson, KE; Bowman, S; Paulsen, IT; James, K; Eisen, JA; Rutherford, K; Salzberg, SL; Craig, A; Kyes, S; Chan, MS; Nene, V; Shallom, SJ; Suh, B; Peterson, J; Angiuoli, S; Pertea, M; Allen, J; Selengut; J; Haft, D; Mather, MW; Vaidya, AB; Martin, DM; Fairlamb, AH; Fraunholz, MJ; Roos, DS; Ralph, SA; McFadden, GI; Cummings, LM; Subramanian, GM; Mungall, C; Venter, JC; Carucci, DJ; Hoffman, SL; Newbold, C; Davis, RW; Fraser, CM;

Barrell, B. Genome sequence of the human malaria parasite *Plasmodium falciparum*, *Nature* **2002**, *419*(6906), 498 – 511.

Gezegen, H; Ceylan, M; Karaman, İ; Şahin, E. Synthesis, characterization and antibacterial activity of novel pyridones. *Synthetic Communications* **2014**, *44*(8), 1084 – 1093.

Giannis, A; Kolter, T. Peptide mimetics for receptor ligands: discovery, development, and medicinal perspectives, *Angew Chem Int Ed Eng* **1993**, *32*, 1244-1267.

GIC (The Genome International Consortium). Initial sequencing and analysis of the human genome, *Nature* **2001**, *409*, 860-921.

Gluzman, IY; Francis, SE; Oksman, A; Smith, CE; Duffin, KL; Goldberg, DE. Order and specificity of the *Plasmodium falciparum* hemoglobin degradation pathway, *J Clin Invest* **1994**, *93*(4), 1602–1608.

Goh, SL; Goh, LL; Sim, TS. Cysteine protease FP-1 in P. falciparum is biochemically distinct from its isozymes, *Parasitol Res* **2005**, *97*(4), 295-301.

Greenbaum, DC; Baruch, A; Grainger, M; Bozdech, Z; Medzihradszky, KF; Engel, J; DeRisi, J; Holder, AA; Bogyo, M. A role for the protease falcipain 1 in host cell invasion by the human malaria parasite, *Science* **2002**, *298*(5600), 2002-2006.

Hachiya, I; Ogura, K; Shimizu, M. Novel 2-Pyridone Synthesis via Nucleophilic Addition of Malonic Esters to Alkynyl Imines, *Org Lett* **2002**, *4*(16), 2755–2757.

Hanada, K; Tamai, M; Yamagishi, M; Ohmura, S; Sawada, J; Tanaka, I. Isolation and Characterization of E-64, a New Thiol Protease Inhibitor, *Agric Biol Chem* **1978**, *42*, 523 – 528.

Hancock, REW; Falla, T; Brown, M. Cationic Bactericidal Peptides, *Adv Microb Physiol* **1995**, *37*, 135.

Jomaa, H; Wiesner, J; Sanderbrand, S; Altincicek, B; Weidemeyer, C; Hintz, M; Türbachova, I; Eberl, M; Zeidler, J; Lichtenthaler, HK; Soldati, D; Beck, E. Inhibitors of nonmevalonate pathway of isoprenoid biosynthesis as antimalarial drugs, *Science* **1999**, *285*, 1573–1576.

Kemp, LE; Bond, CS; Hunter, WN. Structure of 2C-methyl-d-erythritol 2,4-cyclodiphosphate synthase: An essential enzyme for isoprenoid biosynthesis and target for antimicrobial drug development, *Proc Natl Acad Sci* **2002**, *99*, 6591–6596.

Kerr, LK; Lee, JH; Faraday, CJ; Marion, R; Rickert, M; Sajid, M; Pandey, KC; Caffrey, CR; Legac, J; Hansell, E; Mckerrow, JH; Craik, CS; Rosenthal PJ; Brinen, LS. Vinyl Sulfones as Antiparasitic Agents and a Structural Basis for Drug Design, *J Biol Chem* **2009a**, *284*, 25697-25703.

Kerr, ID; Lee, JH; Pandey, KC; Harrison, A; Sajid, M; Rosenthal, PJ; Brinen, LS. Structures of falcipain-2 and falcipain-3 bound to small molecule inhibitors: implications for substrate specificity, *J Med Chem* **2009b**, *52*(3), 852–857.

Kohara, Y; Imamiya, E; Kubo, T; Inada, Y; Naka, T. A new class of angiotensin II receptor antagonists with a novel acidic bioisostere, *Bioorg Med Chem Lett* **1995**, *5*, 1903 – 1908.

Konno, H; Nosaka, K; Akaji, K. Synthesis of tokaramide A, a cysteine protease inhibitor from marine sponge *Theonella aff. mirabilis*, *Tetrahedron* **2011**, *67*, 9067 – 9071.

Krogstad, DJ; Schlesinger, PH. The basis of antimalarial action: non weak base effects of chloroquine on acid vesicle pH, *Amer J Tropical Med Hyg* **1987**, *36*, 213 – 220.

Kumar, A; Kumar, K; Korde, R; Puri, SK; Malhotra, P; Chauhan, VS. Falcipain 1, a *Plasmodium falciparum* Cysteine Protease with Vaccine Potential, *Infect Immun* **2007**, *75*, 2026-2034.

Lee, BJ; Singh, N; Chiang, P; Kemp, SJ; Goldman, EA; Weinhouse, MI; Vlasuk, GP; Rosenthal, PJ. Antimalarial Activities of Novel Synthetic Cysteine Protease Inhibitors, *Antimicrob Agents Chemother* **2003**, *47*, 3810 – 3814.

Linington, RG; Clark, BR; Trimble, EE; Almanza, A; Ureña, LD; Kyle, DE; Gerwick, WH. Antimalarial peptides from marine cyanobacteria: isolation and structural elucidation of gallinamide A, *J Nat Prod* **2009**, *72*(1), 14-17.

Lipinski, CA; Lombardo, F; Dominy, BW; Feeney, PJ. Experimental and computational approaches to estimate solubility and permeability in drug discovery and development settings, *Advanced Drug Delivery Reviews* **1997**, *23*, 3-25.

Lv, Z; Sheng, C; Wang, T; Zhang, Y; Liu, J; Feng, J; Sun, H; Zhong, H; Niu, C; Li, K. Design, synthesis, and antihepatitis B virus activities of novel 2-pyridone derivatives, *J Med Chem* **2010**, *53*(2), 660-668.

Machon, U; Büchold, C; Stempka, M; Schirmeister, T; Gelhaus, C; Leippe, M; Gut, J; Rosenthal, PJ; Kisker, C; Leyh, M; Schmuck, C. On-bead screening of a combinatorial fumaric acid derived peptide library yields antiplasmodial cysteine protease inhibitors with unusual peptide sequences, *J Med Chem* **2009**, *52*, 5662-5672.

Maelicke, A. Proteomics, *Nachr Chem Tech Lab* **1999**, *47*(12), 1433 – 1435.

Makungo, T. *The Search for Novel Leads Targeting PfCDPK4 for Therapeutic Treatment of Malaria*. MSc dissertation, University of Venda, **2015**.

Martin, SF; Dwyer, MP; Hartmann, B; Knight, KS. Cyclopropane-derived peptidomimetics. Design, synthesis, and evaluation of novel enkephalin analogues, *J Org Chem* **2000**, *65*, 1305-1318.

McKerrow, JH; Sun, E; Rosenthal, PJ; Bouvier, J. The proteases and pathogenicity of parasitic protozoa, *Ann Rev Microbiol* **1993**, *47*, 821-853.

Medebielle, M; Ait-Mahand, S; Burkhloder, C; Dolbier, WR; Laumond, G; Aubertin, AM. Syntheses of new difluoromethylene benzoxazole and 1,2,4-oxadiazole derivatives, as potent non-nucleoside HIV-1 reverse transcriptase inhibitors, *J Fluorine Chem* **2005**, *126*, 533-535.

Messer, WS; Abuh, YF; Liu, Y; Periyasamy, S; Ngur, DO; Edgar, MA; El-Assadi, AA; Sbeih, S; Dunbar, PG; Roknich, S; Rho, T; Fang, Z; Ojo, B; Zhang, H; Huzl, JJ; Nagy, PI. Synthesis and Biological Characterization of 1,4,5,6-Tetrahydropyrimidine and 2-Amino-3,4,5,6-tetrahydropyridine Derivatives as Selective m1 Agonists, *J Med Chem* **1997**, *40*, 1230-1246.

Mijin, DZ; Baghbanzadeh, M; Reidlinger, C; Kappe, CO. The microwave-assisted synthesis of 5-arylazo-4,6-disubstituted 3-cyano-2-pyridone dyes, *Dyes Pigments* **2010**, *85*, 73-78.

Morera, E; Nalli, M; Pinnen, F; Rossi, D; Lucente, G. 4-Amino-1,2-dithiolane-4-carboxylic acid (Adt) as cysteine conformationally restricted analogue. Synthetic protocol for Adt containing peptides, *Bioorg Med Chem Lett* **2000**, *10*, 1585-1588.

Nam, T; Ku, J-M; Rector, CL; Choi, H; Porter, NA; Jeong, BS. Pyridoxine-derived bicyclic aminopyridinol antioxidants: synthesis and their antioxidant activities, *Org Biomol Chem* **2011**, *9*, 8475-8482.

Nguyen, J-T; Hamada, Y; Kimura, T; Kiso, Y. Design of potent aspartic protease inhibitors to treat various diseases, *Arch Pharm Chem Life Sci* **2008**, *341*, 523-535.

Osterberg, AE. *Organic Syntheses*, *Vol. 7*, p. 78 (**1927**); *Coll. Vol. 1*, p. 271 (**1941**).

Pandey, KC; Dixit, R. Structure-function of falcipains: Malaria cysteine proteases, *J Trop Med* **2012**, Article ID 345195, 11 pages.

Patel, V; Mazitschek, R; Coleman, B; Nguyen, C; Urgaonkar, S; Cortese, J; Barker, RH; Greenberg, E; Tang, W; Bradner, JE; Schreiber, SL; Duraisingh, MT; Wirth, DF; Clardy, J. Identification and Characterization of Small Molecule Inhibitors of a Class I Histone Deacetylase from *Plasmodium falciparum, J Med Chem* **2009**, *52*, 2185–2187.

Przybylski, P; Schilf, W; Brzezinski, B. **2005**. ^{13}C, ^{15}N NMR and CP-MAS as well as FT-IR and PM5 studies of Schiff base of gossypol with L-phenylalanine methyl ester in solution and solid, *J. Molec. Struc.* **734**, 123–128.

Qiu, W; Gu, X; Soloshonok, VA; Carducci, MD; Hruby, VJ. Stereoselective synthesis of conformationally constrained reverse turn dipeptide mimetics, *Tetrah Letters* **2001**, *42*, 145-148.

Ralph, SA; D'Ombrain, MC; McFadden, GI. The apicoplast as an antimalarial drug target, *Drug Resist Update* **2001**, *4*, 145 – 151.

Ramjee, MK; Flinn, NS; Pemberton, TP; Quibell, M; Wang, Y; Watts, JP. Substrate mapping and inhibitor profiling; Implication for peptide antimalaria drug discovery, *Biochem J* **2006**, *399*, 47-57.

Roberts, R. Lysosomal Cysteine Proteases: Structure, Function and Inhibition of Cathepsins, *Drug News Perspect* **2005**, *18*(10), 605.

Rose, GD; Gierasch, LM; Smith, JA. Turns in peptides and proteins, *Adv Protein Chem* **1985**, *37*, 1-109.

Rosenthal, PJ. Proteases of malaria parasites: new targets for chemotherapy. *Emerg Infect Dis* **1998**, *4*(1), 49-57.

Rosenthal, PJ. Cysteine proteases of malaria parasites, *Int J Parasitol* **2004**, *34*, 1489-1499.

Rosenthal, PJ; Meshnick, SR. Hemoglobin catabolism and iron utilization by malaria parasites, *Mol Biochem Parasitol* **1996**, *83*, 131-139.

Sajid, M; McKerrow, JH. Cysteine proteases of parasitic organisms, *Mol Biochem Parasitol* **2002**, *120*, 1-120.

Santos, MMM; Moreira, R. Michael acceptors as cysteine protease inhibitors, *Mini-Rev Med Chem* **2007**, *7*, 1040-1050.

Scheffelaar, R; Roel, A; Nijenhuis, K; Paravidino, M; Lutz, M; Spek, AL; Ehlers, AW; de Kanter, FJJ; Groe, MB; Orru, RVA; Ruijter, E. Synthesis of conformationally constrained peptidomimetics using multicomponent reactions, *J Org Chem* **2009**, *74*, 660-668.

Scheidt, KA; Roush, WR; McKerrow, JH; Selzer, PM; Hansell, E; Rosenthal, PJ. Structure-based design, synthesis and evaluation of conformationally constrained cysteine protease inhibitors, *Bioorg Med Chem* **1998**, *6*, 2477.

Selzer, PM; Pingel, S; Hsieh, I; Ugele, B; Chan, VJ; Engel, JC; Bogyo, M; Russell, DG; Sakanari, JA; McKerrow, JH. Cysteine protease inhibitors as chemotherapy: Lessons from a parasite target, *Proc Natl Acad Sci USA* **1999**, *96*, 11015 – 11022.

Shenai, BR; Sijwali, PS; Singh, A; Rosenthal, PJ. Characterization of native and recombinant falcipain-2, a principal trophozoite cysteine protease and essential hemoglobinase of *Plasmodium falciparum*, *J Biol Chem* **2000**, *275*, 29000–29010.

Sijwali, PS; Shenai, BR; Gut, J; Singh, A; Rosenthal, PJ. Expression and characterization of the *Plasmodium falciparum* haemoglobinase falcipain-3, *Bioremediation J* **2001**, *360*, 481–489.

Silva, AM; Lee, AY; Gulnik, SV; Majer, P; Collins, J; Bhat, TN; Collins, PJ; Cachau, RE; Luker, KE; Gluzman, IY; Francis, SE; Oksman, A; Goldberg, DE; Erickson, JW. Structure and inhibition of plasmepsin II, a hemoglobin-degrading enzyme from *Plasmodium falciparum*, *Proc Natl Acad Sci USA* **1996**, *93*, 10034-10039.

Singh, N; Sijwali, PS; Pandey, KC; Rosenthal, PJ. *Plasmodium falciparum*: biochemical characterization of the cysteine protease falcipain-2', *Exper Parasitol* **2006**, *112*, 187–192

Sureshbabu, VV; Hemantha, HP; Naik, SA. Synthesis of 1,2,4-oxadiazole-linked orthogonally urethane-protected dipeptide mimetics, *Tetrahedron Lett* **2008**, *49*, 5133-5136.

Tietze, L-F; Eicher, T. **1981**. *Reaktionen und Synthesen im organisch-chemischen Praktikum*, p. 115-116. Thieme: Stuttgart.

Turk, B. Targeting proteases: successes, failures and future prospects, *Nat Rev Drug Discov* **2006**, *5*(9), 785-799.

Upadhyay, PK; Prasad, R; Pandey, M; Kumar, P. A facile synthesis of 5,6-dihydro-5-hydroxy-2(1*H*)-pyridone, *Tetrah Lett* 2009, *50*, 2440-2442.

van Ree, T; Steglich, W. Two novel syntheses of substituted 1,2,4-oxadiazoles from amidoximes, *Synth Comm* **1982**, *12*(6), 457-461.

Verissimo, E; Berry, N; Gibbons, P; Lurdes, S; Cristiano, M; Rosenthal, PJ; Gut, J; Ward, SA; O'Neill, PM. Design and synthesis of novel 2-pyridone peptidomimetic falcipain 2/3 inhibitors, *Bioorg Med Chem Lett* **2008**, *18*, 4210-4214.

Vivas, L; Rattray, L; Stewart, LB; Robinson, BL; Fugmann, B; Haynes, RK; Peters, W; Croft, SL. Antimalarial efficacy and drug interactions of the novel semi-synthetic endoperoxide artemisone *in vitro* and *in vivo, J Antimicrob Chemother* **2007,** 59, 658-665.

Watjen, F; Baker, R; Angelstoff, M; Herbert, R; Macleod, A; Knight, A; Merchant, K; Moseley, J; Saunders, J; Swain, CJ; Wong, E; Springer, JP. Novel benzodiazepine receptor partial agonists: oxadiazolylimidazobenzodiazepines, *J Med Chem* **1989**, *32*, 2282 – 2291.

White, NJ. Antimalarial Resistance, *J Clin Invest* **2004**, *113*(8), 1084-1092.

WHO. The World Health Report, **2014**. World Health Organization: Geneva.

Zhang, JH; Chung, TDY; Oldenburg, KR. A simple statistical parameter for use in evaluation and validation of high throughput screening assays, *Journal of Biomolecular Screening* **1999**, *4*, 67–73.